Dynamics of Hydrogen and Local Structure in Ti-V-H(D) System as Studied by Nuclear Magnetic Resonance and Neutron Inelastic Scattering

By

TAKAHIRO UEDA

National Institute of

Materials and Chemical Research

May 1995

Dynamics of Hydrogen and Local Structure in Ti-V-H(D) System as Studied by Nuclear Magnetic Resonance and Neutron Inelastic Scattering

By

TAKAHIRO UEDA

National Institute of

Materials and Chemical Research

May 1995

DOCTORAL DISSERTATION

Dynamics of Hydrogen and Local Structure in Ti-V-H(D) System as Studied by Nuclear Magnetic Resonance and Neutron Inelastic Scattering

A Dissertation Presented

by

TAKAHIRO UEDA

Department of Physical Chemistry,

National Institute of

Materials and Chemical Research.

Submitted to the Faculty of Science,

Osaka University.

in partial fulfillment of the

Doctor of Science

May 1995

Doctoral Committee:

Professor Nobuo Nakamura, Chairman

Professor Takasuke Matsuo,

Professor Tomoji Kawai,

Associate Professer Akira Inaba.

Acknowledgments

I would like to express my most sincere thanks to Professor Nobuo Nakamura for his kind guidance, criticism, heartful encouragement and a number of variable suggestions filled with his deep insight into science, and for his critical reading of this manuscript. Under his guidance throughout my graduate course I could learn much things about the nuclear magnetic resonance, solid state physics and other related fields.

I wish to express my gratitude to Professor Takasuke Matsuo, Professor Tomoji Kawai and Associate Professor Akira Inaba for their critical reading of this manuscript and for their variable comments.

I wish to thank Emeritus Professor Hideaki Chihara for his attractive guidance into physical chemistry and many helpful suggestions.

I am indebeted to Associate Professor Taro Eguchi, Dr. Sadamu Takeda, Dr. Hirokazu Nakayama and other members of Quantum Chemistry Laboratories for their valuable discussion and encouragement in pursuing my graduate course study. Especially, I am very grateful to Dr. Hiroshi Ohki and Dr. Shin'ichi Ishimaru for fruitful discussions with them, their encouragement and their friendship in Tsukuba as well as in my graduate course of Osaka University.

I am grateful to Dr. Shigenobu Hayashi of Department of Physical Chemistry in National Institute of Materials and Chemical Research for his valuable comments in this study. Dr. Etsuo Akiba and co-workers of Department of Inorganic Materials in National Institute of Materials and Chemical Research helped my X-ray diffraction experiment and synthesis of my samples. Associate Professor Susumu Ikeda of National Laboratory for High Energy Physics and the other members of his research group collaborated with me about neutron inelastic scattering study and permitted to use data in this thesis.

Finally, I deeply appreciate my parents with all my heart, who give me a chance to study the world of chemistry and have a heart to my selections.

Abstract

The dynamics of interstitial hydrogen atoms and the local structure of the host metal lattice in Ti-V disordered alloy were investigated by solid state NMR and neutron scatterng methods to clarify the mechanism of the hydrogen absorption in the alloy, and to characterize the types of the interstitial sites occupied by H in the Ti-V-H(D) system.

The local structural model around an interstitial hydrogen atom in the disordered Ti-V alloy was necessary to relate the macroscopic properties of the T-V-H(D) system with the microscopic informations obtained by NMR and neutron scattering measurements. A cluster model for the local framework structure of the host alloy was applied. This model assumes that the interstitial site energy is determined by the interaction between the interstitial atom and its the nearest neighbor metals. The original model assumes only $Ti_{4-i}V_i$ type tetrahedral cluster around the interstitial to guest site but it was modified to incorporate the $Ti_{6-i}V_i$ type octahedral clusterin order to apply this model to the hydrides with high hydrogen concentrations. The procedure of the modification of the cluster model was described. Use of this model makes it possible to interpret the alloy composition dependence of the activation energy for the hydrogen diffusion or hopping and of the formation enthalpies of the hydride and the deuteride with the disordered host alloys.

For the disordered metal hydrides, β-$Ti_{1-y}V_yH_x$ ($x \sim 1$ and $0.2 < y < 0.9$), the types of the interstitial hydrogen sites were studied by using incoherent neutron inelastic scattering (INIS) technique at 50 K. Four peaks originated from the β-phase were observed in the energy range between 13 meV and 152 meV. These peaks were assigned to the metal lattice vibrations and the local vibrational modes of hydrogen atoms occupying the octahedral site and two kinds of tetrahedral sites. It was found that the occupancy of the octahedral site increases but of the tetrahedral site decreases with increase in V content in the alloy. The composition dependence of the site population was analyzed using the cluster model described above, and the short-range order parameter for the host alloy was determined to be 0.4 which implies that the Ti-V alloy tend to form microscopically inhomogeneous framework and the distribution of hydrogen are significantly biased.

^2H NMR spectra of β-$Ti_{1-y}V_yD_x$ ($x \sim 1$ and $0.2 \leq y \leq 0.8$) were measured to investigate the diffusive motion of deuteron. The obtained spectrum shows no remarkable

quadrupole broadening even at 125 K, except that a broad shoulder appeaer in the frequency region higher than the main peak. The intensity ratio of the shoulder to the total peak appears to decrease with increase in temperature. The shoulder was assigned to the α-phase which co-exists with the β-phase. The deuteron diffusive motion was revealed to be rapid enough to average out the quadrupole interaction.

Local framework structure of metal lattice around the interstitial atom and the dynamics of the interstitial atoms in disordered metal hydrides and deuterides, β-$Ti_{1-y}V_yH_x$ and β-$Ti_{1-y}V_yD_x$ ($x \sim 1$ and $0.2 \leq y \leq 0.8$) were studied by the ^1H and ^2H spin-lattice relaxation time (T_1) measurements. The present alloy-hydrogen system is in a state of biased disorder with respect to the host framework. Moreover the highly concentrated guest atoms are interacting strongly with each other. Therefore the analyses of the dynamics of the guest atoms become very complex. In the present study the guest motion in such inhomogeneous and strongly correlated system was approximated by taking account of distribution of the correlation time for the motion. By applying the BPP theory taking account of the distribution of the correlation time the activation parameters for the diffusion of the interstitial atoms were determined for all of β-Ti-V-H systems. The alloy composition dependence of the apparent activation energy (E_a) for the diffusion of the interstitial atoms was discussed with respect to the local framework structures of metal lattice around an interstitial atom using the extended cluster model. The magnitudes of the metal-hydorgen and the metal-deuterium interactions were then estimated. The results of the analysis suggest that the cluster model is valid to describe the local framework structure and the macroscopic properties such as the formation enthalpy of alloy-hydrogen system of the disordered Ti-V alloy, and that the local metal-interstitial atom interactions can be interpreted using the potential parameters determined for pure TiH_x and VH_x. It was found that there is a remarkable isotope effect on the potential wells restricting the motion of the interstitial atoms in between the hydride and the deuteride. The isotope effect on the guest motion is caused by the mass effect at Ti rich composition, whereas at V rich compositions isotope effect is caused by both mass effect and the difference in the degree of deformation of potental wells between the T- and the O-sites.

Contents

1. Introduction 1

2. Model

2.1 The cluster model in disordered A-B alloy 14

2.2 Extension of Brouwer' formula 16

2.3 Application of model to activation energy of diffusion in A-B alloy 22

3. Samples

3.1 Preparation 27

3.2 X-ray powder diffraction (XRD) 27

3.3 Differential scanning calorimetry (DSC) 33

4.Incoherent inelastic neutron scattering

4.1 Introduction 34

4.2 Experimental 36

4.3 Results 37

4.4 Discussion 40

5. Spin-lattice relaxation times (T_1)

5.1 Introduction

5.1.1 General description of BPP equation 52

5.1.2 Distribution of correlation time 54

5.2 ^{1}H NMR

5.2.1 Experimental 56

5.2.2 Results and analysis 57

5.2.3 Discussion 71

5.3 ^{2}H NMR

5.3.1 Experimental 80

5.3.2 Results and analysis 80

5.3.3 Discussion 88

6. ^{2}H NMR spectra

6.1 Introduction 98

6.2 Experimental 100

6.3 Results and discussion 101

7. Summary 113

1. Introduction

Metal hydrides have been studied over almost a century from the fundamental and applicative points of view. Studies on the hydrogen storage and on the separation and purification of the hydrogen isotope. Enormous efforts were made to identify and characterize simple binary metal hydrides, MH_x, and to establish their phase diagrams [1]. Owing to such extensive works it is now known that almost all the metallic elements in the Periodic Table can form the hydrides. Among them the IV A (Ti, Zr, and Hf) and the V A (V, Nb, and Ta) elements have been recognized to form stable hydrides and extensive investigations on the crystal structure and the electronic and the thermodynamic properties of their hydrides were performed so far [2]. Recently, for the purpose of realizing lighter materials with higher hydrogen-absorbing capacity numerous alloy systems among IV A and V A metals, the alkaline earths such as Mg and Ca, and the rare earth metals such as La draw much attention. For the above purpose the most interesting host materials are the ternary metal hydrides [3]; Such ternary alloy systems can be classified into two groups by the type of the host alloy. One is the hydrides of the ordered alloys such as $LaNi_5H_x$ ($x \leq 6$) [4] and Mg_2NiH_x ($x \leq 4$) [5], which belong to so-called Laves phase and a lot of host materials with this structure have been known. The other is the hydrides of the disordered alloys such as $Ti_{1-y}V_yH_x$ ($x \leq 2$) [6, 7] and $Nb_{1-y}V_yH_x$ ($x \leq 2$) [8]. In former systems the composition and the crystal structure of the host alloys are well-defined and it is relatively easy to characterize the hydrogen sites and the local structure around the guest hydrogens. In addition, hydrogen can be absorbed or desorbed at relatively low temperatures, because the equilibrium pressure of these hydrides is in the range of several atom at room temperature (*ca.* ~ 2 atom at 40 °C for $LaNi_5$ alloy [4]). Therefore, these materials are much concerned with the industrial field. On the other hand, in the latter systems the composition of the host alloys can be changed appropriately and the structure of the host alloys is usually simple, i.e., body-centered-cubic (bcc), face-centered-cubic (fcc) or hexagonal-closed-packed (hcp). However, these disordered-alloy hydrides have not been studied extensively in comparison with the Laves phase, because high temperature and high pressure conditions are necessary to introduce hydrogen into the alloy and these conditions do not suit the industrial purposes.

Although the researches of the new host materials have advanced so quickly, the characters of the metal hydrides, i.e., the state of the hydrogen in the metals, the mechanism of the hydrogenation of the metal and the ability of the hydrogen absorption, have not been clarified yet. These points are necessary to understand the physical properties and the structures of the metal hydrides. In order to investigate the above basic characters the quantitative evaluation of the interaction among the metals and the hydrogens as well as the study of both crystal and electronic structures of the hydrides is necessary. One of the methods to evaluate the interaction among metals and hydrogens in the metal hydrides is to study the composition dependence of the thermodynamic quantities and the activation parameters for the hydrogen dynamics in the hydrides. In a lot of binary metal hydrides such as TiH_x and VH_x the structure and the physical properties such as the hydrogen dynamics and the enthalpy of solution of hydrogen in the host metal have been studied [2]. However, the lattice structure of almost all the member of the binary metal hydrides varies with the hydrogen contents. So, it is very difficult to evaluate quantitatively the interaction among the metals and hydrogens in the hydrides as a function of the hydrogen contents.

In ternary metal hydrides it is possible to change the composition of the metals consisting the alloy, leaving the hydrogen content constant. To evaluate the interaction quantitatively, the host alloy has to satisfy the following two conditions ; (1) The alloy assumes a well-defined monophase over the extended range of composition. (2) The metals consisting the alloy assume the clear difference from each other in the metal-hydrogen interaction. A typical material which satisfies these conditions is Ti-V alloy. Ti and V form stable alloy over arbitrary compositions as shown in Fig. 1.1 [9]. The crystal structure of the Ti-V alloy is bcc at room temperature, the lattice parameter of which varies nearly linearly with the alloy composition. The remarkable point in this system is that the Ti-V alloy is a disordered alloy, that is, it assumes always the disordered structure and any ordering with respect to the arrangements of the two metal species does not take place. It is noted that the hydrides of the individual metal, TiH_x and VH_x, are the most popular metal hydrides, for which a great number of investigations have been reported on the structures and the chemical and the physical properties in detail from both the macroscopic and the microscopic points of view [2]. These

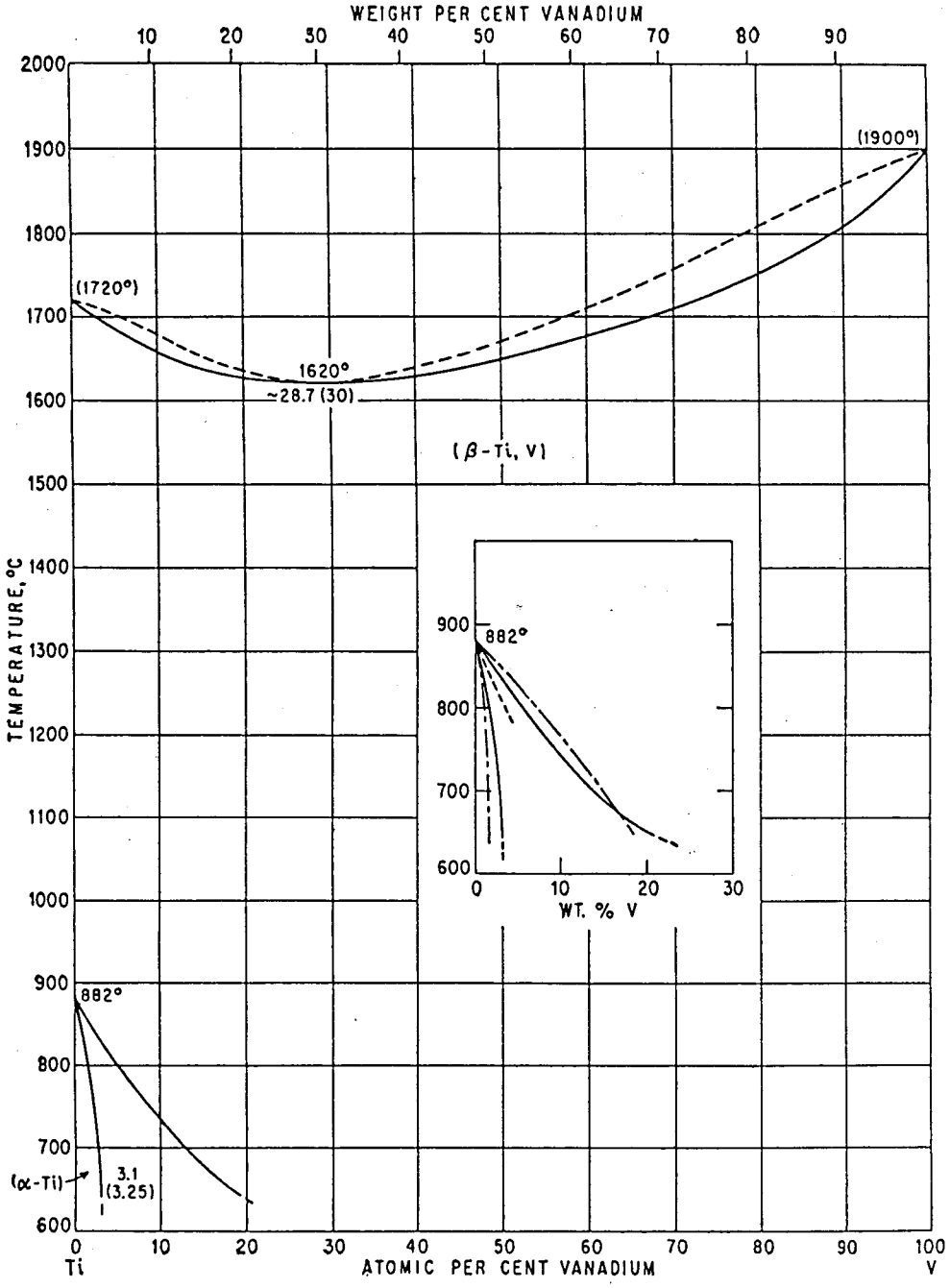

Figure 1.1 Phase diagram of Ti-V alloy [9].

metal hydrides show the clear difference from each other in the metal-hydrogen interaction and in the way of accommodation of hydrogen. The enthalpy of solution of hydrogen in Ti, which is one of the criteria for the affinity between the metal and the hydrogen, is -52.98 kJ/mol, whereas in V it is -31.98 kJ/mol at 573 K [10, 11]. Ti and V accommodate hydrogens in different sites from each other. Figure 1.2 describes fcc and bcc metal lattices and the types of the interstices in the lattices. In TiH_x the hydrogen atoms occupy only the tetrahedral (T-) sites, although the crystal structure varies as the hydrogen content varies. On the other hand, in VH_x the hydrogen atoms can occupy the octahedral (O-) sites as well as T-sites depending on the hydrogen content and the temperature. These differences between Ti-H and V-H systems can be recognized through the measurement of the isotope effect between the hydrides and the deuterides. The pure Ti has been known to show weak isotope effect; The phase transitions of $TiH_{1.99}$ and $TiD_{1.98}$ from tetragonal to cubic phase occur at almost the same temperatures (310 ± 4 K). In both phases the interstitial hydrogen atoms occupy the T-sites. On the other hand, the pure V has been known to show strong isotope effect; The hydride and the deuteride show different phase morphology from each other. The typical example is the phase relations of $VH_{0.5}$ and $VD_{0.5}$. These hydrides have a monoclinic structure called β-phase in which the interstitial atoms occupy the O-sites at low temperature. At high temperature the bcc structure called α-phase appears in which the interstitial atoms occupy the T-sites. There is an intermediate phase called ε-phase for the hydride $VH_{0.5}$, which is isomorphous with the β-phase but with different arrangement of hydrogen atoms, on the other hand no ε-phases exists in the deuteride. When the hydrogen and/or deuterium atoms are absorbed in an alloy consisting of Ti and V, it is expected that hydrogens behave in a different manner from those in the above two pure metal-hydrogen systems because the local metal-hydrogen and/or metal-deuterium interaction and the types of the interstitial sites accommodating the hydrogen atom in the alloy are considered to be significantly different from those in individual pure metal hydrides. Thus Ti-V alloy is one of the most suitable material for examining the interactions among the metals and hydrogens in the metal hydride.

Next, the characteristics of the hydride for Ti-V alloy are described. The alloy absorbs hydrogen up to 2 in the molar ratio of hydrogen to metal atoms [6]. The hydrides have three

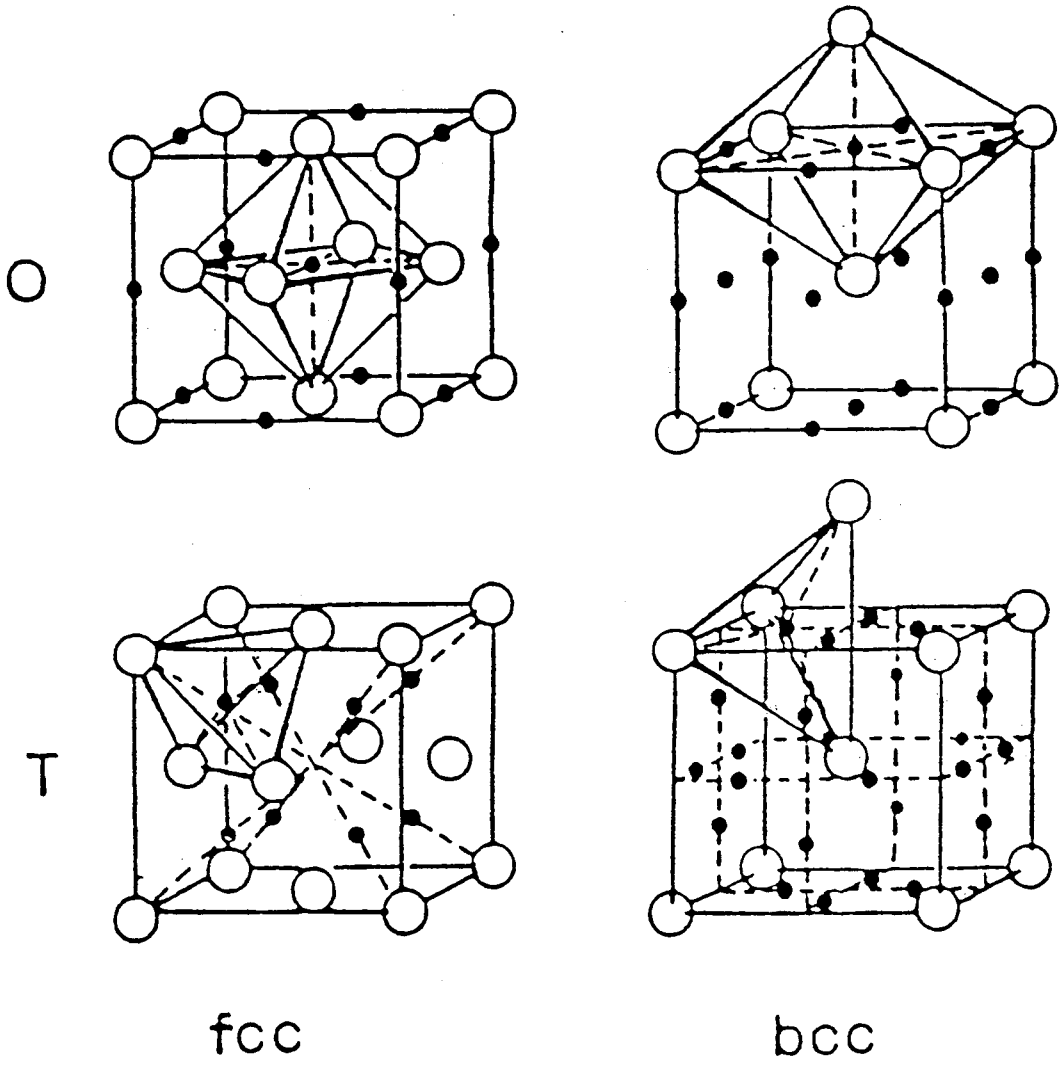

Figure 1.2 The types of interstitial sites in bcc and fcc host lattice.

different phases depending on the degree of hydrogenation. The relation between the hydrogen concentration and the three phases is described schematically as follows;

phase	α-phase	β-phase	γ-phase
host lattice	bcc	bcc, bct	fcc
H site	T-site	?	T-site

0 1 2

x / Hydrogen concentration

Hydride with very low hydrogen concentration (i.e. $x < 0.1$ in $Ti_{1-y}V_yH_x$) are called "α-phase" in which the metal atoms form a bcc lattice. The hydrogen diffusion in this phase was investigated by means of the resistivity measurement [12,13]. These studies revealed that the hydrogen is diffusing randomly over the tetrahedral sites (T-sites see in Figure 1.2), and the diffusion constant D varies from 10^{-6} at 40 °C to 10^{-4} cm^2/s at 200 °C. The pressure-composition isotherms were measured for the alloy composition from $Ti_{0.01}V_{0.99}$ to $Ti_{0.3}V_{0.7}$ and the standard enthalpy and entropy of solution of hydrogen were determined in the alloy [14]. The standard enthalpy varies from -31.7 kJ/molH to -43.5 kJ/molH and the standard entropy varies from -56.7 J/K molH to -47.5 J/K molH, as the alloy composition changes from $Ti_{0.01}V_{0.99}$ to $Ti_{0.3}V_{0.7}$. The composition dependence of the enthalpy of solution of hydrogen and the activation energy of hydrogen diffusion in the alloy were examined by Brouwer *et al.* [15]. They succeeded to explain the composition dependence of the enthalpy of solution of hydrogen and the activation energy of hydrogen diffusion in the alloy by means of a cluster model which takes account of microscopic inhomogeneity in the arrangement of Ti and V atoms. They applied this model to Ti-V-H system in which the hydrogen atoms are assumed to be distributed among the "T-sites" only. They determined the short-range order parameter which measure the degree of inhomogeneity in Ti-V alloy lattice. The short-range order parameter is one of the most important parameter to characterize the disordered and/or amorphous alloys.

The hydride with very high hydrogen to metal ratio (i.e. $x \sim 2$) is called "γ-phase" in which the metal atoms form a fcc lattice and the hydrogen atoms occupy the tetrahedral site (T-

site) fully [6]. Therefore, it is considered that the hydrogen can hardly diffuse in this phase at room temperature. The crystal and electronic structure of this phase have extensively been studied. Nowak *et al.* [16, 17] investigated the electronic structure of the γ-phase by means of the ^{1}H and ^{51}V NMR and stated that the increase of the vanadium composition in the alloy brings about the increase in the metallic character of this phase. Nagel and Perkins [6] investigated the crystal structure of this phase and the structural change associated with the addition of vanadium to the pure titanium hydrides. They found that the transition point (320 K) of the cubic-tetragonal structural phase transition in TiH_2 goes up by the partial substitution of Ti by V but it disappears at the composition of $Ti_{0.64}V_{0.35}H_2$. Switendick [18] performed one-electron energy band calculations on the electronic structure of $Ti_{1-y}V_yH_{2-x}$ system and gave a qualitative interpretation of the cubic-tetragonal structural phase transition in terms of its relation to the existence of degenerate state at the Fermi level.

At the intermediate region of hydrogen content between the α- and the γ-phases, the Ti-V alloy forms monohydride which is called β-phase. The existence of this phase was found for the first time by means of a measurement of the pressure-composition isotherm by Ono *et al.* [7] between 80 and 150 °C as shown in Fig. 1.3(a) and (b). They observed a plateau-like depression in the pressure-composition isotherms around H/M = 1.0 for $Ti_{0.2}V_{0.8}$ and $Ti_{0.4}V_{0.6}$. In this phase the metal atoms form a bcc lattice similar to the α-phase. This phase was obtained by dehydrogenation of the γ-phase under reduced pressure (< 1 atom) and above 400 °C. On the precipitation of the β-phase, it has been known that the dehydrogenation of the γ-phase brings about the phase separation of Ti-V-H system as follows [19, 20] ;

$$Ti_{1-n}V_nH_m = \alpha'\text{-}Ti_{1-x}V_xH_y + \beta\text{-}Ti_{1-x_1}V_{x_1}H_{y_1} + \gamma\text{-}Ti_{1-x_2}V_{x_2}H_{y_2} + \Gamma\text{-}TiH_{y_3} \quad ,$$

where the α'-phase has a hcp structure similar to the α-Ti phase containing a small amounts of V and H and appears only by dehydrogenation. Hayashi *et al.* [21] investigated the fraction of individual phase and the compositions in the dehydrogenated product using X-ray powder diffraction and ^{1}H and ^{51}V NMR. They found that the precipitation conditions depends on the treated temperature and the hydrogen pressure of hydrogenation. The ^{1}H and ^{51}V Knight shifts

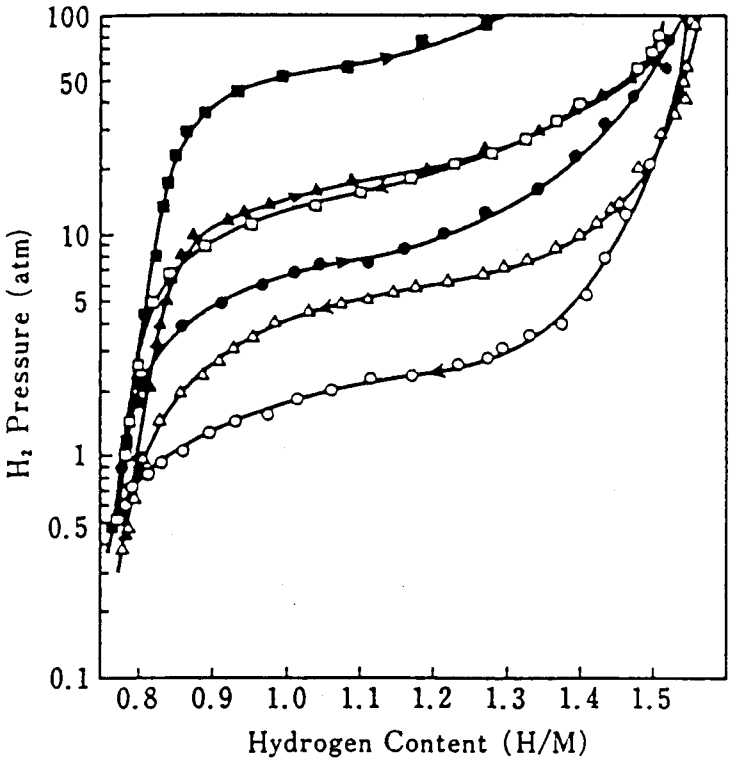

Figure 1.3(a) Pressure-composition isotherms for the $Ti_{0.2}V_{0.8}$-H_x system at 80 °C (○, ●), 100 °C (△, ▲) and 130 °C (□, ■). (from Ono *et al.* (1980) [7])

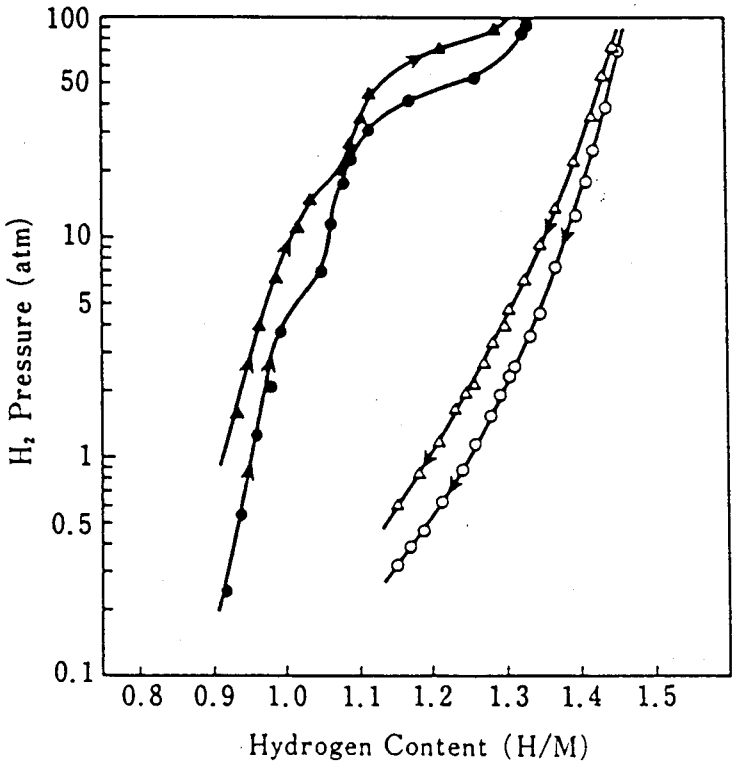

Figure 1.3(b) Pressure-composition isotherms for the $Ti_{0.4}V_{0.6}$-H_x system at 130 °C (△, ▲) and 150 °C (○, ●). (from Ono *et al.* (1980) [7])

Summary of ^{51}V NMR results

Sample	*β (or α) phase*			*γ phase*		
	K[a] (%)	*FWHM* (Oe)	*f*[b] (%)	*K*[a] (%)	*FWHM* (Oe)	*f*[b] (%)
B-5	0.598	ND[c]	10	0.038	60	90
B-15	0.609	27	100			
B-50	0.646	28	63	0.038	ND	37
C-5				0.008	62	100
C-15				0.002	47	100
C-50	0.636	ND	1	0.004	50	99
D-5	0.609	23	100			
D-15	0.693	ND	3	0.012	42	97
D-50	0.670	ND	5	0.010	47	95
B-5-1	0.580	22	100			
B-15-1	0.566	27	100			
B-50-1	0.539	26	100			
C-5-1	0.631	23	100			
C-15-1	0.629	24	100			
C-50-1	0.636	23	100			
D-15-1	0.670	22	100			
D-50-1	0.670	22	100			
B-5-0	0.478	25	100			
B-15-0	0.461	26	100			
B-50-0	0.461	26	100			
C-5-0	0.502	24	100			
C-15-0	0.482	29	100			
C-50-0	0.498	29	100			
D-5-0	0.514	27	100			
D-15-0	0.529	27	100			
D-50-0	0.523	25	100			

[a]Shift from $NaVO_3$ aqueous solution with the low field being positive.
[b]Fraction of this component.
[c]ND: not determined.

Summary of ^{1}H NMR results[a]

Sample	*Narrow component (β)*			*Broad component (γ)*			
	K (ppm)	*FWHM* (Oe)	*f* (%)	*K* (ppm)	M_2 (Oe^2)	M_4 (Oe^4)	*f* (%)
B-5	−65	2.0	8.6	−220	34	2800	91.4
B-15	−54	1.3	82	ND[b]	ND	ND	18
B-50	−65	1.8	19.7	−170	30	2500	80.3
C-5	−76	2.1	1.7	−210	40	3800	98.3
C-15	−87	2.2	1.0	−230	42	4200	99.0
C-50	−76	1.5	2.3	−230	43	4400	97.7
D-5	−42	1.5	100				
D-15	−54	1.4	6.1	−230	45	4800	93.9
D-50	−54	1.4	4.6	−220	45	4700	95.4
B-5-1	−54	1.2	100				
B-15-1	−54	1.3	100				
B-50-1	−65	2.2	19.4	−130	23	1300	80.6
C-5-1	−44	1.2	100				
C-15-1	−49	1.4	100				
C-50-1	−49	1.3	100				
D-15-1	−44	1.2	100				
D-50-1	−44	1.2	100				

[a]The following notations are used: K, shift from TMS, measured at 90.0 MHz; FWHM, full width at half maximum in the absorption spectra measured at 90.0 MHz; f, fraction of the component; M_2, second moment; M_4, fourth moment.
[b]ND: this value cannot be determined.

Table 1.1 Summary of ^{51}V (upper) and ^{1}H (lower) NMR results (from Hayashi et al. (1990) [21]). In the table, the samples are represented by the form *X-m-n*. *X*(= A, B, C and D) denote the [Ti]/[V] ratios which are 8/2 (A), 6/4 (B), 4/6 (C) and 2/8 (D). *m* represents the hydrogen pressure used to the hydrogenation of Ti-V alloy (*m* = 5, 15, and 50 atm). *n* represents the hydrogen content (*n* = 1, 0). The dihydrides are represented by *X-m*, whereas the monohydrides and the alloys with no hydrogen are represented by *X-m-1* and *X-m-0*, respectively.

in the β- and the γ-phases they determined are listed in Table 1.1. The ^{51}V Knight shift in the β-phase referred to $NaVO_3$ aqueous solution increases from 0.57 % to 0.75 % with increase in the V content from 0.4 to 1. In the γ-phase, the ^{1}H Knight shift was observed in the range between -130 and -230 ppm referring to TMS, whereas the ^{1}H Knight shift in the β-phase increases from -65 ppm to -44 ppm with increase in V content from 0.2 to 0.6. The difference in the ^{1}H Knight shift in between the β- and the γ-phases comes probably from higher electron density of hydrogen in the γ-phase than in the β-phase. They have also measured the ^{1}H spin-lattice relaxation time (T_1) for the β-phase to study the hydrogen dynamics and observed a T_1 minimum below room temperature for $Ti_{0.6}V_{0.4}H_{0.90}$, $Ti_{0.4}V_{0.6}H_{0.79}$ and $Ti_{0.2}V_{0.8}H_{0.77}$, but did not discussed the hydrogen dynamics in detail [22]. In the high temperature region between 620 K and 830 K, the hydrogen diffusion constants in $Ti_{0.92}V_{0.08}H_{0.41}$ and $Ti_{0.96}V_{0.04}H_x$ (x = 0.39, 0.54, 0.70) were measured by Sevilla and Cotts [23] using pulse-field-gradient technique of ^{1}H NMR and they discussed the hydrogen diffusion in comparison with that in β-TiH_x whose lattice is bcc.

In the β-phase, the property of hydrogen sites and the hydrogen dynamics below room temperature have not yet been clarified. Also, although qualitative discussions were done on the composition dependence of the activation energy for the hydrogen diffusion in the α-phase by a few researchers [15, 24], no systematic works have been done on the composition dependence of the physical properties of the various phases of $Ti_{1-y}V_yH(D)_x$ system. These informations are necessary to understand the dependence of the structural change on the hydrogen content. It is expected that the investigation of the hydrogen dynamics in various alloy compositions will provide one with the way for evaluating the interaction among Ti, V and H quantitatively.

The present study aims to investigate the structure of the β-form of Ti-V-H system and the dynamical behavior of hydrogen atoms in the alloy system by means of nuclear magnetic resonance and neutron inelastic scattering experiments: these experiments are done on the Ti-V-H and Ti-V-D systems with various Ti-V compositions. The analyses of the data will provide informations on the nature of the available interstitial sites for the hydrogen and the deuterium atoms and the dynamical behavior of the interstitial atoms in the β-phase of the $Ti_{1-y}V_yH(D)_x$.

In addition, the local framework structure of the β-phase will be discussed on the basis of the nature of the hydrogen dynamics. The final goal of this work is to evaluate the metal-hydrogen interaction and the short-range order parameter of the $Ti_{1-y}V_y$ alloy quantitatively and to discuss the static and dynamical structure of the β-phase of the $Ti_{1-y}V_yH(D)_x$ in comparison with those of the α- and γ-phases.

At first, the alloy composition dependence of the activation energy for the diffusion of interstitial atoms in the β-phase will be interpreted by introducing a local structural model with respect to the central interstitial atom in the $Ti_{1-y}V_yH(D)_x$. Thus, the cluster model introduced by Brouwer *et al.* [15] which apply only to the hydrogen T-sites formed by a cluster, $Ti_{4-i}V_i$, was extended to $Ti_{6-i}V_i$ clusters with seven configurations which provide guest hydrogen with both the T- and O-sites in Chapter 2. Chapter 3 describes the sample preparation and the characterization of the sample by means of X-ray power diffraction (XRD) and differential scanning calorimetry (DSC). The specific hydrogen sites in the $Ti_{1-y}V_yH_x$ were distinguished and characterized by means of the vibrational spectra obtained by the incoherent inelastic neutron scattering measurements, and the alloy composition dependence of the stability of the individual sites will be discussed in Chapter 4. The dynamics of the interstitial atoms in the $Ti_{1-y}V_yH(D)_x$ were investigated by measuring the spin-lattice relaxation times of ^1H and ^2H. The information on the strength of the metal-hydrogen and metal-deuterium interaction will be deduced from the alloy composition dependence of the experimental activation energy for the hydrogen diffusion, and the isotope effect of the interaction will be discussed in Chapter 5. ^2H NMR spectra were measured to study the deuterium dynamics in the $Ti_{1-y}V_yD_x$ (Chapter 6). On the basis of the results, the structural feature of the β-phase in the Ti-V-H(D) system will be discussed from the microscopic point of view in comparison with that of the α- and the γ-phases (Chapter 7).

References

[1] J. P.Blackledge, *Metal Hydrides. An Introduction to the Nature and Technology of Hydrides*, edited by W. M. Mueller, J. P. Blackledge and G. G. Libowitz, Academic Press, New York, 1968, pp. 1.

[2] R. L. Beck and W. M. Mueller, *Metal Hydrides. Zirconium Hydrides and Hafnium Hydrides*, edited by W. M. Mueller, J. P. Blackledge and G. G. Libowitz, Academic Press, New York, 1968, pp. 241; W. M. Mueller, *Metal Hydrides. Titanium Hydrides*, edited by W. M. Mueller, J. P. Blackledge and G. G. Libowitz, Academic Press, New York, 1968, pp. 336; T. Schober and H. Wenzl, *Hydrogen in Metals II. The Systems NBH(D), TaH(D), VH(D): Structures, Phase Diagrams, Morphologies, Methods of Preparation*, edited by G. Alfled and J. Völkl, Springer-Verlag, Berlin, 1978, pp. 11 and references cited therein.

[3] W. Bronger, *Angew. Chem. Int. Ed. Engl.*, **30**, 759(1991).

[4] B. S. Bowerman, C. A. Wulff, T. B. Flanagan, *Z. Phys. Chem.*, **116**, 197(1979); W. N. Hubbard, P. L. Rawlins, P. A. Connick, R. E. Stedwell, P. A. G. O'Hare, *J. Chem. Thermo.*, **13**, 785(1983).

[5] J. J. Reilly, R. H. Wiswall, *Inorg. Chem.*, **7**, 2254(1968); P. Zolliker, K. Yvon, J. D. Jorgensen, F. J. Rotella, *ibid.*, **25**, 3590(1986).

[6] H. Nagel and R. S. Perkins, *Z. Metallkd.*, **66**, 362(1975).

[7] S. Ono, K. Nomura and Y. Ikeda, *J. Less-Common Met.*, **72**, 159(1983).

[8] R. C. Brouwer, E. Salomons and R. Griessen, *Phys. Rev.* **B38**, 10217(1988).

[9] *Constitution of Binary Alloys, 2nd edition*, edited by M. Hansen and K. Anderko, McGraw-Hill, New York, 1958, pp. 1241.

[10] P. Dantzer, O. J. Kleppa and M. E. Melnichak, *J. Chem. Phys.*, **64**, 139(1976).

[11] O. J. Kleppa, P. Dantzer and M. E. Melnichak, *J. Chem. Phys.*, **61**, 4048(1974).

[12] D. J. Pine and R. M. Cotts, *Phys. Rev.* **B28**, 641(1983).

[13] S. Tanaka and H. Kimura, *Trans. Jpn. Inst. Met.*, **20**, 647(1979).

[14] D. T. Peterson and S. O. Nelson, *Metall. Trans.* **16A**, 367(1985).

[15] R.C. Brouwer, J. Rector, N. Koeman and R. Griessen, *Phys. Rev.* **B40**, 3546(1989).

[16] B. Nowak, M. Minier, *J. Less-Common Met.*, **101**, 245(1984).

[17] B. Nowak, Y. Chabre and R. Andreani, *J. Less-Common Met.*, **130**, 193(1987).

[18] A. C. Switendick, *J. Less-Common Met.*, **49**, 283(1976).

[19] S. Hayashi, K. Hayamizu and O. Yamamoto, *J. Less-Common Met.*, **113**, 1(1985).

[20] B. Nowak, S. Hayashi, K. Hayamizu amd O. Yamamoto, *J. Less-Common Met.*, **123**, 75(1986).

[21] S. Hayashi and K. Hayamizu, *J. Less-Common Met.*, **161**, 61(1990).

[22] S. Hayashi, K. Hayamizu and O. Yamamoto, *J. Chem. Phys.*, **78**, 5096(1983).

[23] E. H. Sevilla and R. M. Cotts, *Phys. Rev.* **B37**, 6813(1988).

[24] R. B. Mclellan and M. Yoshihara, *J. Phys. Chem. Solids*, **48**, 661(1987).

2 Model

2.1 The cluster model for disordered A-B alloy

Disordered binary A-B alloy which consists of well-defined crystal lattice and assume that every lattice point can be occupied by two kinds of metals A and B with equal probability. In other words there is no long range order with respect to the arrangement between A atoms and B atoms in the A-B alloy. However previous experiments pointed out that the sub-unit extract randomly from the ensemble of the A-B alloy will locally possess a certain order with respect to the arrangement of the metal atoms. Such a local order in the atomic arrangement is called a short-range ordering of metals. The degree of short-range order of metal atoms is one of the parameters characterizing the properties of the disordered A-B alloy. Short-range order parameter σ which represents the degree of short-range order of metal atoms have been determined by X-ray [1, 2] and neutron diffuse scattering [3]. The structural relaxation of the disordered and amorphous alloys is discussed through this parameter from the microscopic point of view. The structural relaxation of amorphous alloys which takes place during successive annealing below the crystallization temperature can be separated into the contributions of preferential topological relaxation and of preferential chemical relaxation. The former is interpreted by a topological long-range order of metal atoms associated with the annihilation of the free volume and with the diffusion of different species of metal atoms. The latter is caused by a chemical short-range order of metal atoms which depends on the atomic rearrangement [4]. In our model, we will also take account of the short-range order parameter to describe the local framework structure of metal atoms around a hydrogen atom.

For a random bcc alloy with interstitial atoms which occupy only the tetrahedral sites and with dilute hydrogen concentrations, Brouwer and co-workers proposed a cluster model with short-range ordering of metals to interpret their hydrogen diffusion data [5,6]. They considered $A_{4-i}B_i$ clusters as local structure around a hydrogen atom, and derived the formulation for the populations of sites $A_{4-i}B_i$ in an alloy with the composition $A_{1-y}B_y$ [6]. They applied their cluster model successfully to describing the composition dependence of the hydrogen diffusion coefficients and the activation energy in several disordered alloys with dilute hydrogen concentrations [7-10]. In addition, the short-range order parameter, which was

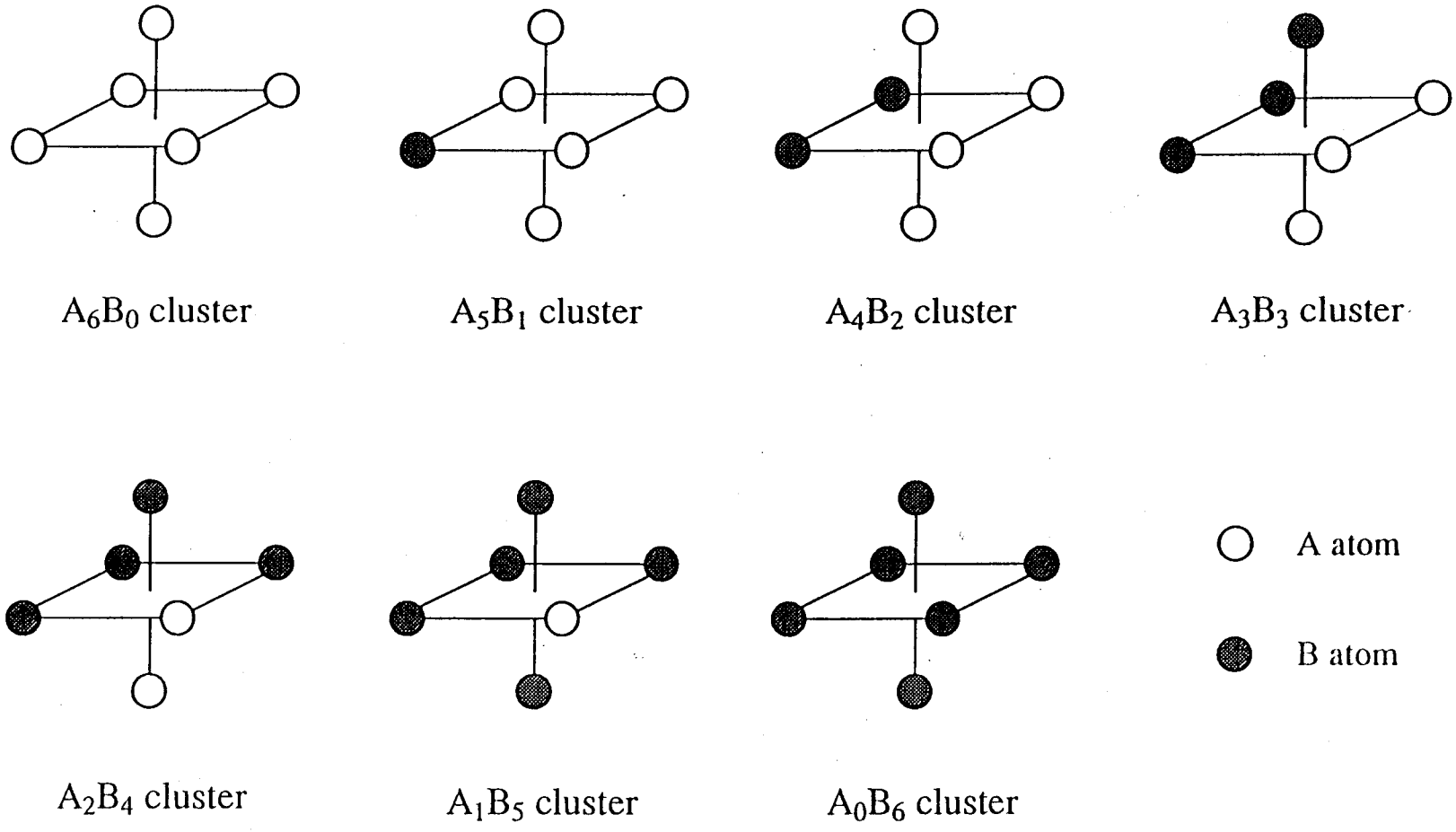

Figure 2.1 Model cluster, $A_{6-i}B_i$ (i = 0 ~ 6) in $A_{1-y}B_y$ alloy.

elucidated from the diffusion data by means of the cluster model, has known to agree well with those deduced by other methods such as X-ray diffuse scattering [1,2].

However, the application of their model is limited to the alloys with dilute interstitial atom concentrations, because their cluster model takes account of only tetrahedral site as the site symmetry of an interstice. In the metal hydrides with higher hydrogen concentrations there are some cases that hydrogen atoms are occupying octahedral sites as has been seen in VH_x [11]. The hydrogens in some systems are occupying both of T- and O-site simultaneously as seen in δ-phase of VH_x [11]. Especially, in our systems Ti-V-H, the hydrogen or deuterium atoms occupy both of tetrahedral and octahedral sites as will be described below. Therefore, it is necessary to incorporate both of T- and O-sites into the cluster model. In practice, we should adopt the cluster with the composition $A_{6-i}B_i$ as well as $A_{4-i}B_i$ cluster as the available site. Hence, the model consists of the octahedrons with seven different configurations as shown in Fig. 2.1. In the following section we will extend the Brouwer's formula to make it possible to calculate the population of $A_{6-i}B_i$ clusters and apply the formula to calculation of the activation energy for H(D) diffusion in disordered A-B alloy to analyze the alloy composition dependence of activation energy.

2.2 Extension of Brouwer's formula

For random distribution, the population of sites of a certain type $A_{6-i}B_i$ in the $A_{1-y}B_y$ alloy is given by the binomial distribution,

$$p(i) = \begin{bmatrix} 6 \\ i \end{bmatrix} (1 - y)^{6-i} y^i \, . \qquad (2.1)$$

In the cluster model proposed by Brouwer and co-workers[6] the inclination of the distribution of the populations is described by means of a short-range order parameter, σ. σ is zero the completely random distribution of metal atoms, and is defined by the following pair probabilities (with p_A = 1-y and p_B = y)[12,13] :

$$p_{AA} = p_A + (1 - p_A)\sigma , \tag{2.2a}$$

$$p_{AB} = p_B - p_B\sigma , \tag{2.2b}$$

where p_{AA} is the probability to find an A atom as the nearest neighbor of the first A atom and p_{AB} is the probability to find a B atom as the nearest neighbor of the first A atom. The pair probabilities are related to each other by

$$p_{AA} + p_{AB} = 1 , \tag{2.3a}$$

$$p_A p_{AB} - p_B p_{BA} = 0 . \tag{2.3b}$$

(Relations for p_{BA} and p_{BB} are obtained by exchanging A and B in the above equations.)

Statistically, the parameter σ represents the size of the ensemble consisting of both A and B atoms. As σ approaches zero, the size of the ensemble approaches the infinite value and the distribution becomes completely random. On the other hand, as absolute value of σ approaches 1 the size of the ensemble approaches zero and the distribution is not random. Physically, these situations represent the pass probability for the phase separation. That is, in the $A_{1-y}B_y$ alloy complete ordering occurs for $\sigma = -1$. The Phase separations of $A_{1-y}B_y$ alloy to the each metals occurs for $\sigma = 1$ and $A_{6-i}B_i$ clusters disappear.

Next we derive the equation for the population of sites of a certain type $A_{6-i}B_i$. In this cluster metal atoms form an octahedron and the resultant cluster has twelve interatomic bonds. So, the cluster model incorporates all twelve bonds in an octahedron. At first, consider an A_6 cluster. The probabilities to find the first and the second A atoms are simply p_A and $p_{AA}(\sigma)$ as represented by Eqs. (2.2), respectively. Consider a third A atom placed in the cluster. The probability for this third atom, $p_{AAA}(\sigma)$, must be at least $p_{AA}(\sigma)$ and at most 1. Modifying Eq. (2.2a) we get

$$p_{AAA} = p_{AA} + (1 - p_{AA})\sigma , \tag{2.4}$$

and the probabilities form the fourth to sixth A atom cluster are similarly derived as follows:

$$p_{AAAA} = p_{AAA} + (1 - p_{AAA})\sigma\,, \tag{2.5}$$

$$p_{AAAAA} = p_{AAAA} + (1 - p_{AAAA})\sigma\,, \tag{2.6}$$

$$p_{AAAAAA} = p_{AAAAA} + (1 - p_{AAAAA})\sigma\,. \tag{2.7}$$

So, each probability can be calculated from the p_A and p_B. As the result, the probability to find an A_6B_0 cluster in the alloy is given by

$$p(i=0, \sigma) = p_A p_{AA} p_{AAA} p_{AAAA} p_{AAAAA} p_{AAAAAA} \tag{2.8}$$

as the function of y and σ. Calculations for other clusters are possible with the analogous expressions described above. The clusters A_5B_1, A_4B_2 and A_3B_3, which represent $A_{6-i}B_i$ with i = 1, 2, and 3, respectively, have the populations derived as follow:

$$\begin{aligned} p(i=1, \sigma) = {} & p_A p_{AA} p_{AAA} p_{AAAA} p_{AAAAA} p_{AAAAAB} + p_A p_{AA} p_{AAA} p_{AAAA} p_{AAAAB} p_{AAAABA} \\ & + p_A p_{AA} p_{AAA} p_{AAAB} p_{AAABA} p_{AAABAA} + p_A p_{AA} p_{AAB} p_{AABA} p_{AABAA} p_{AABAAA} \\ & + p_A p_{AB} p_{ABA} p_{ABAA} p_{ABAAA} p_{ABAAAA} + p_B p_{BA} p_{BAA} p_{BAAA} p_{BAAAA} p_{BAAAAA}, \end{aligned} \tag{2.9}$$

$$\begin{aligned} p(i=2, \sigma) = {} & p_A p_{AA} p_{AAA} p_{AAAA} p_{AAAAB} p_{AAAABB} + p_A p_{AA} p_{AAA} p_{AAAB} p_{AAABA} p_{AAABAB} \\ & + p_A p_{AA} p_{AAB} p_{AABA} p_{AABAA} p_{AABAAB} + p_A p_{AB} p_{ABA} p_{ABAA} p_{ABAAA} p_{ABAAAB} \\ & + p_B p_{BA} p_{BAA} p_{BAAA} p_{BAAAA} p_{BAAAAB} + p_A p_{AA} p_{AAA} p_{AAAB} p_{AAABB} p_{AAABBA} \\ & + p_A p_{AA} p_{AAB} p_{AABA} p_{AABAB} p_{AABABA} + p_A p_{AB} p_{ABA} p_{ABAA} p_{ABAAB} p_{ABAABA} \\ & + p_B p_{BA} p_{BAA} p_{BAAA} p_{BAAAB} p_{BAAABA} + p_A p_{AA} p_{AAB} p_{AABB} p_{AABBA} p_{AABBAA} \\ & + p_A p_{AB} p_{ABA} p_{ABAB} p_{ABABA} p_{ABABAA} + p_B p_{BA} p_{BAA} p_{BAAB} p_{BAABA} p_{BAABAA} \end{aligned}$$

$$+ p_A p_{AB} p_{ABB} p_{ABBA} p_{ABBAA} p_{ABBAAA} + p_B p_{BA} p_{BAB} p_{BABA} p_{BABAA} p_{BABAAA}$$
$$+ p_B p_{BB} p_{BBA} p_{BBAA} p_{BBAAA} p_{BBAAAA}, \qquad (2.10)$$

$$p(i=2, \sigma) = p_A p_{AA} p_{AAA} p_{AAAB} p_{AAABB} p_{AAABBB} + p_A p_{AA} p_{AAB} p_{AABA} p_{AABAB} p_{AABABB}$$
$$+ p_A p_{AA} p_{AAB} p_{AABB} p_{AABBA} p_{AABBAB} + p_A p_{AA} p_{AAB} p_{AABB} p_{AABBB} p_{AABBBA}$$
$$+ p_A p_{AB} p_{ABA} p_{ABAA} p_{ABAAB} p_{ABAABB} + p_A p_{AB} p_{ABA} p_{ABAB} p_{ABABA} p_{ABABAB}$$
$$+ p_A p_{AB} p_{ABB} p_{ABBA} p_{ABBAA} p_{ABBAAB} + p_A p_{AB} p_{ABB} p_{ABBA} p_{ABBAB} p_{ABBABA}$$
$$+ p_A p_{AB} p_{ABB} p_{ABBB} p_{ABBBA} p_{ABBBAA} + p_A p_{AB} p_{ABA} p_{ABAB} p_{ABABB} p_{ABABBA}$$
$$+ p_B p_{BA} p_{BAA} p_{BAAA} p_{BAAAB} p_{BAAABB} + p_B p_{BA} p_{BAA} p_{BAAB} p_{BAABB} p_{BAABBA}$$
$$+ p_B p_{BA} p_{BAB} p_{BABB} p_{BABBA} p_{BABBAA} + p_B p_{BA} p_{BAA} p_{BAAB} p_{BAABA} p_{BAABAB}$$
$$+ p_B p_{BA} p_{BAB} p_{BABA} p_{BABAA} p_{BABAAB} + p_B p_{BA} p_{BAB} p_{BABA} p_{BABAB} p_{BABABA}$$
$$+ p_B p_{BB} p_{BBA} p_{BBAA} p_{BBAAA} p_{BBAAAB} + p_B p_{BB} p_{BBA} p_{BBAA} p_{BBAAB} p_{BBAABA}$$
$$+ p_B p_{BB} p_{BBA} p_{BBAB} p_{BBABA} p_{BBABAA} + p_B p_{BB} p_{BBB} p_{BBBA} p_{BBBAA} p_{BBBAAA},$$
$$(2.11)$$

[$p(i=4, \sigma)$, $p(i=5, \sigma)$ and $p(i=6, \sigma)$ are obtained from $p(i=2, \sigma)$, $p(i=1, \sigma)$ and $p(i=0, \sigma)$ by exchanging A and B]. In Eqs. (2.9)-(2.11), it is difficult to estimate all of probabilities composed of $p(i, \sigma)$ using p_A and p_B. Two assumptions are made to simplify the equations and to represent with using p_A and p_B [6]. At first, the probability p_{AAAAAB} corresponds to the chance to find a B atom next to five A atoms. This must be $p_{AAAAAB} = 1 - p_{AAAAAA}$, which represents the influence of five A atoms in an analogous way as for one A atom in p_{AB}. The another probabilities p_{AAAAB}, p_{AAAB} and p_{AAB} are represented by the analogous way in Eq. (2.3a). Second, in the case of finding an A atom next to B atom, for example, AAABAA, the influence of one A and one B atom cancel each other, therefore, $p_{AAABAA} = p_{AAAA}$. This assumption come from the fact that the B atom in the cluster increases the probability to find another B atom, whereas the A atom decreases it. Using these assumptions, Eqs. (2.9)-(2.11) are rewritten in the following forms,

$$p(i=1, \sigma) = p_A p_{AA} p_{AAA} p_{AAAA} p_{AAAAA} p_{AAAAAB} + p_A p_{AA} p_{AAA} p_{AAAA} p_{AAAAB} p_{AAAA}$$

$$+ p_A p_{AA} p_{AAA} p_{AAAB} p_{AAA} p_{AAAA} + p_A p_{AA} p_{AAB} p_{AA} p_{AAA} p_{AAAA}$$

$$+ p_A p_{AB} p_A p_{AA} p_{AAA} p_{AAAA} + p_B p_{BA} p_A p_{AA} p_{AAA} p_{AAAA}, \qquad (2.12)$$

$$p(i=2, \sigma) = p_A p_{AA} p_{AAA} p_{AAAA} p_{AAAAB} p_{AAAB} + p_A p_{AA} p_{AAA} p_{AAAB} p_{AAA} p_{AAAB}$$

$$+ p_A p_{AA} p_{AAB} p_{AA} p_{AAA} p_{AAAB} + p_A p_{AB} p_A p_{AA} p_{AAA} p_{AAAB}$$

$$+ p_B p_{BA} p_A p_{AA} p_{AAA} p_{AAAB} + p_A p_{AA} p_{AAA} p_{AAAB} p_{AAB} p_{AA}$$

$$+ p_A p_{AA} p_{AAB} p_{AA} p_{AAB} p_{AA} + p_A p_{AB} p_A p_{AA} p_{AAB} p_{AA}$$

$$+ p_B p_{BA} p_A p_{AA} p_{AAB} p_{AA} + p_A p_{AA} p_{AAB} p_{AB} p_A p_{AA}$$

$$+ p_A p_{AB} p_A p_{AB} p_A p_{AA} + p_B p_{BA} p_A p_{AB} p_A p_{AA}$$

$$+ p_A p_{AB} p_B p_{BA} p_A p_{AA} + p_B p_{BA} p_B p_{BA} p_A p_{AA}$$

$$+ p_B p_{BB} p_{BBA} p_{BA} p_A p_{AA}, \qquad (2.13)$$

$$p(i=2, \sigma) = p_A p_{AA} p_{AAA} p_{AAAB} p_{AAB} p_{AB} + p_A p_{AA} p_{AAB} p_{AA} p_{AAB} p_{AB}$$

$$+ p_A p_{AA} p_{AAB} p_{AB} p_A p_{AB} + p_A p_{AA} p_{AAB} p_{AB} p_B p_{BA}$$

$$+ p_A p_{AB} p_A p_{AA} p_{AAB} p_{AB} + p_A p_{AB} p_A p_{AB} p_A p_{AB}$$

$$+ p_A p_{AB} p_B p_{BA} p_A p_{AB} + p_A p_{AB} p_B p_{BA} p_B p_{BA}$$

$$+ p_A p_{AB} p_B p_{BB} p_{BBA} p_{BA} + p_A p_{AB} p_A p_{AB} p_B p_{BA}$$

$$+ p_B p_{BA} p_A p_{AA} p_{AAB} p_{AB} + p_B p_{BA} p_A p_{AB} p_B p_{BA}$$

$$+ p_B p_{BA} p_B p_{BB} p_{BBA} p_{BA} + p_B p_{BA} p_A p_{AB} p_A p_{AB}$$

$$+ p_B p_{BA} p_B p_{BA} p_A p_{AB} + p_B p_{BA} p_B p_{BA} p_B p_{BA}$$

$$+ p_B p_{BB} p_{BBA} p_{BA} p_A p_{AB} + p_B p_{BB} p_{BBA} p_{BA} p_B p_{BA}$$

$$+ p_B p_{BB} p_{BBA} p_{BB} p_{BBA} p_{BA} + p_B p_{BB} p_{BBB} p_{BBBA} p_{BBA} p_{BA}. \qquad (2.14)$$

These equations are used to calculate the populations of $A_{6-i}B_i$ cluster with short-range order between metals. To study the effect of σ on the populations of $A_{6-i}B_i$ cluster, the populations of $A_{6-i}B_i$ cluster are calculated for $A_{0.5}B_{0.5}$ alloy by using Eqs. (2.2)-(2.11) and are plotted as a function of σ in Fig. 2.2. In the figure the populations when $\sigma = 0$ correspond to the population of each cluster with binomial distributions. As $\sigma = 0$, the populations of A_5B_1, A_4B_2 and A_3B_3 clusters are relatively large and the population of A_6B_0 is very small. As σ

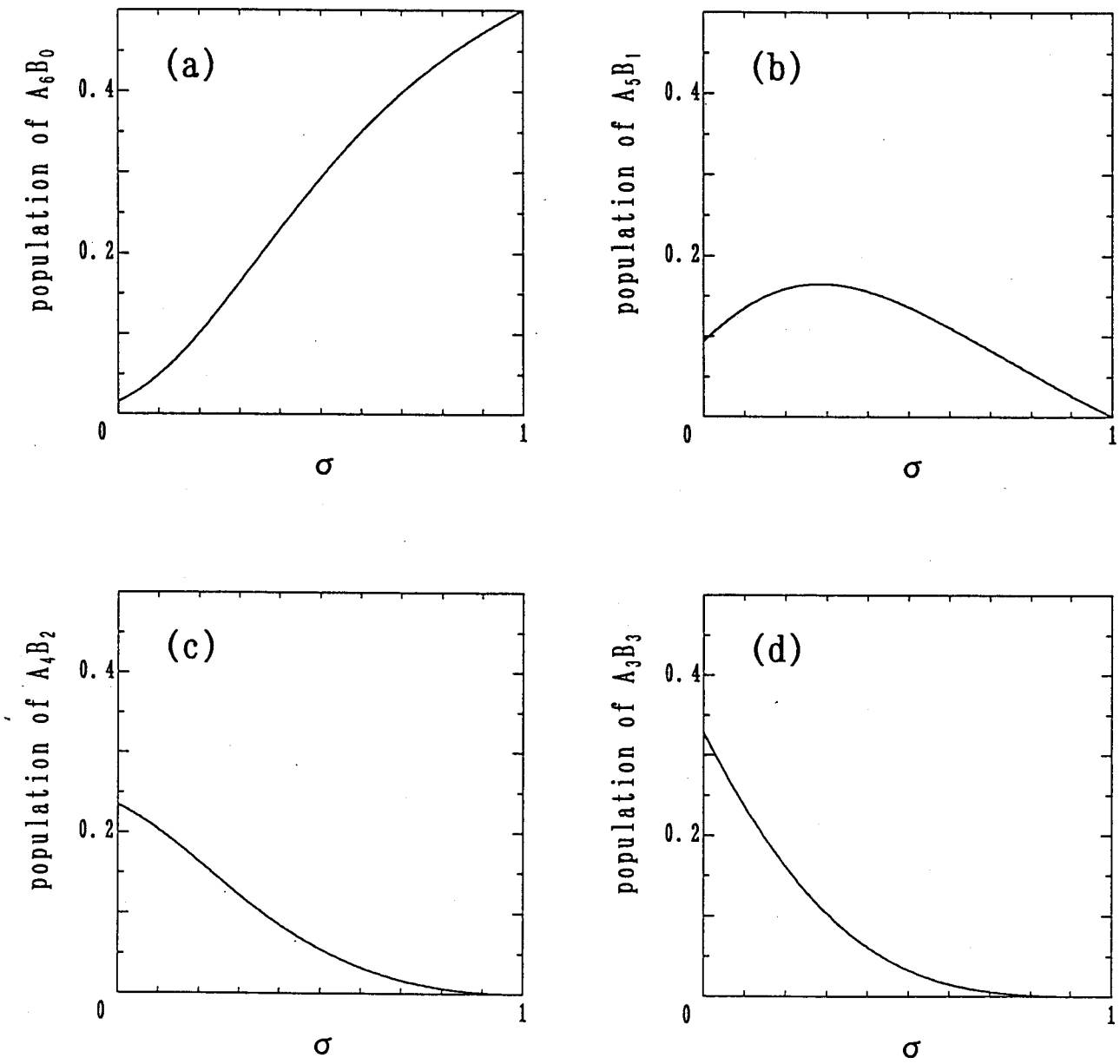

Figure 2.2 Simulations of populations of four kinds of $A_{6-i}B_i$ clusters using Eqs. (2.8) and (2.12) - (2.14) ; A_6B_0 cluster [i = 0] (a), A_5B_1 cluster [i = 1] (b), A_4B_2 cluster [i = 2] (c) and A_3B_3 cluster [i = 3] (d).

increases, the population of A_6B_0 cluster monotonically increases and reaches to 0.5 at $\sigma = 1$. On the other hand, the population of A_5B_1 cluster initially increases and decreases to zero after taking a maximum value at $\sigma = 0.3$, and the populations of A_4B_2 and A_3B_3 clusters monotonically decrease and reach 0 with increase in σ. These situations imply that the phase separation of $A_{0.5}B_{0.5}$ alloy to pure A and B metals occurs at $\sigma = 1$.

In the present work the above equations will be used to the analysis of the variation in the population of the hydrogen sites with alloy composition obtained by the neutron inelastic scattering experiments, and the analysis of the activation energy of the hydorgen and deuterium diffusion which are determined from nuclear spin-lattice relaxation times. As an example of the application of this model the composition dependence of activation energy for H(D) diffusion in A-B alloy is described as the function of alloy composition, y, and of the short-range order parameter, σ, in the next section.

2.3 Application of model to activation energy of diffusion in A-B alloy

In order to obtain the theoretical activation energy for H(D) diffusion in A-B alloy, we need the energy scheme describing stability of interstitial sites among the clusters. Consider a simple energy scheme as shown in Fig. 2.3. The interstitial atoms are hopping among the individual sites, the stability of which depends on the type of cluster which provides the corresponding sites. Each of clusters $A_{6-i}B_i$ has its characteristic site energy, $\Delta\overline{H}_i(y)$, specified by the subscript i. The site energy is defined as the energy which is necessary to excite the interstitial atom in a cluster to infinite point. Now an interstitial atom moves form an initial site (type j) to the nearest neighbor site (type k). Then, the interstitial atom passes through the saddle point located between the two sites. This saddle point energy is denoted by Q as shown in the figure. In general, the saddle point energy is correlated with the site energy: if the site energy decreases, the saddle point energy is also lowered [1]. However, in this model, the saddle point energy is the same for all of interstitial sites in different clusters due to the simplification of the treatment. Hence the activation energy $E_{a(jk)}$ for hopping from the site j to the site k corresponds to the difference between the site energy $\Delta\overline{H}_j(y)$ and the saddle point

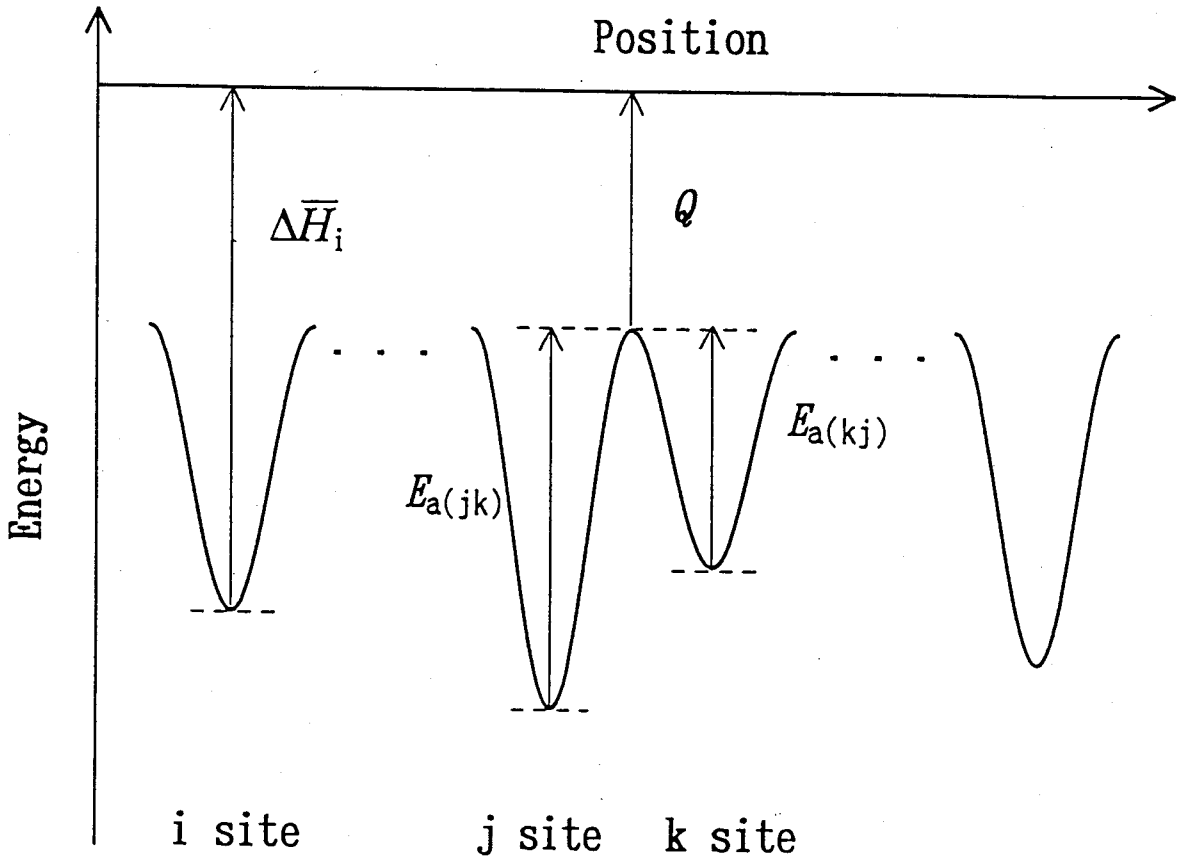

Figure 2.3 Schematic representation of site energies $\Delta\overline{H}_i(y)$ and saddle point energy Q depending on the kinds of clusters.

energy Q. The activation energy $E_{a(jk)}$ for hopping from the site j to the site k is different from $E_{a(kj)}$ for hopping from the k to j sites, and each of activation energies are characterized by only the site energy $\Delta\overline{H}_j(y)$ and $\Delta\overline{H}_k(y)$. The total activation energy E_a will be derived as the mean value of activation energies for the individual sites. In other words the total activation energy E_a will be represented by the difference between the average values of the individual site energies $\Delta\overline{H}_i(y)$ and the saddle point energy Q [6]. It is necessary to calculate the population c_i of interstitial atoms in the clusters $A_{6-i}B_i$ using the average value of the site energies $\Delta\overline{H}_i(y)$. Assuming that the long-range interstitial-interstitial interaction can be ignored and taking into acount the metal-interstitial interaction, the population is given as a function of y and σ by Fermi-Dirac distribution using the population of $A_{6-i}B_i$ sites, $p(i, \sigma)$, as follows [5, 6, 14]:

$$c_i(y, \sigma) = \frac{p(i, \sigma)}{s_i + \exp\{[\Delta\overline{H}_i(y) - \mu]/RT\}}, \qquad (2.15)$$

where μ is the chemical potential of the system, and s_i is called selective-blocking factor originated from the blocking effect of the repulsive interactions between the interstitial atom occupying a site and a new atom which want to enter a nearest neighbor empty site. For hydrogen atoms in a bcc lattice of host metals, good agreement between the experimental and the theoretical entropies has been obtained by taking a constant value $s_i = 4$ for the blocking factor. Also, the analytical treatment for blocking factor were made by Boureau,[15] and the value ($s_i = 4$) was deduced for high hydrogen concentrations. Hence, we assume that $s_i = 4$. Using $c_i(y, \sigma)$, $p(i, \sigma)$ and s_i the average site energy (enthalpy of formation) is represented by [12]

$$\Delta\overline{H}(y, \sigma) = \frac{\sum_i \Delta\overline{H}_i(y) c_i(y, \sigma)\left[1 - \frac{s_i}{p(y, \sigma)} c_i(y, \sigma)\right]}{\sum_i c_i(y, \sigma)\left[1 - \frac{s_i}{p(y, \sigma)} c_i(y, \sigma)\right]}. \qquad (2.16)$$

So the activation energy for H(D) diffusion, defined by the difference between $\Delta\overline{H}(y, \sigma)$ and Q as described above, is given by

$$E_a(y, \sigma) = Q - \Delta\overline{H}(y, \sigma) . \qquad (2.17)$$

The analysis of alloy composition (y) dependence of E_a with Eq. (2.17) gives a short-range order parameter for host metals. Also, equation (2.16) can be applied to the analysis of the experimental thermodynamic quantities such as enthalpy and entropy of formation [6].

References

[1] P. S. Rudman, *Acta Metall.*, **12**, 1381(1964).

[2] D. T. Peterson and S. O. Nelson, *Metall. Trans.*, **16A**, 367(1985).

[3] H. Roelofs, B. Schönfeld, G. Kostorz and W. Bührer, *Phys. stat. sol.*, (b)**187**, 31(1995).

[4] B. Porscha and H. Neuhäuser, *Phys. stat. sol.*, (b)**186**, 119(1994).

[5] R.C. Brouwer, E. Salomons and R. Griessen, *Phys. Rev.* **B38**, 10217(1988).

[6] R.C. Brouwer, J. Rector, N. Koeman and R. Griessen, *Phys. Rev.* **B40**, 3546(1989).

[7] S. Tanaka, H. Kimura, *Trans. Jpn. Inst. Met.*, **20**, 647(1979).

[8] D. T. Peterson and H. M. Herro, *Metall. Trans.*, **18A**, 249(1987).

[9] D. J. Pine and R. M. Cotts, *Phys. Rev.* **B28**, 641(1983).

[10] T. Eguchi and S. Morozumi, *J. Jpn. Inst. Met.*, **41**, 795(1977).

[11] T. Schober and H. Wenzl, *in Hydrogen in Metals II. The Systems NbH(D), TaH(D), VH(D): Structures, Phase Diagrams, Morphologies, Methods of Preparation*, edited by G. Alfled and J. Völkl, Springer-Verlag, Berlin, 1978, pp. 11.

[12] R. Griessen, *in Hydrogen in Disordered and Amorphous Solids*, edited by G. Bambakidis and R. C. Bowman (Plenum, New York, 1986), pp. 153-172.

[13] D. Nguyen Manh, D. Mayou, A. Pasturel and F. Cyrot-Lackman, *J. Phys.*, **F15**, 1911(1985).

[14] R. Kirchheim, *Acta Metall.*, **30**, 1069(1982).

[15] G. Boureau, *J. Phys. Chem. Solids*, **42**, 743(1981).

3. Sample

3.1 Preparations

Titanium powder (purity 99.9 %, -100 mesh) and vanadium powder (99.9%, -50 mesh) were purchased from Soekawa Chemical Co., Ltd. and High Purity Chemicals Co., Ltd., respectively. Binary alloys $Ti_{1-y}V_y$ were prepared by arc-melting of the mixture of Ti and V powders with the appropriate molar ratios under an argon atmosphere. The five samples of $Ti_{1-y}V_y$ alloy with y (V content) = 0.2, 0.4, 0.6, 0.8 and 0.9 were used to synthesis of the hydrides and deuterides.

The alloy buttons were cut to some small blocks with diamond cutter. After washing of the blocks with acetone the alloys were hydrogenated. In the case of the dihydride and dideuteride of $Ti_{0.8}V_{0.2}$ the alloy was degassed for 3 hr at 700 °C, hydrogenated by contacting with H_2 or D_2 gas of the pressure less than 1 atom at 700 °C and cooled slowly down to room temperature. For another alloys the syntheses of the dihydrides and dideuterides were carried out under higher pressure. The alloys in a stainless-steel pressure bottle with the volume of 300 ml were degassed at 500 °C for 3hr. The H_2 or D_2 gas was brought into the bottle and its pressure was kept at 50 atom. The bottle was then taken out from the furnace and cooled down to room temperature. The H_2 or D_2 gas was absorbed by the alloys in the above procedure and the final pressure in the bottle was reduced to less than 3 atom. The dihydrides and dideuterides thus synthesized were crushed into fine powders (less than -200 mesh) by the stainless-steel mill and the agate mortar.

The monohydrides and monodeuterides were prepared by partial dehydrogenation of the dihydrides or dideuterides by heating under reduced pressures. The hydrogen and/or deuterium content in each of hydrides and deuterides was determined up to ± 1 % by volumetric method which measure the volume of the H_2 or D_2 gas evolved at a high temperature (800 °C). The compositions of the systems prepared in the present study is listed in Table 3.1.

3.2 X-ray powder diffraction (XRD)

X-ray powder diffraction patterns were measured using Rigaku Electronic Co. RAX01 X-ray diffractometer at room temperature over the range of the reflection angle, $30° \leq 2\theta \leq 90°$.

The mean X-ray wavelength was 1.5404 Å (the mean value of Cu $K\alpha 1$ and $K\alpha 2$). The voltage and the current through the x-ray filament were 40 kV and 30 mA, respectively.

Figures 3.1 and 3.2 show the x-ray powder diffraction (XRD) patterns of β-$Ti_{1-y}V_yH_x$ and β-$Ti_{1-y}V_yD_x$ at room temperature. All XRD patterns consist of a typical bcc reflections which are superimposed by the reflections due to small amount of γ-phase (fcc) or γ-Ti (hcp). The hydries contain larger amount of undesired γ-modifications than the deuterides. $Ti_{0.8}V_{0.2}H_{0.73}$ contains the largest amount of γ-phase. The amount of γ-phase in the hydrides was estimated to be less than 10 % from the ratio of the (110) reflection for bcc to the (111) for fcc by taking account of the multiplicity and structure factor for each reflection. $Ti_{0.2}V_{0.8}H_{0.86}$ contains similar amounts of γ-Ti and the alloy γ-phase. The amount of γ-phases coexisting with the γ-deuterides were undetectable and so it was estimated to be less than 1 %. The reflections are significantly broad in these alloy systems. This suggests that the crystalline lattices are not ideal and the lattice constants are distributed to some extent in the disordered Ti-V-H(D) alloys. In both hydrides and deuterides, the (110) reflection locates in the range $37° < 2\theta < 41°$ and shifts linearly to higher angle direction as the V content increases. The mean lattice constant of each bcc lattice was determined from the 2θ value of (110) reflection and listed in Table 3.1. The lattice constants increase linearly with the increase in the Ti content. On the other hand, the lattice constant is almost independent of hydrogen isotope. Other hydrides prepared in the present study were also examined by XRD. Figure 3.3 shows the XRD patterns of these systems. Three hydrides with y = 0.8, 0.6, and 0.4 were confirmed to belong to the bcc lattice. XRD indicates that the hydride, $Ti_{0.4}V_{0.6}H_{0.92}$, is a monophase but the hydrides, $Ti_{0.8}V_{0.2}H_{0.94}$ and $Ti_{0.1}V_{0.9}H_{0.98}$, are mixture of the β- and γ-phases. The amount of γ-phase in the specimen was estimated to be about 20 % for both of $Ti_{0.8}V_{0.2}H_{0.94}$ and $Ti_{0.1}V_{0.9}H_{0.98}$ from the intensity ratio between (110) reflection for bcc and (111) reflection for fcc lattices. $Ti_{0.1}V_{0.9}H_{0.98}$ (Fig. 3.3d) has a body-centered tetragonal (bct) lattice [1] as in the case of pure metal hydride, β-VH_x [2].

Table 3.1 Lattice constants and transition points for β-$Ti_{1-y}V_yH_x$ and β-$Ti_{1-y}V_yD_x$

composition	lattice constant (nm)	transition point[1] (K)
$Ti_{0.2}V_{0.8}H_{0.86}$	0.320±0.002	------
$Ti_{0.2}V_{0.8}H_{0.83}$	0.321±0.002	------
$Ti_{0.2}V_{0.8}D_{0.79}$	0.319±0.003	192, 255
$Ti_{0.4}V_{0.6}H_{0.86}$	0.323±0.002	------
$Ti_{0.4}V_{0.6}H_{0.91}$	0.326±0.002	------
$Ti_{0.4}V_{0.6}D_{0.80}$	0.325±0.003	------
$Ti_{0.6}V_{0.4}H_{1.1}$	0.329±0.002	------
$Ti_{0.6}V_{0.4}H_{0.91}$	0.330±0.002	------
$Ti_{0.6}V_{0.4}D_{0.86}$	0.329±0.003	254
$Ti_{0.8}V_{0.2}H_{0.73}$	0.333±0.002	------
$Ti_{0.8}V_{0.2}H_{0.89}$	0.333±0.002	------
$Ti_{0.8}V_{0.2}D_{0.79}$	0.334±0.001	251

1) These phase transition points are determined by DSC measurements.

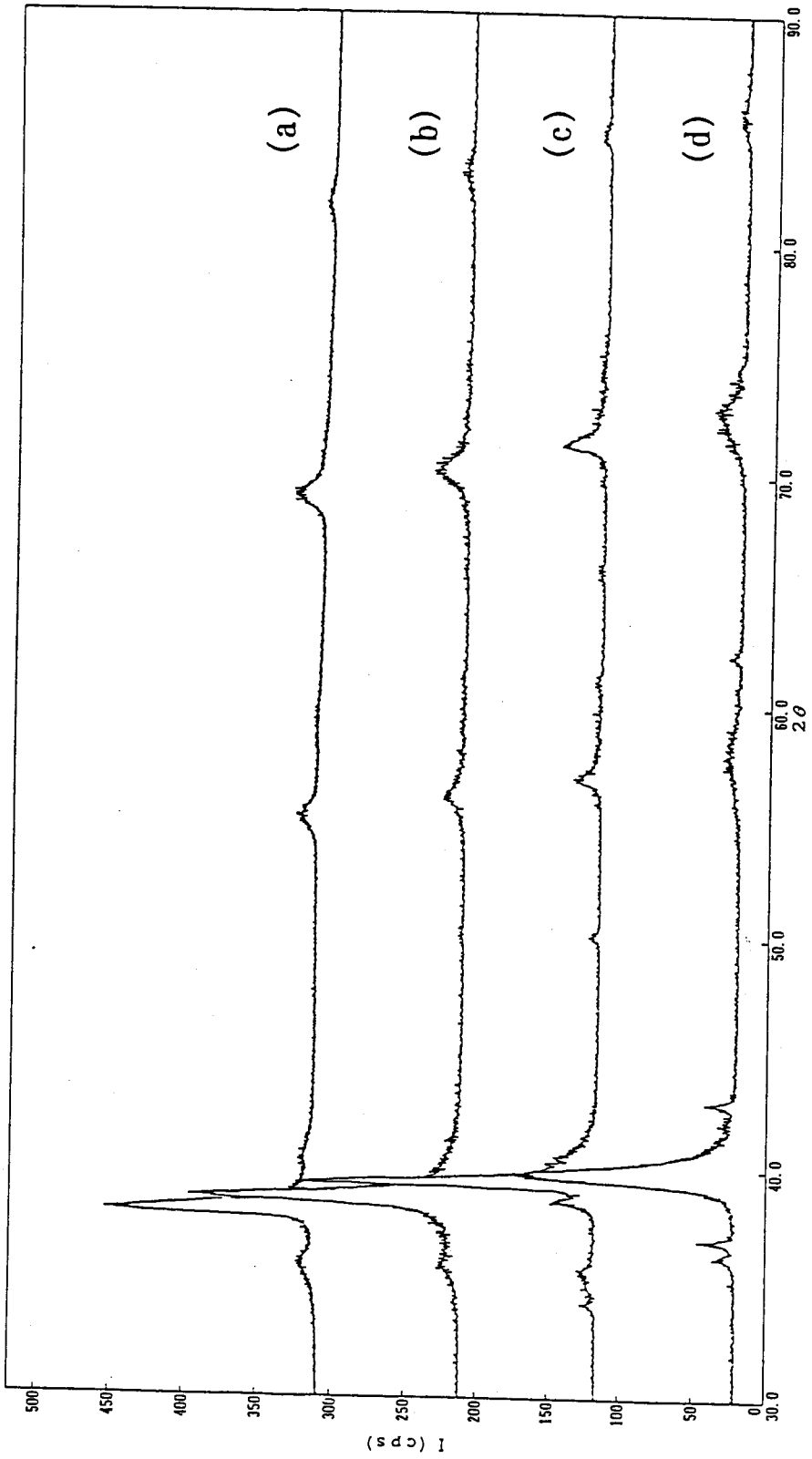

Figure 3.1 X-ray powder diffraction patterns of β-$Ti_{1-y}V_yH_x$ at room temperature; $Ti_{0.8}V_{0.2}H_{0.73}$ (a), $Ti_{0.6}V_{0.4}H_{1.1}$ (b), $Ti_{0.4}V_{0.6}H_{0.86}$ (c) and $Ti_{0.2}V_{0.8}H_{0.86}$ (d).

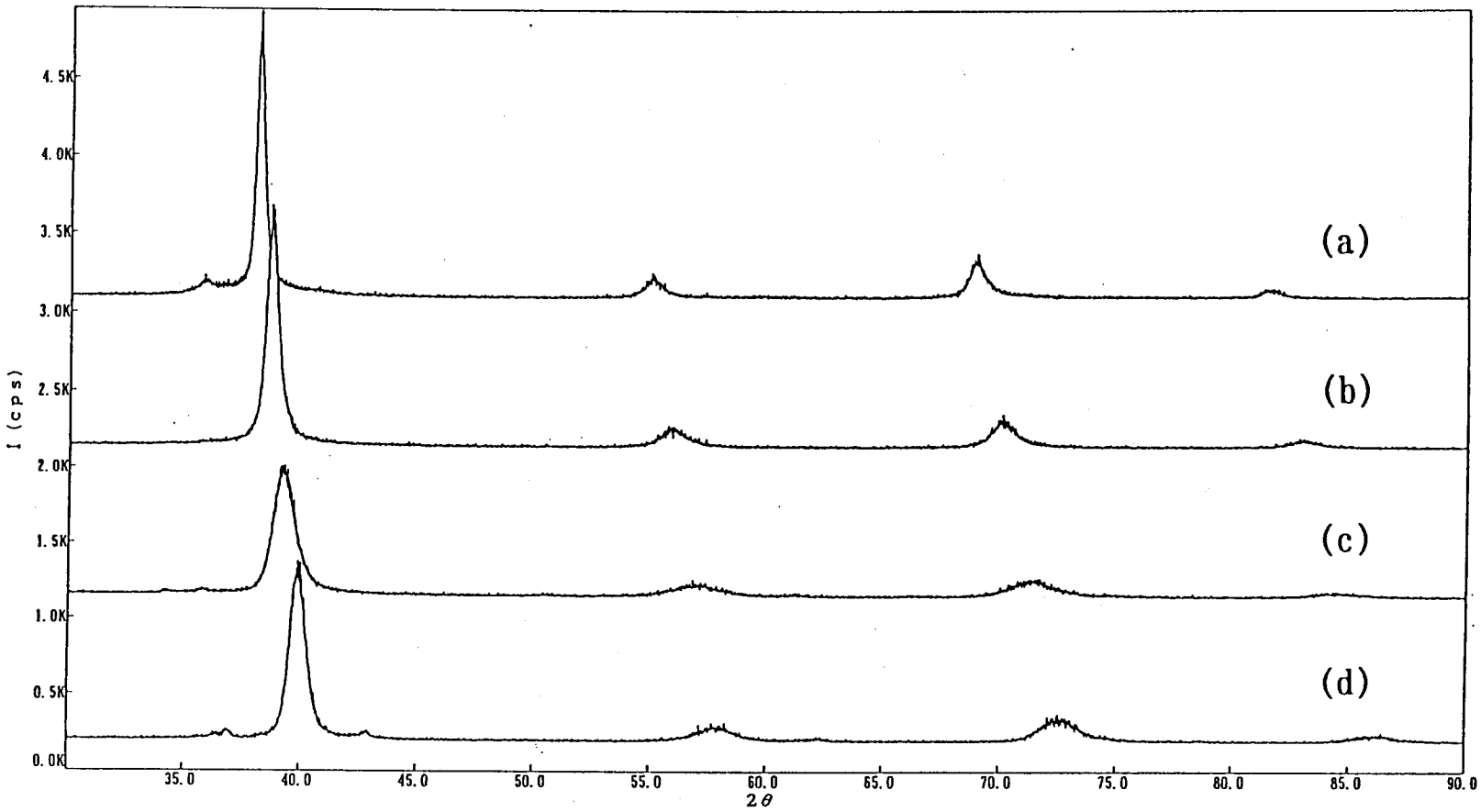

Figure 3.2 X-ray powder diffraction patterns of β-$Ti_{1-y}V_yD_x$ at room temperature; $Ti_{0.8}V_{0.2}D_{0.79}$ (a), $Ti_{0.6}V_{0.4}D_{0.86}$ (b), $Ti_{0.4}V_{0.6}D_{0.80}$ (c) and $Ti_{0.2}V_{0.8}D_{0.79}$ (d).

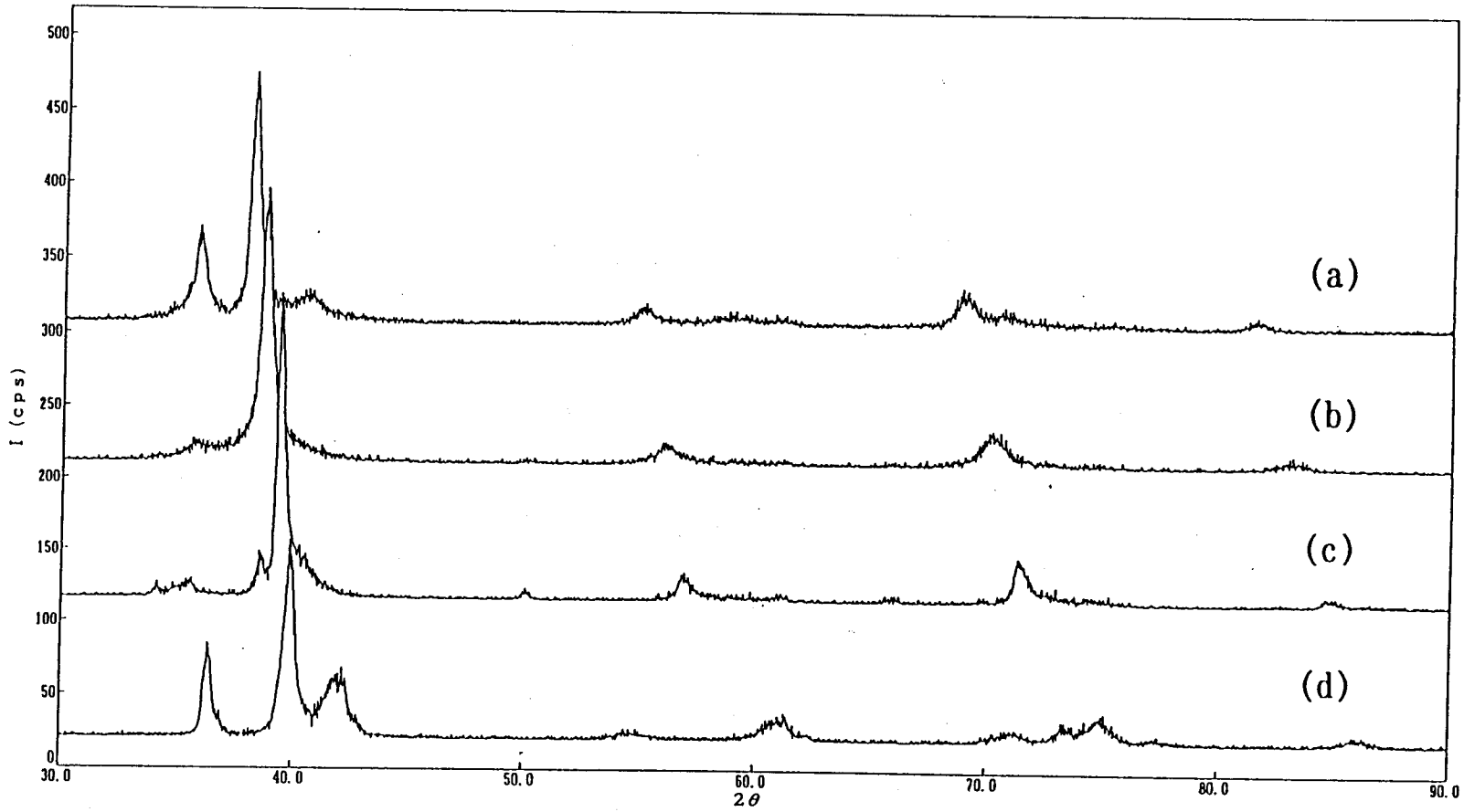

Figure 3.3 X-ray powder diffraction patterns of β-$Ti_{1-y}V_yH_x$ at room temperature; $Ti_{0.8}V_{0.2}H_{0.94}$ (a), $Ti_{0.6}V_{0.4}H_{1.1}$ (b), $Ti_{0.4}V_{0.6}H_{0.92}$ (c) and $Ti_{0.1}V_{0.9}H_{0.98}$ (d).

3.3 Differential scanning calorimetry (DSC)

Differential scanning calorimetry (DSC) were carried out with Rigaku Electronic Co. Model TAS 100 - DSC 8230 over the temperature range between 120 K and 360 K. The heating rate was 10 K/min.

For β-$Ti_{1-y}V_yH_x$ there was no thermal anormaly but endothermic peaks were observed below room temperature in β-$Ti_{1-y}V_yD_x$ except in $Ti_{0.4}V_{0.6}D_{0.80}$. $Ti_{0.2}V_{0.8}D_{0.79}$ gave two thermal anormalies at 192 K and 255 K. The former transition had a peak maximum at 220 K and was accompanied by relatively large enthalpy change. The latter had a peak maximum at 260 K and was accompanied by a small enthalpy of transition. $Ti_{0.8}V_{0.2}D_{0.79}$ gave a thermal anormaly at 251 K and its peak maximum was 283 K. $Ti_{0.6}V_{0.4}D_{0.86}$ gave a small endothermic peak at 254 K. These thermal anormalies reproduced at the second run of the DSC measurements. Therefore, the thermal anormalies observed were caused by second order structural phase transitions or the phase separations. Although the crystal structure at the room temperature which is the high temperature phase is bcc as described above, the characteristices such as the crystal structure for the low temperature phases have not been known yet. We will discuss this point in a later section. The transition points observed by DSC were listed in Table 3.1 with the lattice constants.

References

[1] S. Ono, K. Nomura and Y. Ikeda, *J. Less-Common Met.*, **72**, 159(1983).

[2] T. Schober and H. Wenzl, *in Hydrogen in Metals II. The Systems NbH(D), TaH(D), VH(D): Structures, Phase Diagrams, Morphologies, Methods of Preparation*, edited by G. Alfled and J. Völkl, Springer-Verlag, Berlin, 1978, pp. 11.

4. Incoherent inelastic neutron scattering

4.1 Introduction

Incoherent Neutron Inelastic Scattering (INIS) measurements have been applied extensively to some metal hydrides to study the location sites and the dynamics of hydrogens in the metallic lattice [1-7]. Energy transfer corresponding to the local vibrational modes of hydrogen in metal hydrides is observed in the INIS spectra. The excitation energy of the local vibration of a hydrogen atom, ΔE, is described by the following equation [6]:

$$\Delta E(\mathrm{lmn}) = E(\mathrm{lmn}) - E(000),$$

where E(lmn) is the perturbed energy of the vibrational level specified by the vibrational quantum numbers l, m and n corresponding to the three degrees of freedom. The E(lmn) local vibrational frequencies of the hydrogen atoms reflect the feature of potential well in which the hydrogen locates. The shape of the potential well depends on the chemical and topological environment around the hydrogen atom (i.e., crystal symmetry, the size of the space which the hydrogen occupies, degree of lattice distortion and the kinds of host metals). Especially, the potential energy function and the vibrational energy level scheme for the hydrogen are mainly governed by the symmetry of the hydrogen site when the metallic species are unchanged. Therefore, the vibrational spectra of the metal hydrides are used to discuss the hydrogen site symmetry through the local vibrational modes corresponding to the first excitation which are observed at the lowest energy range and have the largest intensity than those of the higher excitation. In addition, if the higher excitation such as the second, third and fourth harmonics are observed in the vibrational spectra, it is possible to discuss the shape of the hydrogen potential in the hydrides. For example, the TiH_2 and $VH_{0.33}$, which are well-known metal hydrides, have been studied in detail by INIS [6]. The TiH_2 has a fcc lattice, in which the hydrogen atom occupy the tetrahedral site (T-site). The local vibrational modes of hydrogen atom in TiH_2 are triply degenerated and $\hbar\omega$ = 147.6 meV at 300 K. The vibrational excitations are observed at 147.6 meV (first), 285 meV (second), 420 meV (thrid), 540 meV (fourth), and 670 meV (fifth harmonics). The hydrogen potential is approximately described by a harmonic potential as shown in Fig. 4.1(a). On the other hand, the $VH_{0.33}$ has a body-centered-tetragonal (bct) lattice, in which the hydrogen atom occupies (0,0,c/2) and its equivalent lattice

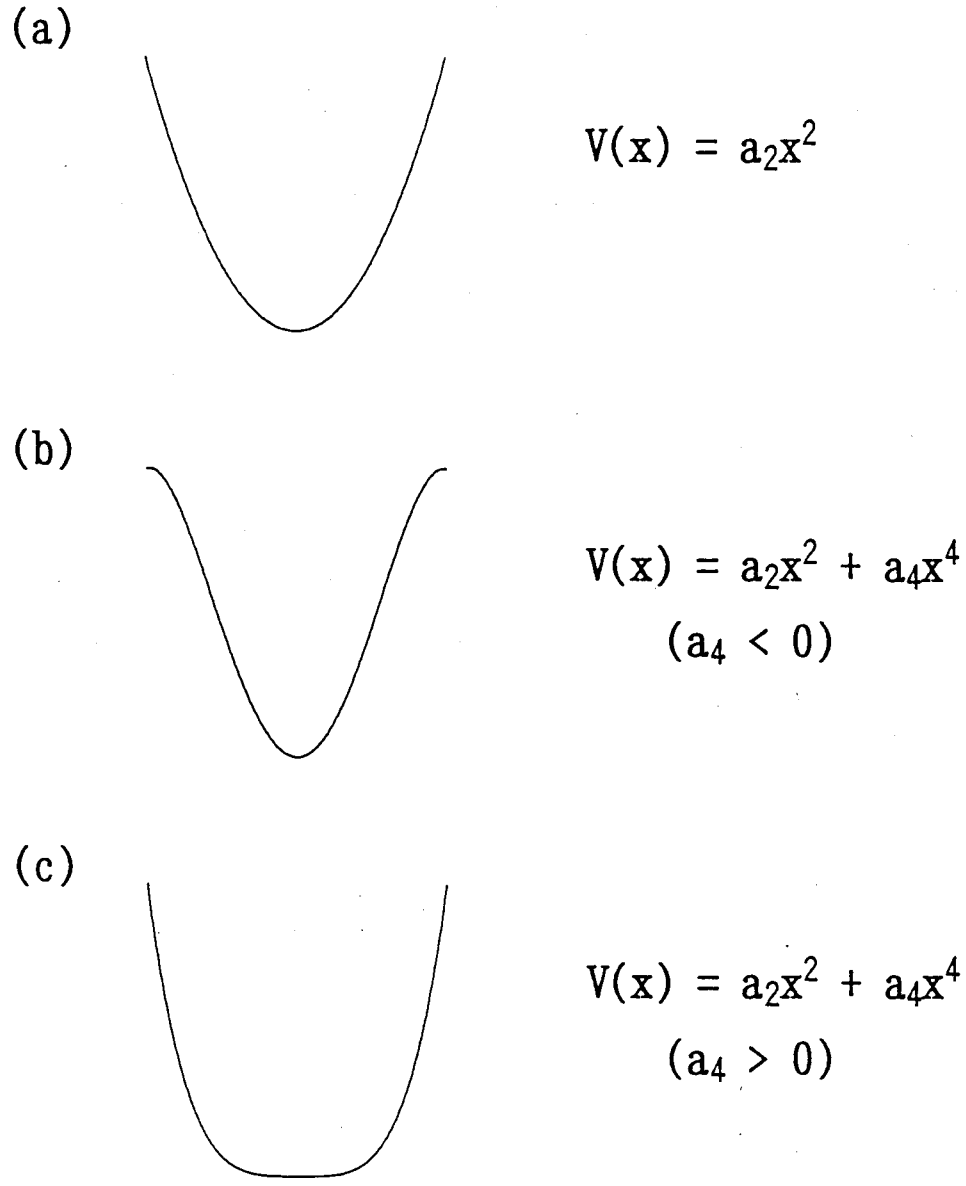

Figure 4.1 Three types of hydrogen potential: (a) Harmonic potential, (b) trumpet like potential and (c) well like potential.

points called O_Z-site. The degeneracy of the local vibrational modes is removed in this hydride, and the doubly degenerate in-plane modes are observed at 50 and 57 meV whereas the mode perpendicular to the plane is observed at 220 meV at 30 K. The hydrogen potential is described by a well-like potential as shown in Fig. 4.1(b). These results on the TiH_2 and $VH_{0.33}$ can be the starting point for the discussion ofthe potential function in the Ti-V-H system, in which the hydrogen sites symmetry, the dynamics and the potentials are expected to be discussed in reference to those for TiH_x and VH_x.

In this chapter we will discuss the INIS spectra of the hydrides β-$Ti_{1-y}V_yH_x$ measured at 50 K in order to investigate the potential energy function for the hydrogen sites and the local structure of metallic lattice surrounding the hydrogen atom. A cluster model [8] which is established on the basis of short-range ordering scheme of either Ti or V is applied to determine the site symmetry of each of the different hydrogen sites and to interpret the dependence of the population of specified hydrogen site on the alloy composition, from which we try to estimate the short-range order parameter, σ. The correlation between the distributions of metal atoms, Ti and V, around a hydrogen atom and the types of sites occupied by the hydrogen atom is also discussed.

4.2 Experimental

INIS measurements were performed using a CAT spectrometer (a Crystal Analyzer Time-of-flight spectrometer) [6, 9] which was installed in the neutron scattering facility (KENS) with the pulsed spallation neutron source at the National Laboratory for High Energy Physics (KEK, Japan). The energy resolution of the CAT is $\Delta\varepsilon/\varepsilon \sim 2$ % over a wide energy range of 1 - 1000 meV. The correction for the peak intensities was necessary to compare the intensities between the peaks observed at the different energy regions, because of the intensity distribution of the incident neutron source. The correction of the peak intensity was performed by the use of the intensity distribution function function $I(\lambda)$ which is well-defined for the neutron source in KENS. The hydrides were wrapped with aluminum foil (70 x 70 x 2 mm^3)

and sealed in an aluminum sample cell (70 x 70 x 5 mm^3) under the atmosphere of He gas. The INIS spectra were measured at 50 K and accumulated for 12 hr.

4.3 Results

Figure 4.2 shows the INIS spectra obtained for the four samples with different composition at 50 K. The spectrum consists of two peaks and two shoulders in $Ti_{0.8}V_{0.2}H_{0.94}$. One peak at 13 meV is relatively narrow and the other at 140 meV is broad. The two broad shoulders appear at 40 meV and 100 meV. The peak positions and intensities of two peaks in the spectrum are similar to those for TiH_2 [6]. However, the spectrum of $Ti_{0.8}V_{0.2}H_{0.94}$ has two shoulders in addition to two well-defined peaks and the line width of each peak is broader than that for TiH_2. In $Ti_{0.6}V_{0.4}H_{1.1}$ the specrtum is similar to that of $Ti_{0.8}V_{0.2}H_{0.94}$, although the peak intensity at 140 meV is weaker than that of $Ti_{0.8}V_{0.2}H_{0.94}$. In $Ti_{0.4}V_{0.6}H_{0.92}$ the spectrum consists of four peaks; the first peak locates at 13 meV, the second at 40 meV, the third at 100 meV and the forth at 140 meV. The peak intensities are comparable to each another except for the peak at the lowest energy. Finally, in $Ti_{0.1}V_{0.9}H_{0.98}$, the spectrum appears to consist of three peaks and one shoulder. The first peak locates at 16 meV, the second locate at 40 meV and the third at 145 meV. The broad shoulder is observed at 110 meV. This spectrum possesses the characteristic of the spectrum of $VH_{0.33}$ [6]. The above results indicate that the intensities of the peaks locating at 40, 100, and 140 meV depend on the alloy composition. Thus the INIS spectrum of Ti-V-H system can approximately be represented by the weighted superposition of those of TiH_2 and $VH_{0.33}$.

It is necessary to estimate the relative intensity of each peak to discuss the composition dependence of the spectra. The vibrational spectrum of metal hydride has usually been analyzed by assuming that the spectrum consists of the superposition of three peaks corresponding to the three normal modes with the excitation energies $\Delta E(100)$, $\Delta E(010)$ and $\Delta E(001)$. In the present study, it was difficult to analyze using such procedure owing to the weak intensity and the low signal-to-noise ratio. Thus the gaussian curve fitting of the INIS spectra was used to determine the integrated intensities of peaks. Four gaussian curves were

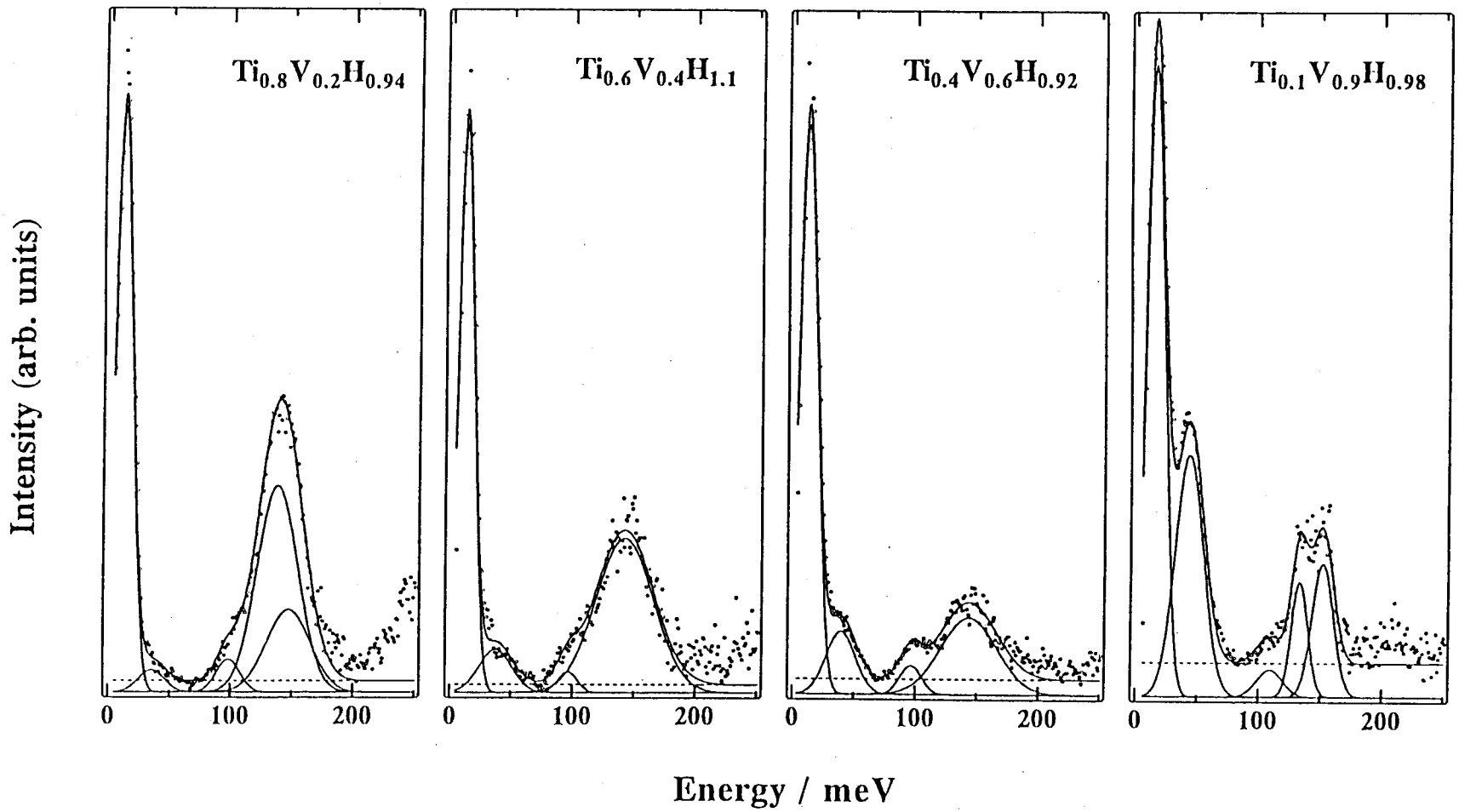

Figure 4.2 Incoherent neutron inelastic scattering spectra of β-$Ti_{1-y}V_yH_x$ (x ~1; y = 0.2, 0.4, 0.6, 0.9) at 50 K. The spectra are normalized by the hydrogen concentrations, the total count and the energy distribution of incident neutrons. The solid lines indicate the results of the least squares' curve fitting of data with 4 gaussians for y = 0.4 and 0.6 and with 5 gaussians for y= 0.2 and 0.9, and the broken lines represent the background noise.

Table 4.1 The peak energies, the line widths Γ and relative intensity of the vibrational modes of a hydrogen atom and a metal lattice in Ti-V alloys, and the number fraction of the corresponding hydrogen site.

Substance	Peak	Γ	Intensity	fraction
	(meV)	(meV)	$I/I_{max.}$	(%)
$Ti_{0.8}V_{0.2}H_{0.94}$	13 ± 1	9.7 ± 0.2	1.0	-----
	36 ± 3	14.8 ± 1.0	0.04 ± 0.01	8.6
	99 ± 3	13.6 ± 1.0	0.06 ± 0.01	7.6
	139 ± 3	23.4 ± 0.5	0.35 ± 0.02	83.8
	148 ± 2[a)]	25.2 ± 0.5	0.14 ± 0.02	-----
$Ti_{0.6}V_{0.4}H_{1.1}$	13 ± 1	8.9 ± 0.3	1.0	-----
	38 ± 3	18.7 ± 1.0	0.08 ± 0.01	19.3
	97 ± 2	11.0 ± 1.0	0.04 ± 0.01	3.7
	143 ± 2	33.1 ± 0.5	0.27 ± 0.02	77.0
$Ti_{0.4}V_{0.6}H_{0.92}$	13 ± 1	10.1 ± 0.2	1.0	-----
	40 ± 1	16.7 ± 0.5	0.11 ± 0.01	35.7
	97 ± 2	12.4 ± 0.5	0.05 ± 0.01	8.1
	144 ± 2	32.2 ± 1.0	0.14 ± 0.01	56.2
$Ti_{0.1}V_{0.9}H_{0.98}$	16 ± 1	10.1 ± 0.2	1.0	-----
	44 ± 1	16.1 ± 0.2	0.38 ± 0.01	93.6
	110 ± 3	14.7 ± 1.0	0.04 ± 0.01	6.4
	134 ± 3[a)]	9.3 ± 0.5	0.18 ± 0.02	-----
	152 ± 3[a)]	12.0 ± 0.5	0.21 ± 0.03	-----

a) This peak is assumed to be originated from the γ-phase.

used to describe the INIS spectra of $Ti_{0.4}V_{0.6}H_{0.92}$ and $Ti_{0.6}V_{0.4}H_{1.1}$, and five gaussian curves were assumed for $Ti_{0.1}V_{0.9}H_{0.98}$ and $Ti_{0.8}V_{0.2}H_{0.94}$. As $Ti_{0.8}V_{0.2}H_{0.94}$ and $Ti_{0.1}V_{0.9}H_{0.98}$ are the mixtures of the β- and γ-phases, an extra gaussian curve was necessary for these two hydrides to take account of contribution from the γ-phase, which was expected to give an INIS peak around 145 meV by analogy with the spectrum of TiH_2 [6]. The results of the least squares' fitting are shown in Fig. 4.2 by solid lines and the parameters used for the data fitting are listed in Table 4.1.

4.4 Discussion

The peak observed at the lowest energy, which is 13 meV for $Ti_{0.8}V_{0.2}H_{0.94}$, $Ti_{0.6}V_{0.4}H_{1.1}$ and $Ti_{0.4}V_{0.6}H_{0.92}$ and is 16 meV for $Ti_{0.1}V_{0.9}H_{0.98}$, has assigned to the acoustic branch of metal lattice vibrational mode in the crystal [2]. This mode can be ignored in the following discussion because this mode is independent of the existence of hydrogen. The integrated intensities of other peaks depend on the Ti content, as was mentioned above. This suggests that the observed peaks are originated from the local vibrational modes of three different types of hydrogen sites. As described in introduction, we refer to the structure of TiH_2 and $VH_{0.33}$ for the assignmant of the observed peaks to the specific hydrogen sites. The excitation energies $\Delta E(100)$, $\Delta E(010)$ and $\Delta E(001)$ of a hydrogen atom occupying the O-site in $VH_{0.33}$ are 50 meV, 57 meV and 220 meV, whereas the excitation energy of a hydrogen atom at the T-site in TiH_2 is 147.6 meV [6]. By comparing the observed spectra with those in previous works, the peaks observed at 36 meV < ε < 44 meV can be assigned to the in-plane local vibrational modes of a hydrogen atom at the O-site, and those at 134 meV < ε < 152 meV to the local vibrational modes of hydrogen atoms at the T-site. Although the local out of plane mode at the O-site is observed at 220 meV in $VH_{0.33}$, the intensity and the S/N ratio in our spectra are not high enough to discuss this mode. Hence this mode is omitted from the following discussion. The peak at 97 meV < ε < 110 meV locates at an intermediate energy range between those of the O- and T-sites. In fact, Hempelmann *et al.* observed a well-defined peak is the similar energy region (about 108 meV) for $ZrV_2H_{4.5}$, and assigned it to a hydrogen

atom occupying the V_4 site [10]. Although the crystal structure of $ZrV_2H_{4.5}$ is different from that in our system, we assume that Ti-V-H system and Zr-V-H system have similar the local structure around a hydrogen atom to each other and to assign the peak in this energy range to the T-site surrounded by four V atoms by referring to Ref.[10]. The hydrogen sites corresponding to the three peaks are denoted as T_1-, T_2- and O-site in the decreasing order of the excitation energy in following discussion; T_1-site is the site surrounded by four Ti and T_2-site by four V atoms.

Before we discuss the composition dependence of the INIS spectra, we perform the correction for the coexistence of the γ-phase in $Ti_{0.1}V_{0.9}H_{0.98}$ and $Ti_{0.8}V_{0.2}H_{0.94}$. If we assume that two peaks observed at 134 and 152 meV for $Ti_{0.1}V_{0.9}H_{0.98}$ and a peak observed at 148 meV for $Ti_{0.8}V_{0.2}H_{0.94}$ are originated by the γ-phase, the fractions of the γ-phase deduced in the neutron scattering experiments are consistent with those in the X-ray diffraction as interpreted follows. The integral peak intensities of the γ-phase are about 30 and 27 % in $Ti_{0.1}V_{0.9}H_{0.98}$ and $Ti_{0.8}V_{0.2}H_{0.94}$, respectively, of the total integral peak intensities, if the contribution from the peak at the lowest energy is excluded. To estimate the fraction of the γ-phase in metal atom base we consider the ratio of the hydrogen contents in the β- and γ-phase. For example, the ratio of the β- and γ-phases in the metal atom base is 70 : (30/2) in $Ti_{0.1}V_{0.9}H_{0.98}$ because the hydrogen-to-metal ratios in the β- and γ-phases are 1 and 2, respectively. Consequently, the fractions of the γ-phase in $Ti_{0.1}V_{0.9}H_{0.98}$ and $Ti_{0.8}V_{0.2}H_{0.94}$ are 18 and 15 %, respectively, which agree with about 20 % estimated in the X-ray diffraction experiments.

After removing the contributions from the γ-phase and the metal lattice vibration the resultant spectra consist of at most three peaks. Their intensities and positions vary with the metal composition of the alloy. The relative intensity of the peak corresponding to the hydrogen atom at the O-site decreases and the peak position shifts slightly to lower energies with increasing Ti content in the alloys. According to the simple lattice dynamical model used by Hempelmann *et al.* for the assignment of the different vibrational peaks to certain hydrogen sites [10], the vibrational frequency is proportional to the inverse of metal-hydrogen distance. Thus this variation of the peak position is considered to be due to the lattice expansion caused

by Ti incorporation. However, an additional perturbations such as the shape change of the hydrogen potential might bring about further lower energy shift. For the peaks corresponding to the T_2-site the relative peak intensity is approximately constant, and the peak position is unshifted within the experimental error except for $Ti_{0.1}V_{0.9}H_{0.98}$. The peak position 110 meV for $Ti_{0.1}V_{0.9}H_{0.98}$ is greater by 10 meV than those of the other hydrides. We consider that this shift is caused by the difference in the crystal structure. For the peaks corresponding to the T_1-site the relative peak intensity increases with increasing Ti content in the alloys and the peak position is unshifted within the experimental error.

The line widths Γ in Table 4.1 are relatively large compared with those of other pure metal hydrides such as TiH_2 ,$VH_{0.33}$ [6] and ZrV_2H_x [10], due probably to the lowering of the site symmetry which causes to lift the three fold degenercy of the local modes for the T-site and two for the O-site. In addition, the distribution of the metal-hydrogen force constant brought about by the distribution of the lattice constants due to the formation of the disordered alloys causes further broadening.

Next, we discuss the composition dependence of the relative number of each hydrogen site. The occupancy of hydrogen sites is analyzed in terms of only the relative number of hydrogen atoms at each site in the hydrides because of the difficulty in determining the absolute occupancy. The integral peak intensities were corrected for the degeneracy of the vibrational modes; 2 and 3 for the O- and T-sites, respectively. The ratio of the corrected integral peak intensities gives the relative populations of the hydrogen sites in the Ti-V alloys. The relative populations of hydrogen atoms at the three kinds of hydrogen sites are listed in Table 4.1 and are plotted against the content of Ti atoms, 1-y, in Fig. 4.3. The relative population of hydrogen atoms at the T_1-site increases and that at the O-site decreases with increase in the Ti content. The relative population of hydrogen atoms at the two sites become comparable when the Ti content is 0.4. These populations change monotonous but not linearly with the Ti content, whereas at the T_2-site remain constant within the experimental error. The relative population of hydrogen sites at the latter site is smaller than those at the other two sites. These results indicate that the types and the number of the hydrogen sites are strongly correlated with the composition of the host alloys.

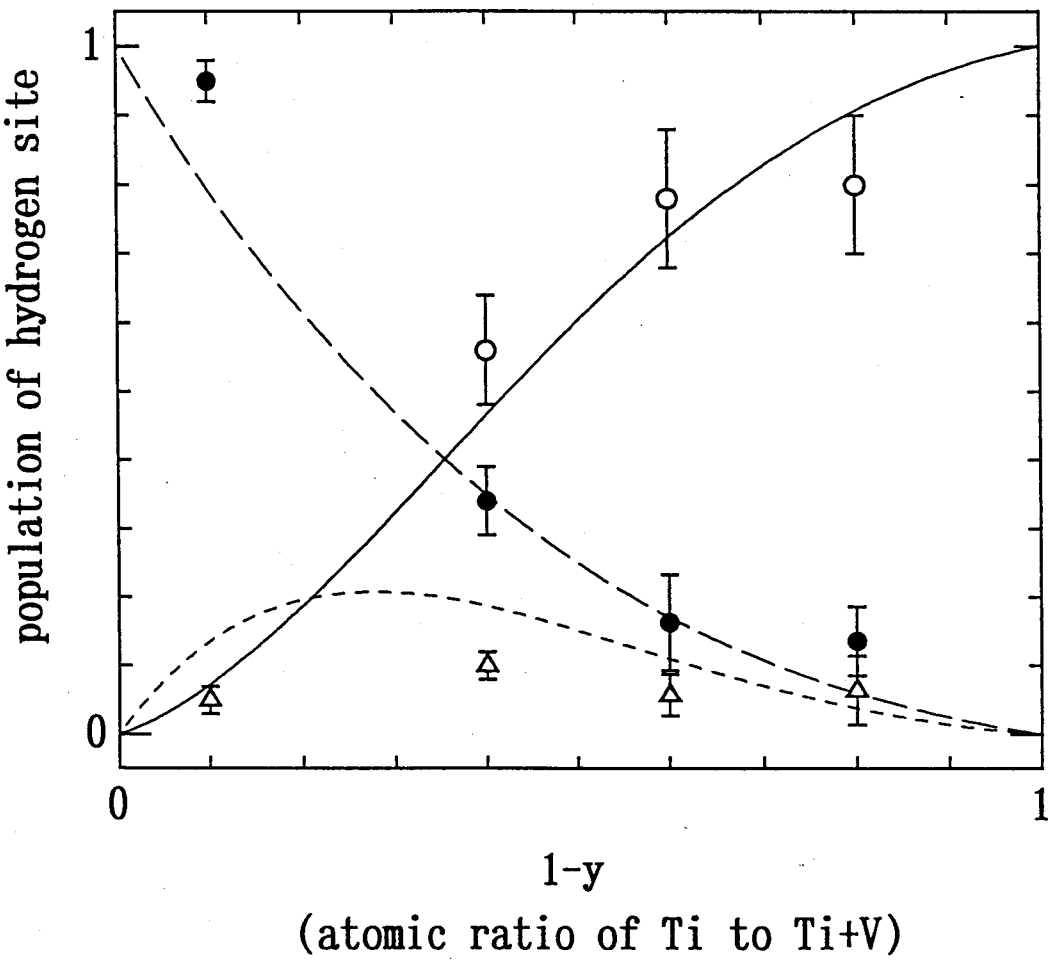

Figure 4.3 The composition dependence of the population of the hydrogen site. The population of the hydrogen site for the O-site (●), T_1-site (○) and T_2-site (△) are plotted against the content of Ti (i.e. 1-y). The degeneracies of the local vibrational modes of the hydrogen atom are taken into account to convert the integralated peak intensities to the population of the hydrogen sites. The lines were calculated values using Eqs. (4.1) with σ = 0.43, n = 4 and m = 5. For $Ti_{0.1}V_{0.9}H_{0.98}$, the population of the T_1-site arising from the β-phase is too small to be estimated.

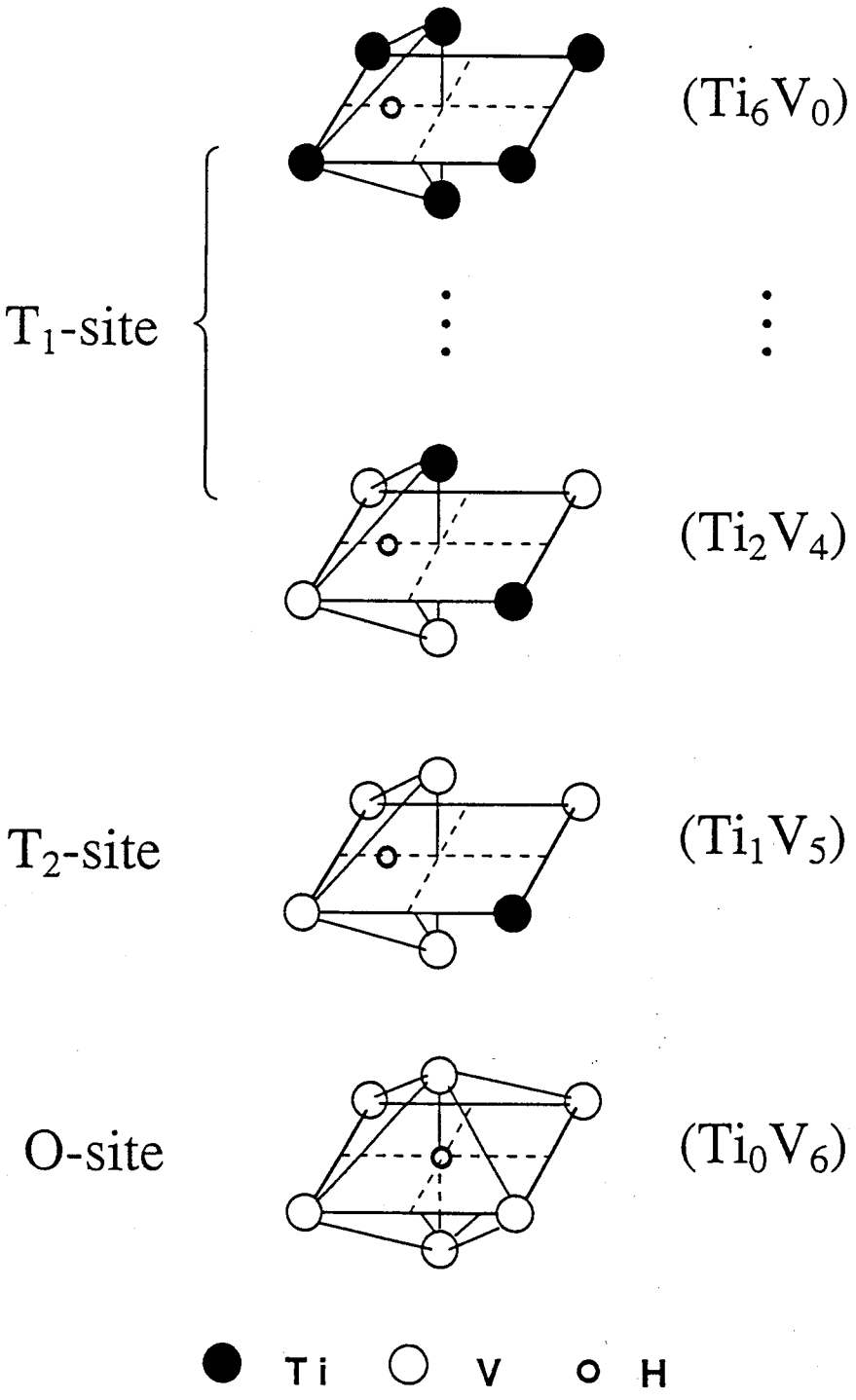

Figure 4.4 Schematic description of the correlation between the arrangement of metals and the hydrogen site in the cluster. This scheme corresponds to the case of n = 4 and m = 5; the hydrogen atom occupys the T_1-site in the clusters from Ti_6V_0 to Ti_2V_4, the hydrogen atom occupys the T_2-site in the cluster Ti_1V_5 and has the hydrogen atom occupys the O-site in the cluster Ti_0V_6.

Such variation of the population at the hydrogen site is discussed on the basis of the various octahedral metal clusters which surround the hydrogen atom [i.e. $Ti_{6-i}V_i$ (i = 0 to 6)]. We now construct a model for the stable hydrogen sites in the clusters, by referring to the hydrogen sites in pure metal hydrides such as $VH_{0.33}$ and TiH_2. This model is schematically shown in Fig. 4.4. The hydrogen atoms occupy the O- or T-sites in the pure metal hydrides composed of only V or Ti [15]. The octahedron in $VH_{0.33}$ is composed of only V atoms and represented by Ti_0V_6, whereas in TiH_2 it is composed of Ti and represented by Ti_6V_0. In our system the octahedrons are composed of Ti and V and so the seven different configurations can be realized in $Ti_{1-y}V_y$. The affinity of Ti to the hydrogen atom is generally greater than that of V [11, 12]. The stability of the hydrogen site is mainly determined by the metal-hydrogen interaction. In the Ti-rich content the site stability is dominated by Ti-H interaction and the tetrahedral site is more stable than the octahedral site in a similar with the hydrogen site of TiH_2. On the other hand, in the V-rich content, the site stability is dominated by V-H interaction and the octahedral site is more stable than the tetrahedral site in a similar with the hydrogen site of $VH_{0.33}$. In fact, we measured the temperature dependence of the INIS spectrum for $Ti_{0.4}V_{0.6}H_{0.92}$ to clarify the potential energy scheme among each hydrogen site at 50 K and 300 K. The peak intensities to the specific hydrogen sites few depended on the temperature, althought the linewidth of the spectra for $Ti_{0.4}V_{0.6}H_{0.92}$ increases as heating. This results suggests that the hydrogen atom at the T_1- and T_2-sites is more stable than that at the O-site, and supports the above model. The affinity of Ti to the hydrogen atom is generally greater than that of V [11, 12]. Taking into account the difference in the affinity of metal to hydrogen between Ti and V and the stability of the hydrogen site, we propose a scheme for the stable hydrogen site in the cluster; as the configuration of the clusters changes from Ti_6V_0 to Ti_0V_6, the relative stability of the T_1-site to the O-site is reduced through the occupation of the T_2-site. The population $p(i, \sigma)$ that a specified cluster, $Ti_{6-i}V_i$ is realized in the $Ti_{1-y}V_y$ alloy is given by Eqs. (2.2)-(2.11) (replaceing A and B to Ti and V, respectively). The number fractions of the T_1-, T_2- and O-sites are then given by

$$P_{T_1}(\sigma) = \sum_{i=0}^{n} p(i, \sigma), \qquad (4.1a)$$

$$P_{T_2}(\sigma) = \sum_{i=n+1}^{m} p(i, \sigma), \tag{4.1b}$$

and

$$P_{O}(\sigma) = \sum_{i=m+1}^{6} p(i, \sigma), \tag{4.1c}$$

where n and m are adjustable parameters representing the border numbers between the T_1- and T_2-sites and between the T_2- and O-sites, respectively. Parameters n and m must be integers which satisfy the conditions $0 \leq n < m < 6$. Thus, in this model, the parameter σ represents the degree of the clustering of metal atoms, and n and m determine the types of sites where the hydrogen atom enters.

Figure 4.5 shows site populations calculated using Eqs. (4.1) for various values of adjustable parameters, σ, n and m to demonstrate dependence of the calculated site populations on the parameters. The O-site population has a linear relation with the Ti content at $\sigma = 1$. When the parameters n and m are constant and σ changes from 1 to 0, the curve for the O-site is no longer linear, as shown in Fig. 4.5(a). The T_2-site population is zero at $\sigma = 1$, and increases as σ varies from 1 to 0 (Fig. 4.5(b)). It reaches a maximum at 1-y = 0.5 irrespective of the value of σ at n = 2 and m = 3. The curve of the O-site and the maximum of the curve of the T_2-site shift from the low concentration side of Ti to the high concentration side with decrease in n and m, when σ is fixed (Fig. 4.5(c) and 4.5(d)). By fitting Eqs. (4.1) to the experimental data (Fig. 4.3) we obtained $\sigma = 0.43 \pm 0.05$, n = 4 and m = 5.

The σ value obtained is compared with literature values [8] which were estimated by Brouwer *et al.* from the activation energy for hydrogen diffusion and the enthalpies of formation of hydrides in various $Ti_{1-y}V_y$ alloys [13-16]. The σ in the literature ranges in $0.36 \leq \sigma \leq 0.51$ as listed in Table 4.2. The cluster model derived above might be too simple to describe the actual local structure in the alloy. In an actual system a hydrogen atom occupying a site will block a hydrogen atom to enter into the nearest neighbor empty sites (selective-blocking), and the site occupancies of hydrogen atoms depend on the temperature because of the differences in the site energy among the three sites. Nevertheless, the σ value obtained

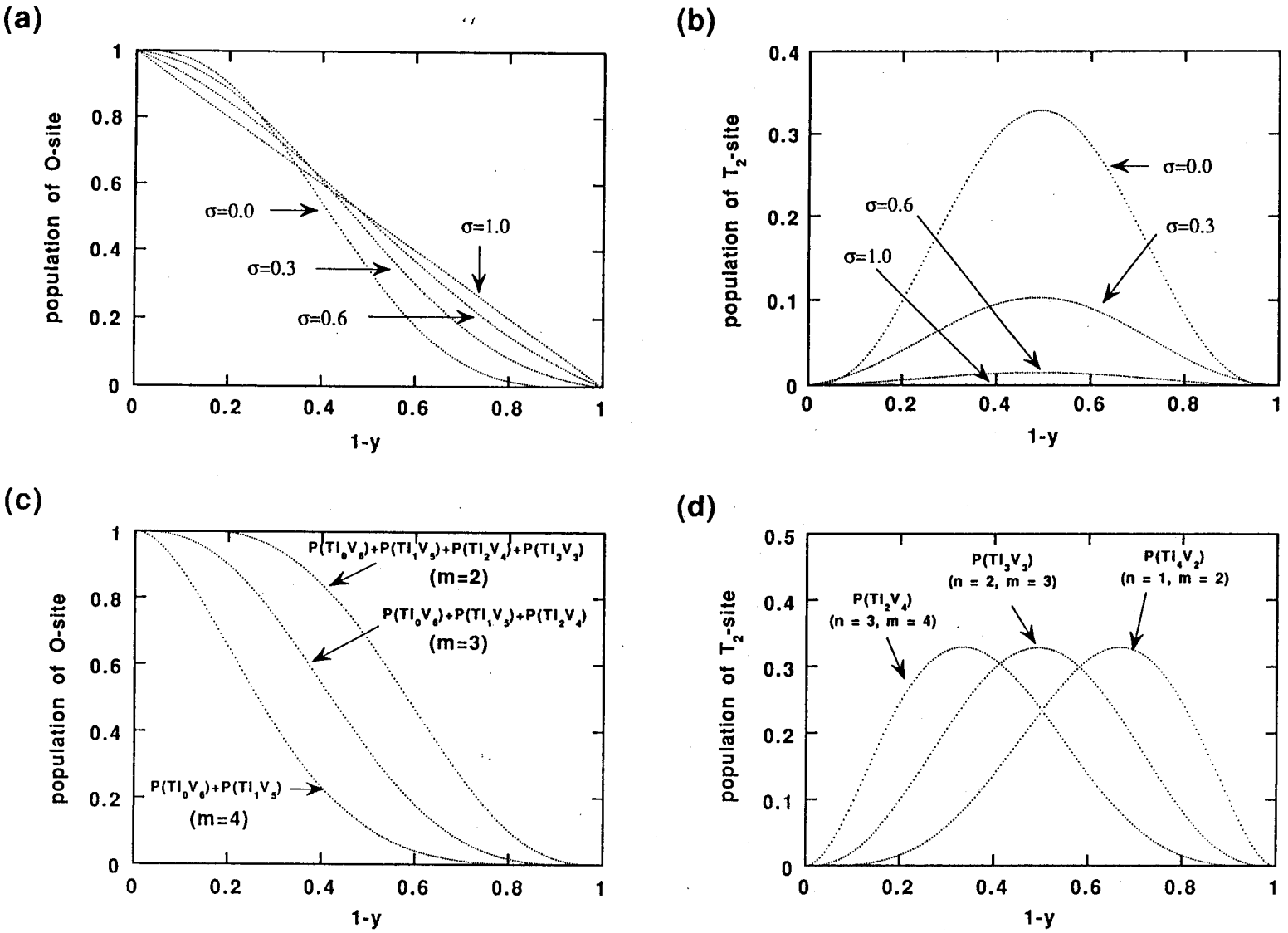

Figure 4.5 Simulations of the populations for the O- and T_2-sites. The short-range order parameter (i.e. σ) dependences of the O-site (a) and T_2-site (b) populations were calculated using Eqs. (4.1) with n=2 and m=3. The dependences of the O-site (c) and T_2-site (d) populations on n and m were calculated with $\sigma = 0$.

Table 4.2 Short-range order parameter of $Ti_{1-y}V_y$ alloys and its annealing temperature.

Source	σ	T_a / K
This work	0.43	quench
Brouwer *et al.*[8]	0.36	1900
Tanaka *et al.*[13]	0.51	1270
Pine *et al.*[14]	0.40	1300 - 1800
Peterson *et al.*[16]	0.41	
	0.39	

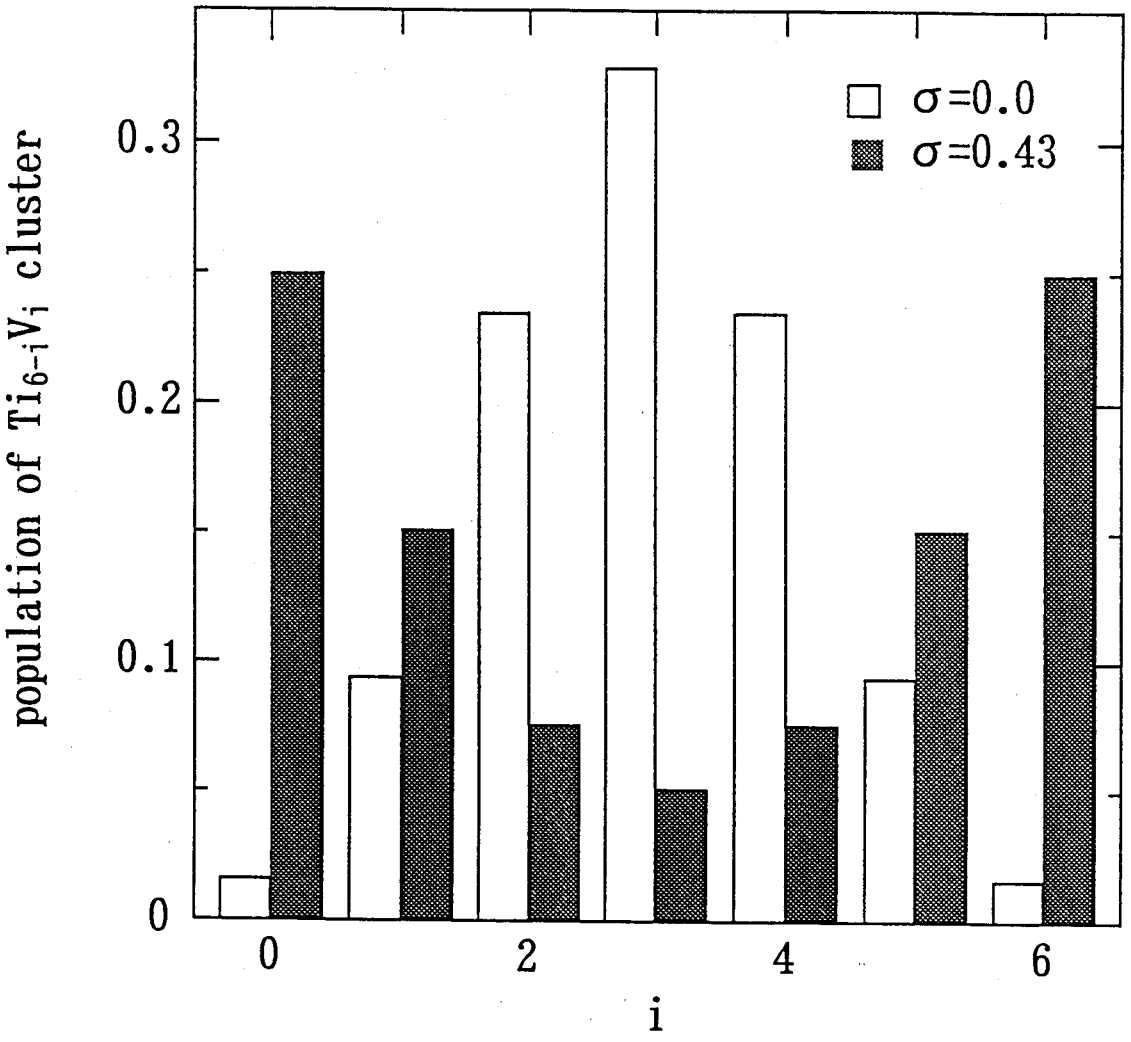

Figure 4.6 The populations of the $Ti_{6-i}V_i$ clusters in the $Ti_{0.5}V_{0.5}$ alloy at two given values of σ.

using the simplest model in this work is in good agreement with literature values. This results suggests strongly that the σ value is intrinsic for the Ti-V alloy system.

However, the degree of short-range ordering of metal atoms depends on the conditions of synthesis and thermal treatments and the hydrogen concentrations in Ti-V alloys. Especially, the annealing temperature is the most effective factor for the relaxation of the structure of the disordered alloy and will be closely related to the short-range order of the metal atoms. Porscha *et al.* [17] found that in the structural relaxation of the amorphous $Cu_{64}Ti_{36}$ alloy the short-range atomic rearrangement is predominant mechanism at low annealing temperatures, whereas the long-range atomic diffusion is predominant mechanism at high annealing temperatures. This result indicates that the annealing at low temperatures affects the short-range order of metal atoms and that the contribution of the short-range order to the structural relaxation becomes small with increase in the annealing temperature. Table 4.2 shows that the σ value decreases with increase in the annealing temperature; σ is 0.36 at T_a = 1900 K, and 0.51 at T_a = 1270 K. This trend is consistent with the result of Porscha *et al.*. In this work on the Ti-V alloys synthesized by quenching the melt, σ assumes an intermediate value between 0.36 and 0.51 which agrees with the value at T_a = 1300 - 1800 K determined by Pine *et al.*.

The short-range order parameter, $\sigma = 0.43 \pm 0.05$, suggests that the clustering of the same kind of metallic species occurs in the alloys. The populations of the $Ti_{6-i}V_i$ clusters in the $Ti_{0.5}V_{0.5}$ alloy are calculated for σ = 0 and 0.43 and the results are shown in Fig. 4.6. For σ = 0.43 the populations of Ti_2V_4, Ti_3V_3 and Ti_4V_2 decreases while those of Ti_0V_6, Ti_1V_5, Ti_5V_1 and Ti_6V_0 increases relative to the case of σ = 0 (the binomial distribution). The population of Ti_3V_3 is only 1/6 and the populations of Ti_2V_4 and Ti_4V_2 are 1/3 when σ = 0.43. The populations of Ti_1V_5 and Ti_5V_1 at σ = 0.43 are twice as much as that at σ = 0, and those of Ti_0V_6 and Ti_6V_0 are about 10 times greater. These considerations show that Ti and V atoms are apt to form clusters between the same kind of metal. Ti and V can form a complete series of the alloy and the resultant alloys appear to be homogeneous in the macroscopic sense. However, the present study revealed that the affinity between the same kinds of metals (Ti-Ti and V-V) is larger than that between Ti and V and therefore, very inhomogeneous distribution of the composition is realized in the microscopic point of view.

References

[1] T. Springer, *Z. Physik. Chem.*, **B115**, S141(1979).

[2] V. A. Semenov, Yu. V. Lisichkin, *Sov. Phys. Soild State*, **24**, 2037(1982).

[3] J. Eckert, J. A. Goldstone, D. Tonks and D. Richter, *Phys. Rev.*, **B27**, 1980(1983).

[4] A. Magerl, J.J. Rush, J. M. Rowe, D. Richter, H. Wipf, *Phys. Rev.*, **B27**, 927(1983).

[5] A. Magerl, J. J. Rush, J. M. Rowe, *Phys. Rev.*, **B33**, 2093(1986).

[6] S. Ikeda and N. Watanabe, *J. Phys. Soc. Jpn.*, **56**, 565(1987).

[7] I. S. Anderson, N. F. Berk, J. J. Rush and T-. J. Udovic, *Phys. Rev.*, **B37**, 4358(1988).

[8] R. C. Brouwer, J. Rector, N. Koeman and R. Griessen, *Phys. Rev.*, **B40**, 3546(1989).

[9] S. Ikeda and N. Watanabe, *Nucl. Inst. Meth.*, **221**, 571(1984).

[10] R. Hempelmann, D. Richter, O. Hartmann, E. Karlsson and R. Wäppling, *J. Chem. Phys.*, **90**, 1935(1989).

[11] O. J. Kleppa, P. Dantzer and M. E. Melnichak, *J. Chem. Phys.*, **61**, 4048(1974).

[12] P. Dantzer, O. J. Kleppa and M. E. Melnichak, *J. Chem. Phys.*, **64**, 139(1976).

[13] S.Tanaka and H. Kimura, *Trans. Jpn. Inst. Met.*, **20**, 647(1979).

[14] D. J. Pine and R. M. Cotts, *Phys. Rev.*, **B28**, 641(1983).

[15] P. S. Rudman, *Acta Metall.*, **12**, 1381(1964).

[16] D. T. Peterson and S. O. Nelson, *Metall. Trans.*, **16A**, 367(1985).

[17] B. Porscha and H. Neuhäuser, Phys. stat. sol., (b)**186**, 119(1994).

5. Spin-lattice relaxation time (T_1)

5.1 Introduction

5.1.1 General description of BPP equation

The random modulation of the dipole-dipole and/or quadrupole interactions, caused by molecular motion such as molecular rotation, reorientation and translational diffusion, is a major origin of spin-lattice relaxation in solid materials. The spin-lattice relaxation time, T_1, can be represented by spectral density which is the Fourier transform of the correlation function of the molecular motion. When the molecular motion is rapid enough and can be represented by a single-exponential correlation function, $g(\tau) = \exp(-|t|/\tau_c)$, the spectral density is given by [1]

$$j(\omega) = \frac{2\tau_c}{1 + \omega^2 {\tau_c}^2}, \qquad (5.1)$$

where τ_c is called correlation time of the motion and its inverse correspond to the rate of the motion. This spectral density leads to the famous BPP equation for T_1. For the nuclei with spin $I = 1/2$ such as ^{1}H the major interaction is dipolar interaction between like spins I or I and unlike spin S, and the modulation of the dipolar interaction due to the fluctuation of the internuclear vector by motion is the dominant mechanism for the magnetic longitudinal relaxation. In the case of like spins as the interacting spins I, the dipolar spin-lattice relaxation time is represented by [2]

$$T_1^{-1} = C_{II}\left[\frac{\tau_c}{1 + \omega_L^2\tau_c^2} + \frac{4\tau_c}{1 + 4\omega_L^2\tau_c^2}\right], \qquad (5.2)$$

where $\omega_L = \omega_I$ is the Larmor frequency for I spins under the static magnetic field H_0 ($\omega_L = \gamma_I H_0$). In the case of unlike spins I and S, the dipolar spin-lattice relaxation time for spin I is represented by

$$T_1^{-1} = C_{IS}\left[\frac{\tau_c}{1 + (1 - \alpha)^2\omega_L^2\tau_c^2} + \frac{3\tau_c}{1 + \omega_L^2\tau_c^2} + \frac{6\tau_c}{1 + (1 + \alpha)^2\omega_L^2\tau_c^2}\right]. \qquad (5.3)$$

C_{II} and C_{IS} represent the magnitude of the dipolar interaction which is supposed to be averaged out by a motional mode. In Eq. (5.3) α is the ratio of gyromagnetic ratio for spin S to for spin I ($\alpha = \gamma_S/\gamma_I = \omega_S/\omega_I$). For quadrupolar nuclei with nuclear spin $I = 1$ such as ^2H, the modulation of the quadrupole interaction due to the fluctuation of the electric-field-gradient (EFG) tensor around a nucleus by motion is the dominant mechanism for the magnetic relaxation. The quadrupolar spin-lattice relaxation time is represented by

$$T_1^{-1} = \frac{3}{40}(1 + \frac{\eta^2}{3})(\frac{e^2Qq}{\hbar})^2[\frac{\tau_c}{1 + \omega_L^2\tau_c^2} + \frac{4\tau_c}{1 + 4\omega_L^2\tau_c^2}] \qquad (5.4)$$

where the quantity e^2Qq/h is quadrupole coupling constant (QCC) and η is the symmetry parameter of the EFG tensor.

T_1^{-1} in Eqs. (5.2)-(5.4) show a characteristic behavior of the limiting values of the correlation time : in the slow motion limit ($\omega_L^2\tau_c^2 \gg 1$) the T_1^{-1} is proportional to ω_L^{-2}, in the rapid motion limit ($\omega_L^2\tau_c^2 \ll 1$) the T_1^{-1} does not depend on the Larmor frequency, and in the intermediate region ($\omega_L^2\tau_c^2 \sim 1$) the T_1^{-1} assumes maximum value where it is proportional to ω_L^{-1}.

When the temperature dependence of T_1^{-1} is treated, Arrhenius activation process is usually assumed to the correlation time of the motion, which is represented by

$$\tau_c = \tau_0 \exp(\frac{E_a}{RT}), \qquad (5.5)$$

where E_a is the activation energy for the motion. Using this equation, we expect that the logarithmic plot of the T_1 vs. reciprocal temperature $1/T$ shows a symmetrical V-shape curve and its slopes at both sides of the minimum are $+E_a/R$ and $-E_a/R$, from which the activation energy can be determined. The minimum values of T_1 are used to determine the coefficients C_{II}, C_{IS} or QCC. The coefficients C_{II} and C_{IS} lead to the determination of the mode of the molecular motion by comparing with the calculated values of theC_{II} and C_{IS} on the basis of

suitable model for the motional mode. The value of QCC and η can be used to discuss the electronic structure and to deduce the symmetry of the site at which the spins are located.

5.1.2 Distribution of correlation time

The BPP equations on the basis of the single-exponential correlation function have been widely used to interpret the dynamical behavior of the condensed matter. However, there are some exceptional cases, particularly in solids, where the spin-lattice relaxation cannot be described by the simple BPP equations. There are several cases where the simple BPP theory does not apply. A type of non-exponential correlation function appears when the motion of the individual spins is not independent from but cooperative with each other. For example, the hopping of the ionic charge carriers in the fast-ion conductors are described by a non-exponential correlation function. For the glassy fast-ion conducting system $0.56Li_2S$ + $0.44Si_2S$ in which Li^+ is the mobile ion [3], the degree of non-exponential property of the correlation function depends on the Li^+ concentration, and only at the extremely dilute concentrations the correlation function can be approximated by the single exponential and the spectral density of Eq. (5.1) can be valid. Also, the spectral density for the diffusive motion of particles moving among the well-defined lattice points in the crystals is different from Eq. (5.1). The spectral densities for such motion were calculated by Sholl *et al.* for the simple lattices such as the simple cubic (sc), the body-centered cubic (bcc) and the face-centered cubic (fcc) [4-7]. The calculated spectral densities were successfully applied to interpret the experimental results of T_1 in PdH_x and PbF_2 crystal lattice of which are the fcc [8]. The Sholl theory cannot be applied to more complex structure with lower symmetries. As the well-defined lattice points are necessary to caluclate the spectral density for the diffusive motion, the application of the theory to disordered solids is extremely difficult. Similar cooperative motions of the molecules and the functional groups have also been reported by some researchers for some molecular crystals [9]. In the case of system in which variety of interatomic or intermolecular interactions works there may be distributions of the rate of motion for even a single motional mode. Consider methyl groups located in the different electrostatic environment such as in the different fragments in a macromolecules. In such case the three-fold

reorientation of each methyl group is characterized by the BPP equation, but the rate of reorientation differ from place to place. The ensemble of these methyl groups as a whole will have a distribution of the correlation times [10-13]. The disordered solids such as binary or ternary metal hydrides [14-17] lies in an intermediate situation between above two categolies. Both an irregularity of environment and some kind of cooperative motion exist in these systems [18, 19] and hence a distribution of correlation timehas to be taken into account to describe the molecular motion.

From a formal point of view, we cannot distinguish whether the spectral density is originated from the molecular reorientiion of which the correlation times is distributed or from a specific molecular reorientation with a non-exponential correlation function [20]. Under such a condition the spectral density of the molecular motion can be represented as follows by using a distribution of correlation times [21]:

$$j(\omega_0, x_1, x_2, \cdots) = \int_0^\infty \Lambda(\tau_c, x_1, x_2, \cdots) \frac{2\tau_c}{1 + \omega_0^2 \tau_c^2} d\tau_c, \qquad (5.6)$$

where $\Lambda(\tau_c, x_1, x_2, \cdots)$ is the distribution function for correlation time τ_c and $\{x_i\}$ is a set of parameters characterizing the distribution of τ_c. The distribution function Λ is normalized to unity:

$$\int_0^\infty \Lambda(\tau_c, x_1, x_2, \cdots) d\tau_c = 1 . \qquad (5.7)$$

Since the Fourier transform is a linear operation, Λ gives rise to the reduced correlation function;

$$g(t, x_1, x_2, \cdots) = \int_0^\infty \Lambda(\tau_c, x_1, x_2, \cdots) e^{-|t|/\tau_c} d\tau_c . \qquad (5.8)$$

The frequency dependence of the T_1 derived from Eq. (5.6) are usually different from that of the simple BPP formalisum, depending on the form of the distrubution function.

Temperature dependence of T_1 is evaluated from Eq. (5.5) by replacingτ_c, τ_0 and E_a with τ_{cm}, τ_{0m} and E_a^{app}, respectively. The parameters τ_{cm} and τ_{0m} are mean correlation time and mean pre-exponential factor, respectively, which are the values at the maximum point of the distribution function for the correlation time and the pre-exponential factor, respectively. E_a^{app} is an apparent activation energy. To describe the temperature dependence using Eq. (5.5) with newly defined parameters Beckmann has introduced a useful parameter $S = \ln(\tau_c/\tau_{cm})$. Using S he defines a new distribution function $F(S)$ as [21]

$$F(S)dS = \Lambda(\tau_c)d\tau_c, \tag{5.9}$$

$$F(S) = \tau_{cm}e^S\Lambda(\tau_c). \tag{5.10}$$

Using Eqs.(5.6), (5.9) and (5.10) the spectral density for the motion and hence the BPP equation for T_1 with distribution of the correlation time are obtained.

5.2 ^{1}H NMR

5.2.1 Experimental

^{1}H NMR measurements were carried out with a Bruker Model CXP-100 pulsed spectrometer with an electromagnet. The proton spin-lattice relaxation times (T_1) were measured using the 90° - τ - 90° methods in the temperature range between 105 and 400 K at four frequencies, 9, 22.5, 52 and 90 MHz. The experimental uncertainty was less than ± 5 %. The temperature was controlled with the accuracy of ± 1 K by Bruker variable temperature unit VT-1000 by the flow of cooled or heated nitrogen gas. The hydrides used for the T_1 measurements had the following compositions ; $Ti_{0.6}V_{0.4}H_{0.91}$, $Ti_{0.4}V_{0.6}H_{0.91}$ and $Ti_{0.2}V_{0.8}H_{0.83}$ which were prepared by S. Hayashi *et al.* [22], and $Ti_{0.8}V_{0.2}H_{0.89}$, $Ti_{0.4}V_{0.6}H_{0.86}$ and $Ti_{0.2}V_{0.8}H_{0.86}$ which were prepared in this work. The samples were

sealed into glass ampoules (10 mmϕ and ca. 100 mm long) with He heat exchange gas (~ 150 mmHg).

5.2.2 Results and Analysis

The proton magnetization recovery curves for $Ti_{0.8}V_{0.2}H_{0.89}$, $Ti_{0.6}V_{0.4}H_{0.91}$, $Ti_{0.4}V_{0.6}H_{0.91}$ and $Ti_{0.2}V_{0.8}H_{0.83}$ were described by a single exponential decay over all temperature range of measurements. For $Ti_{0.4}V_{0.6}H_{0.86}$ and $Ti_{0.2}V_{0.8}H_{0.86}$, the recovery of the magnetization showed the non-exponential decay depending on the temperature. The magnetization recovery curves for $Ti_{0.4}V_{0.6}H_{0.86}$ (163 and 200 K) and $Ti_{0.2}V_{0.8}H_{0.86}$ (182 and 267 K) are shown in Fig. 5.1. In both hydrides the recovery curves at high temperature above 200 K show a single exponential decay, whereas at lower temperature show non-exponential decay. The degree of the non-exponential decay was relatively small. Two origins of such non-exponential behavior are considered; one is the co-exsisting of multi-phase brought about by phase separation, and other is existence of the cooparative motion of the protons in these systems. It is difficult to clearify which origins are dominant. In this work the spin-lattice relaxation times T_1 were represented by the apparent T_1 values, i.e., the time at which the longitudinal magnetization decays down to 1/e of the equilibrium value. The ^1H T_1 values at four Larmor frequencies for $Ti_{0.8}V_{0.2}H_{0.89}$, $Ti_{0.6}V_{0.4}H_{0.91}$, $Ti_{0.4}V_{0.6}H_{0.91}$ and $Ti_{0.2}V_{0.8}H_{0.83}$ are plotted against the reciprocal temperature in Fig. 5.2 (a) - (d), and the ^1H T_1 and the apparent T_1 values of $Ti_{0.4}V_{0.6}H_{0.86}$ and $Ti_{0.2}V_{0.8}H_{0.86}$ at 22.5 MHz are plotted together in these figures.

The protonT_1 values in $Ti_{0.4}V_{0.6}H_{0.86}$ and $Ti_{0.2}V_{0.8}H_{0.86}$ were in good agreement with those in $Ti_{0.4}V_{0.6}H_{0.91}$ and $Ti_{0.2}V_{0.8}H_{0.83}$, respectively, suggesting that the T_1 values in these hydrides not depend on the samples prepared using the different lot of Ti-V alloy. The minimum of T_1 values was observed in each of all samples. The values and the temperatures at whichT_1 assumes minimum depend on the composition of the Ti-V alloys. For example, the temperatures at which the T_1 minimum was observed at 9 MHz are 174, 200, 215 and 217 K for $Ti_{0.2}V_{0.8}H_{0.83}$, $Ti_{0.4}V_{0.6}H_{0.91}$, $Ti_{0.6}V_{0.4}H_{0.91}$ and $Ti_{0.8}V_{0.2}H_{0.89}$, respectively. The T_1 minimum value is longer as the V content becomes lower in the alloy : The minimum values of

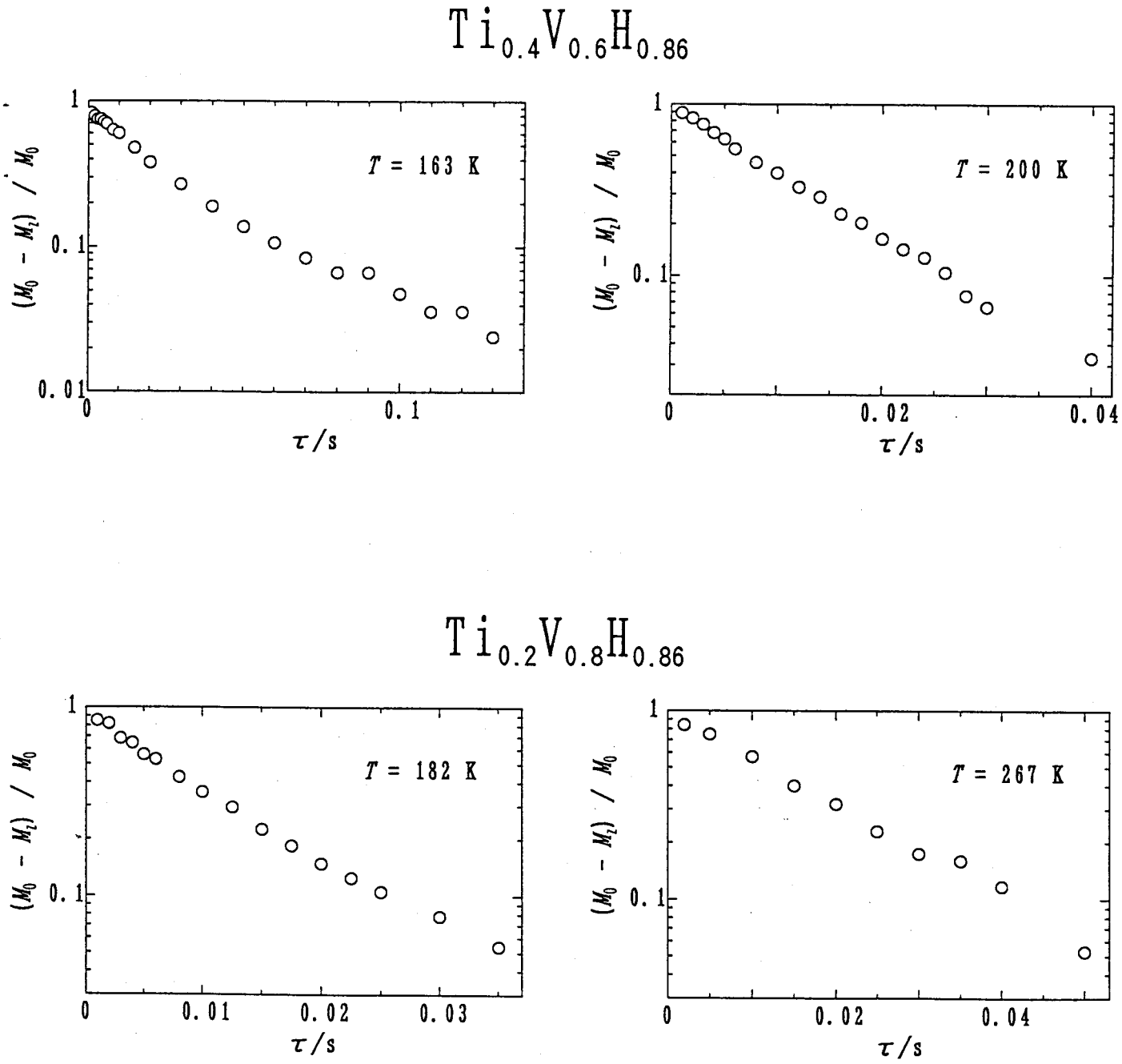

Figure 5.1 Recovery curves of ^1H magnetization in β-$Ti_{0.4}V_{0.6}H_{0.86}$ (upper) and β-$Ti_{0.2}V_{0.8}H_{0.86}$ (lower).

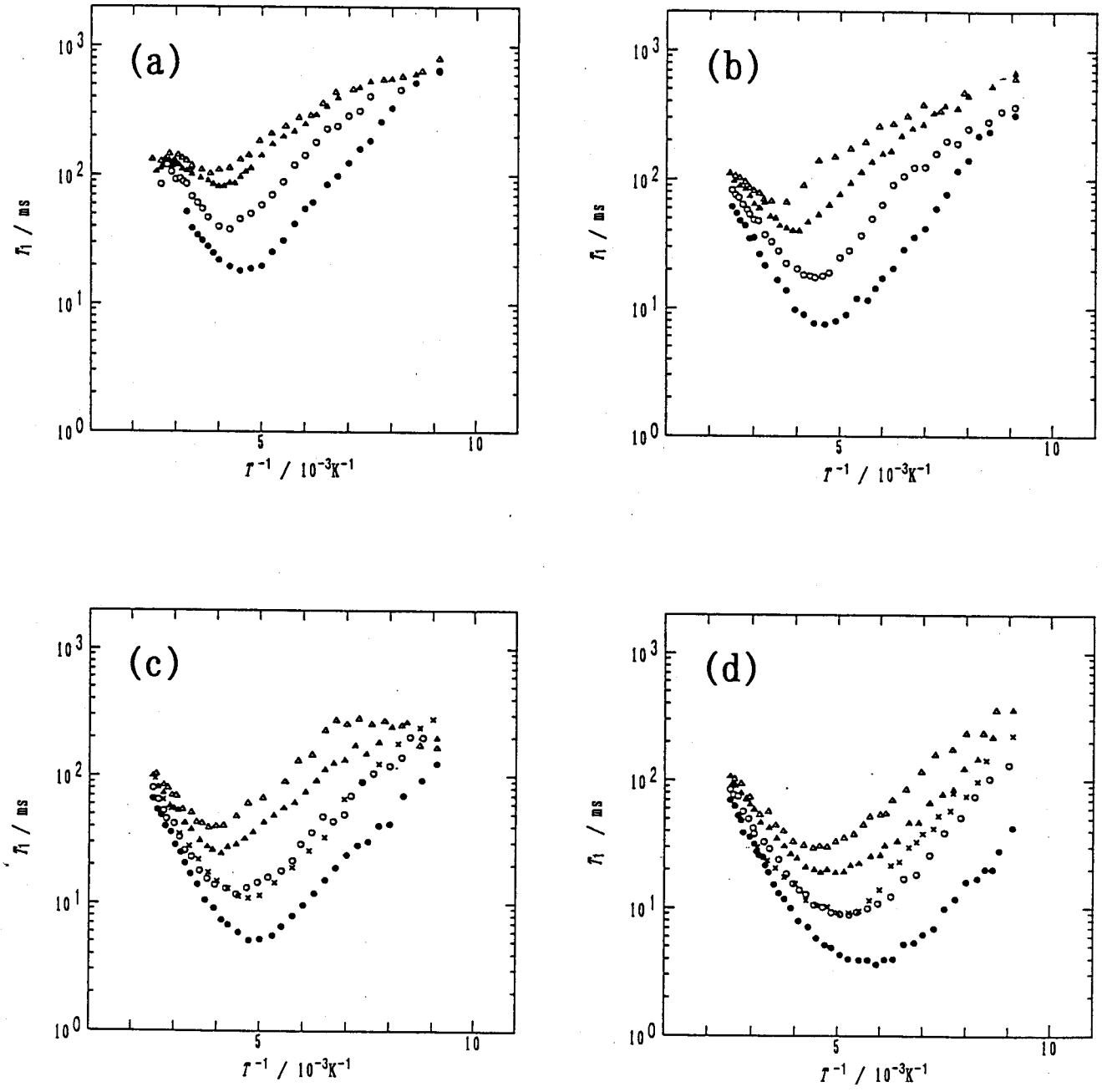

Figure 5.2 Temperature and frequency dependence of ^1H spin-lattice relaxation times (T_1) for $Ti_{0.8}V_{0.2}H_{0.89}$ (a), $Ti_{0.6}V_{0.4}H_{0.91}$ (b), $Ti_{0.4}V_{0.6}H_{0.91}$ (c) and $Ti_{0.2}V_{0.8}H_{0.83}$ (d). The resonance frequency is 9 MHz (●), 22.5 MHz (○), 52 MHz (▲) and 90 MHz (△). Temperature dependence of ^1H T_1 for $Ti_{0.4}V_{0.6}H_{0.86}$ and $Ti_{0.2}V_{0.8}H_{0.86}$ at 22.5 MHz are plotted in (c) and (d), respectively, using the symbol (×) . Solid lines are the theoretical T_1 calculated using Eqs. (1)-(9). The top broken line shows the contribution of the conduction electrons, in which Korringa constant K is assumed to be the weighted average of K's for TiH_x and VH_x.

T_1 were 3.8, 5.2, 7.5 and 18 ms for $Ti_{0.2}V_{0.8}H_{0.83}$, $Ti_{0.4}V_{0.6}H_{0.91}$, $Ti_{0.6}V_{0.4}H_{0.91}$ and $Ti_{0.8}V_{0.2}H_{0.89}$, respectively. These results indicate that the ^1H-^{51}V dipolar interaction contributes dominantly to the total proton relaxation. The slopes of T_1 vs. $1/T$ plot were different between higher and lower temperature regions than the T_1 minimum. The slope in higher temperature region is steeper than in the lower temperature region. On the basis of the above-mentioned dependence of ^1H T_1 on the temperature and frequency for the β-$Ti_{1-y}V_yH_x$ the relaxation data are analyzed to obtain the activation parameters for hydorgen dynamics in the hydrides. The detailed procedure is described below.

For β-$Ti_{1-y}V_yH_x$ the proton spin-lattice relaxation is caused mainly by the fluctuation of the nuclear dipolar interaction due to the diffusional motion of protons. The total spin-lattice relaxation rate (T_1^{-1}) is therefore contributed by following three components [23]:

$$T_1^{-1} = T_{1(HH)}^{-1} + T_{1(HV)}^{-1} + T_{1e}^{-1} \qquad (5.11)$$

under the assumption that the spin-temperature concept holds, where $T_{1(HH)}^{-1}$ is the contribution of the ^1H-^1H dipolar interaction, $T_{1(HV)}^{-1}$ that of the ^1H-^{51}V dipolar interaction and T_{1e}^{-1} that of the interaction of ^1H with conduction electrons which satisfies the Korringa relation, $T_{1e} \cdot T = K$, where K is a constant. Contributions of the ^{47}Ti-^1H and ^{49}Ti-^1H dipolar interactions to the total T_1 are negligible.

The BPP relaxation equations for $T_{1(HH)}^{-1}$ and $T_{1(HV)}^{-1}$, generalized to include the distribution $F(S)$ of correlation times, can be written as follows by using Eqs.(5.6), (5.9) and (5.10) [10, 11, 19]:

$$T_{1(HH)}^{-1} = C_{HH}\int_{-\infty}^{+\infty} F(S)\left[\frac{\tau_c}{1+\omega_L^2\tau_c^2} + \frac{4\tau_c}{1+4\omega_L^2\tau_c^2}\right]dS \qquad (5.12)$$

and

$$T_{1(HV)}^{-1} = 2C_{HV}\int_{-\infty}^{+\infty} F(S)\left[\frac{\tau_c}{1+4(1-\alpha)^2\omega_L^2\tau_c^2} + \frac{3\tau_c}{1+4\omega_L^2\tau_c^2} + \frac{6\tau_c}{1+4(1+\alpha)^2\omega_L^2\tau_c^2}\right]dS,$$

(5.13)

where C_{HH} and C_{HV} are the dipolar strengths representing the magnitudes of the parts of dipolar interactions which are averaged out when the hydorgen diffusion takes place. ω_L is the Larmor frequency of ^1H and α the ratio of gyromagnetic ratio of ^{51}V to ^1H (γ_V/γ_H).

In Eq. (5.12) and (5.13) τ_c is the correlation time describing the fluctuation of the ^1H-^1H dipolar interaction by the proton diffusion. Using this correlation time the effective correlation time describing the fluctuation of the ^1H-^{51}V dipolar interaction is given by $2\tau_c$. The temperature dependence of the correlation time is represented by Arrhenius' activation law using the activation energy E_a^{app} and the pre-exponential factor τ_{0m} for the proton diffusion, as described in Eq. (5.5),

$$\tau_{cm} = \tau_{0m}\exp(\frac{E_a^{app}}{RT}), \tag{5.14}$$

when the fluctuations can be approximated by a thermally activated process.

The dipolar strengths C_{HH} and C_{HV} bring about information about the relative arrangements of the nuclei. These constants are the function of both the interatomic distances r_i for H-H pair and r_j for H-V pair and the concentration of the H and V nuclei. These constants are theoretically represented by

$$C_{HH} = \frac{4}{5}\gamma_H^4\hbar^2 I(I+1)x\sum_i r_i^{-6}, \tag{5.15}$$

and

$$C_{HV} = \frac{2}{15}\gamma_H^2\gamma_V^2\hbar^2 S(S+1)y\sum_j r_j^{-6}, \tag{5.16}$$

on the basis of the structural model [2, 4-6]. In those equations x is the content of H atom in the $Ti_{1-y}V_yH_x$ and y is the content of V atom in the $Ti_{1-y}V_yH_x$. The x and y are equal to the probability for finding H and V on each lattice point, respectively. I and S are nuclear spin quantum number for ^1H (I = 1/2) and ^{51}V (S = 7/2), respectively. The summations with respect to r_i and r_j are taken over the all lattice points occupied by hydrogen and metals.

We represent the distribution of the correlation times by a gaussian or lognormal distribution, as has usually done. The gaussian distribution is represented by [10,11]

$$F(S) = \frac{1}{\beta\sqrt{\pi}} \exp(-S^2/\beta^2) . \qquad (5.17)$$

If τ_{0m} is assumed to be approximately equal to τ_0, the parameter S can also be represented by S = $(E_a^{app} - E_a)/RT$. Usin this relation, the distribution function Eq. (5.17) gives a gaussian distribution of the activation energy. In this case, apparent activation energy E_a^{app} is a value at the maximum point of the distribution for activation energy (hereafter, we denote simply this parameter as E_a). As Eq. (5.14) is used to specify the temperature dependence of correlation time, there are two origins causing the distribution of the correlation time: one is the pre-exponential factor and the other the activation energy. It is reasonable to consider that these two distributions are mutually independent. Introducing the distribution parameters β_0 and β_Q to characterize the distribution of the pre-exponential factor and the activation energy, respectively, we can show that the total distribution parameter β in Eq. (5.17) has temperature-dependent and is represented by [24]

$$\beta^2 = \beta_0^2 + (\beta_Q/RT)^2 . \qquad (5.18)$$

Equation (5.18) implys that β_0 predominates the distribution of the correlation times as the temperature approaches infinite, while β_Q goverms thedistribution at low temperature. In other words, at infinite temperature the distribution of correlation times is governed by a single pre-exponential factor, and on cooling the contribution of the distribution of the activation energy to the distribution of the correlation times become effective. The variation of T_1 vs. $1/T$ curve with the change in β_0 and β_Q are shown in Fig. 5.3 (a) and (b), respectively. In Fig. 5.3 (a) the change in β_0 is affects the curvature around T_1 minimum of T_1 vs. $1/T$ curve; the V-shape of the T_1 vs. $1/T$ curve rounds out and the minimum value longer with increase in β_0 (increase in the width of the distribution of the pre-exponential factor). On the other hand, the change in β_Q affects the slope of T_1 vs. $1/T$ curve as shown in Fig. 5.3 (b); the slope of T_1 vs. $1/T$ curve

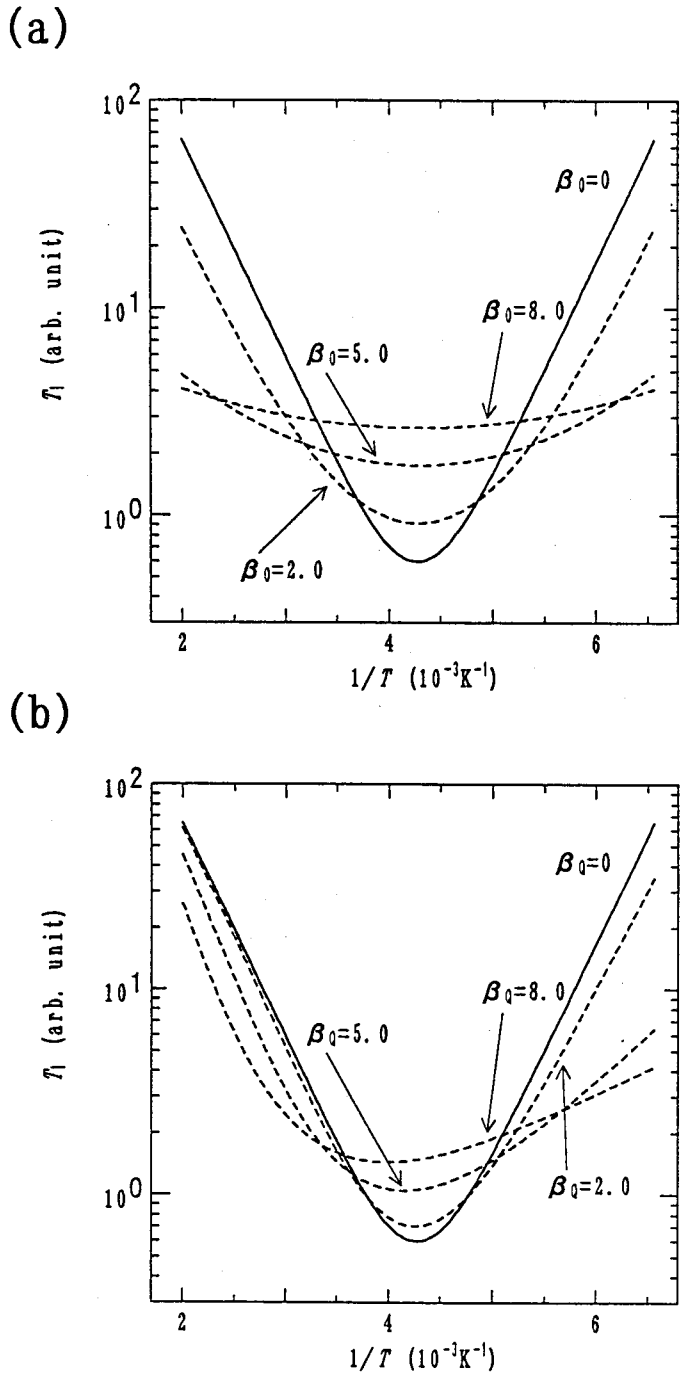

Figure 5.3 Dependence of T_1 on the distribution parameters β_0 (a) and β_Q (b).

at lower temperature than the temperature of T_1 minimum decreases drastically and the minimum value becomes longer with increase in β_Q (corresponding to the increase in the width of the distribution of activation energy), although the slope at the higher temperature than of T_1 minimum varies only slightly with β_Q.

In order to fit the experimental relaxation data and to derive the valuable information on the proton dynamics in Ti-V-H system we have to determine the six parameters, C_{HH}, C_{HV}, β_0, β_Q, τ_{0m} and E_a. The fitting procedure to fix these parameters will bring about the unambiguity and unreliability in these parameters. We then make some assumptions to the fitting parameters τ_{0m}, C_{HH} and C_{HV}.

First we attempt to fix the pre-exponential factor, τ_{0m}. Physically this parameter implies the reciprocal frequency factor of the fluctuation at infinit temperature, and the two types of assumption have been made by previous researchers [25-28] ; One is the simple assumption $\tau_0 = \nu_0^{-1}$ which was proposed by Walstedt *et al.* for diffusion of Na^+ in Na-almina [25]. ν_0 is a local vibrational frequency of the solute atom in an interstitial position. Other is more complicated assumption $\tau_0 = n\nu_0^{-1}\exp(\Delta S /R)$ which was proposed by Wert and Zener for diffusion of C and N in α-Fe [26]. n is the number of the nearest neighbor sites and ΔS is an entropy of excitation. In this workwe assume that $\tau_{0m} = 1/2\nu_0^{-1}$ which was proposed by Walstedt *et al.* [25]. ν_0 is a local vibrational frequency of hydrogen atoms in Ti-V alloy which was determined by the neutron scattering experiments for each hydrides as described in a previous section. We identify the value of the frequency of the most intense peak to $(2\tau_{0m})^{-1}$ in each hydride and value of ν_0 is listed in Table 5.1.

Next we look for a method to evaluate the dipolar strenghts for ^1H-^1H and ^1H-^{51}V. When the dipolar interaction is completely averaged out by the isotropic hydrogen diffusion, these parameters for β-Ti-V-H system are equal to the rigid lattice values. These values can be calculated using Eqs.(5.15) and (5.16), if the spacial arrangements of the lattice points for both H and metals are known in the bcc lattice. We found by the neutron scattering experiments that the hydrogen atoms are distributed at two kinds of tetrahedral (T_1- and T_2-) sites and an octahedral (O-) site and the dominant hydrogen site is specified by the alloy composition. The T_1-site predominates at Ti-rich composition but the O-site does at V-rich composition. As the

Table 5.1 Hydrogen and deuteron local vibrational frequencies in Ti-V alloy

Substance	ν_0^{H} a) (meV)	ν_0^{D} b) (meV)	τ_0^{H} c) (10^{-14} s)	τ_0^{D} c) (10^{-14} s)
$Ti_{0.2}V_{0.8}H_{0.83}$	44[d]	----	4.7	----
$Ti_{0.4}V_{0.6}H_{0.91}$	144	----	1.5	----
$Ti_{0.6}V_{0.4}H_{0.91}$	143	----	1.5	----
$TI_{0.8}V_{0.2}H_{0.89}$	139	----	1.5	----
$Ti_{0.2}V_{0.8}D_{0.79}$	----	31	----	13.0
$Ti_{0.4}V_{0.6}D_{0.80}$	----	102	----	4.2
$Ti_{0.6}V_{0.4}D_{0.86}$	----	101	----	4.2
$Ti_{0.8}V_{0.2}D_{0.79}$	----	98	----	4.2

a) evaluated by incoherent inelastic neutron scattering for β-$Ti_{1-y}V_yH_x$ the energy of the peak intensity of the local vibrational mode.

b) These values are derived from ν_0^{H} using Eq. (5.23).

c) These values are calculated by using the relation, 1meV = 0.2418 THz.

d) The experimental value for $Ti_{0.1}V_{0.9}H_{0.98}$.

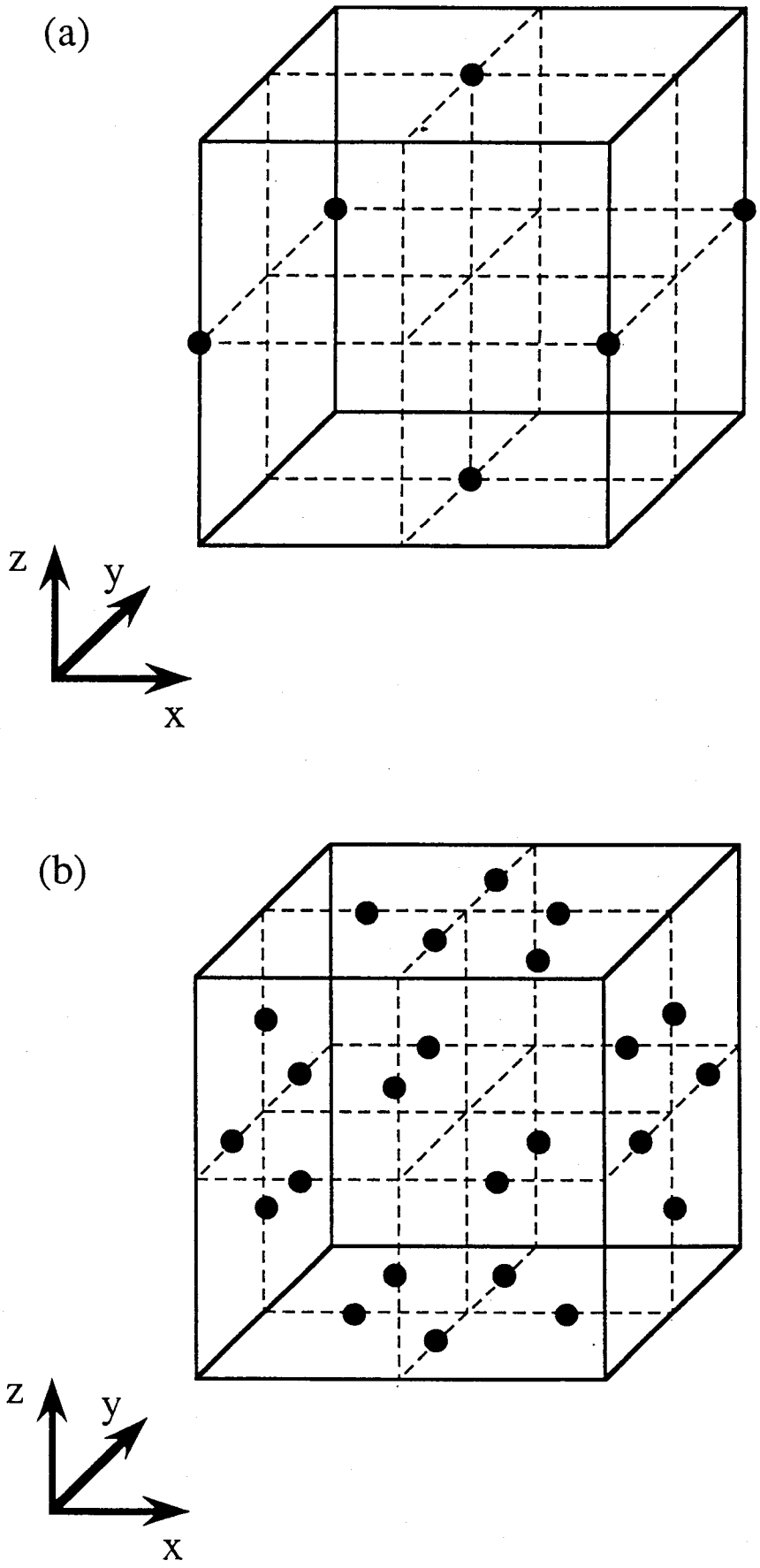

Figure 5.4 Model structure of bcc unit cell. Hydrogen occupys the O-site (a) and deuterium occupys the T-site (b). Metal atoms locate at (0,0,0), (1/2,1/2,1/2) and its equivalent positions. The sites of interstitial atom are denoted by full circles.

fraction of T_2-site is relatively small, this contribution to C is assumed to be negligible (T_1-site is denoted as T-site in the following discussion). To calculate C_{HH} and C_{HV} theoretically, the model structure of bcc unit cell, in which the hydrogen atoms populate the O-site and T-site independently, are made as shown in Fig. 5.4. In Fig. 5.4 (a), the hydrogen atoms locates at (0, 0, 1/2), (1/2, 1/2, 0) and their equivalent positions (O-site) to form a bcc lattice. If the hydrogen atoms occupy the all O-sites, the maximum molar ratio of hydrogen atoms to metals is 1. On the other hand, there are four T-sites on each of the surfaces of a cube, as shown in Fig. 5.4 (b). For example, available sites to a hydrogen atom are (1/4, 0, 1/2), (1/2, 0, 1/4), (1/2, 0, 3/4) and (3/4, 0, 1/2) on the *xz* plane projected along the *y* axis. However, it has been known that when a hydrogen atom enters a specified interstice of the metal lattice, the other T-sites located within 2.1 Å from it the first one are necessarily blocked for other hydrogens to enter there [29, 30]. Because the lattice constant are 3.2 ~ 3.4 Å in β-$Ti_{1-y}V_yH_x$, the distance between the nearest T-sites is less than 2.1Å. Hence, only one T-site among four can be populated by one hydrogen atom. Under this condition the maximum molar ratio of hydrogen atoms to metals is 1.5.

Under such restrictions on the distribution of hydrogens on the interstitial sites we calculated the lattice sum of H-H and H-V distances in the β-form of Ti-V alloy. The lattice sum $\sum r_i^{-6}$ for the H-H vectors is $50.47a_0^{-6}$ for the T-sites and $29.04a_0^{-6}$ for the O-sites. The lattice sum $\sum r_j^{-6}$ for the H-V vectors is $146.53a_0^{-6}$ for the T-sites and $169.56a_0^{-6}$ for the O-sites. In the actual system it has been known that the hydrogen atoms are distributed at both the T- and O-sites simultaniously with a fraction determined by the composition of the Ti-V alloys. In this case, the hydrogen atoms cannot occupy both the T- and O-sites simultaniously within 2.1 Å and the value of the lattice sum for each vector will be the value between for the T- and O-sites. Hence, the theoretical dipolar strengths can be given by the weighted average between the dipolar strength of the T-and the O-sites with the metal composition y, as follows:

$$C_{HH}(\text{av.}) = y \cdot C_{HH}(\text{O-site}) + \frac{2}{3}[1 - y] \cdot C_{HH}(\text{T-site}), \qquad (5.19)$$

and

$$C_{HV}(\text{av.}) = y \cdot C_{HV}(\text{O-site}) + [1 - y] \cdot C_{HV}(\text{T-site}). \qquad (5.20)$$

C_{HH}(T-site), C_{HH}(O-site), C_{HV}(T-site) and C_{HV}(O-site) are the individual dipolar strengths given by Eqs. (5.15) and (5.16). The factor 2/3 (the second term at right hand side in Eq. (5.19)) represents to convert the ratio of the hydrogen sites to the metals, 3 : 2, to the ratio of the hydrogen atoms to the metals, 1 : 1. The theoretical dipolar strength which governs the ^{1}H T_1 is over-estimated and the calculated T_1 minimum values are smaller than the ones for experimental values [31]. The H-H dipolar interaction is considered to contribute to the relaxation as the theory predicts, since the calculated values of the T_1 minimum are in good agreement with the experimental ones for the hydrides such as TiH_x, ZrH_x and HfH_x when this contribution was taken into account [32]. On the other hand, it has known that the experimental value of T_1 minimum in the α-ScH_x [45], TaV_2H_x ($0.22 \leq x \leq 1.54$) [16] and β-VH_x ($0.486 \leq x \leq 0.736$) [34], which is donimated by the H-M dipolar interaction, is much larger than the calculated value on the basis of the crystal structure. In the former two materials, the metal atoms form the hexagonal-closed -packed crystal lattice and the hydrogen atoms occupies one of the T-sites which locates along the c-axis with the separation ~1.35 Å. The localized motion hopping between these two sites brings about the additional T_1 minimum at the lower temperature than that of the proton diffusive motion. This localized motion is one of the origins for the over-estimation in the H-M dipolar interaction. In the latter material, the humps of T_1 appeare at the low temperature side of the T_1minimum and these humps become large with increase in the hydrogen concentration. In β-VH_x, two kinds of octahedral hydrogen sites O_{Z1} and O_{Z2} have been proposed. The hydrogen atom occupy only O_{Z1} site at the low hydrogen concentrations ($x \sim 0.486$) and the O_{Z2} site is partially occupied as more hydrogen atoms are added ($x \sim 0.736$). Hence these humps of T_1 have been assigned to the hydrogen motion occupying the O_{Z2} site. The presence of the tunneling motion of the hydrogen atoms below 100 K may also brings about the over-estimation in the H-V dipolar interaction. However, the origin of the over-estimation in the H-V dipolar interaction has not yet clarified. In order to evaluate the activation parameters the contribution of the H-V dipolar interaction is assumed to be supressed by adjustable parameter f and so the effective dipolar strength defined by $C'_{HV} = f$

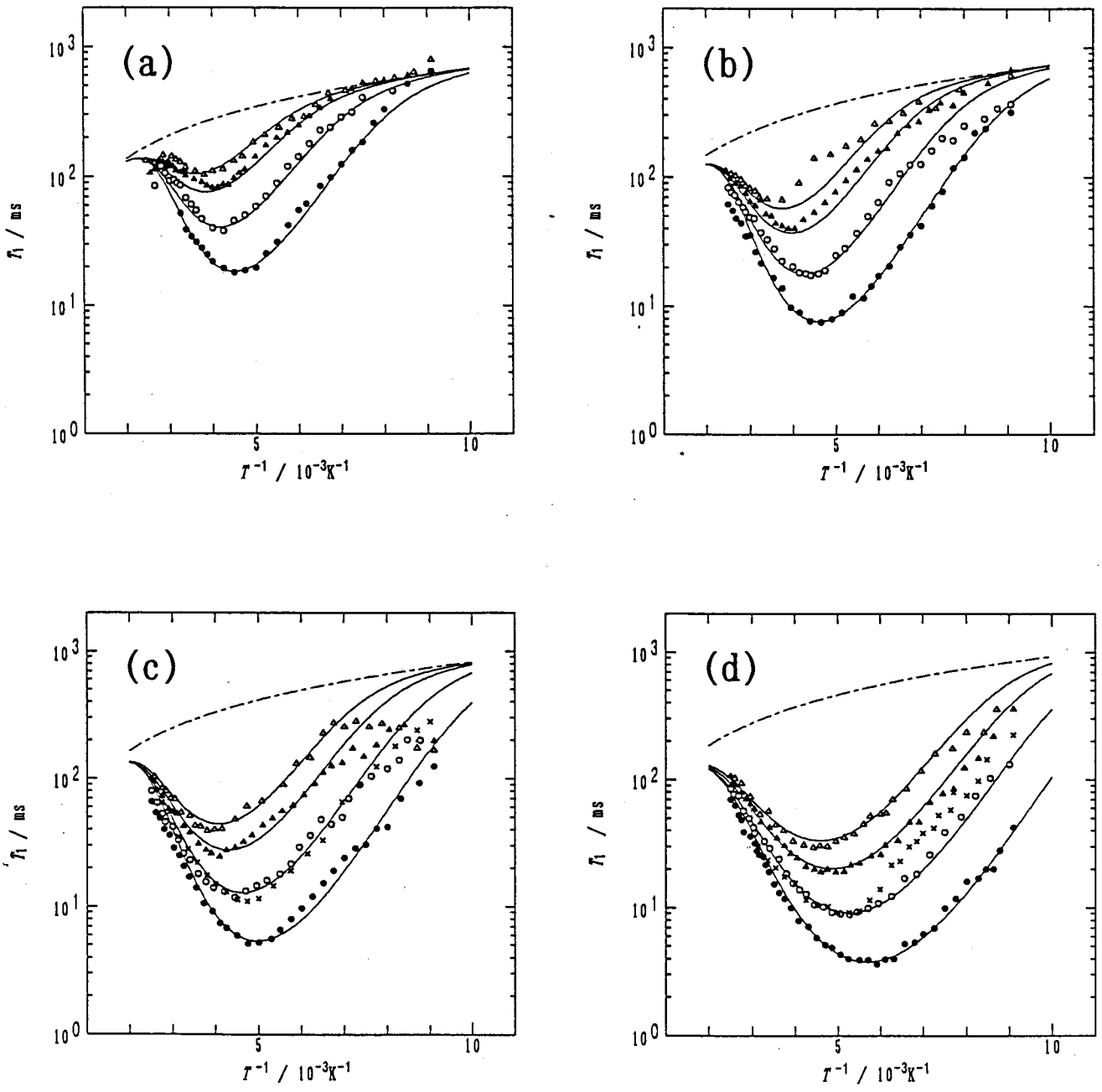

Figure 5.5 ^1H spin-lattice relaxation times, T_1, for $Ti_{0.8}V_{0.2}H_{0.89}$ (a), $Ti_{0.6}V_{0.4}H_{0.91}$ (b), $Ti_{0.4}V_{0.6}H_{0.91}$ (c) and $Ti_{0.2}V_{0.8}H_{0.83}$ (d), fitted by using Eqs. (5.11)-(5.18). The resonance frequency is 9 MHz (●), 22.5 MHz (○), 52 MHz (▲) and 90 MHz (△). The top broken line shows the contribution of the conduction electrons, in which Korringa constant K used are listed in Table 5.2.

Table 5.2 Relaxation parameters for β-$Ti_{1-y}V_yH_x$.

Substance	$C_{calc.}$ (10^9 s^{-2})		f	E_a (kJmol^{-1})	τ_{0m} (10^{-14} s)	β_0	β_Q (kJmol^{-1})	K (Ks)
	C_{HH}	C_{HV}						
$Ti_{0.2}V_{0.8}H_{0.83}$	3.90	10.0	0.6	17.5	4.7	2.7	2.9	93
$Ti_{0.4}V_{0.6}H_{0.91}$	3.98	6.58	0.6	21.8	1.5	2.4	4.2	83
$Ti_{0.6}V_{0.4}H_{0.91}$	3.83	3.98	0.6	23.5	1.5	2.1	4.6	74
$TI_{0.8}V_{0.2}H_{0.89}$	3.62	1.82	0.1	24.0	1.5	1.8	4.9	69

C_{HV} was used in the data fitting. The validity of this treatment will be discussed in the next section.

For the contribution of the conduction electrons to the T_1 in Eq. (5.11), we assume that the K values in the Korringa relation for β-$Ti_{1-y}V_yH_x$ is given by the weighted average of K's for TiH_x [33] and VH_x [34]. The results of the data fitting are shown in Fig. 5.5 (a) - (d) and the activation parameters obtained are listed in Table 5.2.

5.2.3 Discussion

The composition dependence of the apparent activation energy for the hydrogen diffusion in the Ti-V alloys has been known to reflect the degree of the disorder with respect to the arrangements of the metal atoms. The metal composition dependence of E_a determined from the ^1H T_1 data fitting is shown in Fig. 5.6(a) together with other literature data for the α-Ti-V-H system [35]. The apparent activation energy for the hydrogen diffusion decreases gradually from 24 $kJmol^{-1}$ for y = 0.2 to 21.8 $kJmol^{-1}$ for y = 0.6, and decreases rapidly to 17.5 $kJmol^{-1}$ for y = 0.8. The absolute values of E_a in other literature agree with our values very well and the literature data link smoothly to our data in the composition dependence curve despite the phase and the hydrogen concentrations are different. This result suggests that in the Ti-V alloys the activation energy for diffusive motion are dominantly determined by the interaction between metal and hydrogen atoms and by the local framework structure of metal lattice around the hydrogen atom.

At first, we try to interpret the composition dependence of E_a by means of the simple statistical model. In this model we assume two types of the hydrogen site, which are the T- and O-sites with the site populations $P_{T\text{-site}}$ and $P_{O\text{-site}}$. The site populations $P_{T\text{-site}}$ and $P_{O\text{-site}}$ are the probability to find the hydrogen atom at each interstitial site and depend on the alloy composition as shown in INIS experiments. The hydrogen atoms distributes both on the T- and the O-site with the site energy $\Delta H_{T\text{-site}}$ and $\Delta H_{O\text{-site}}$, respectively. In the case that the hydrogen distribution can be described by Boltzmann distribution function, the mean site energy $\Delta\overline{H}$ between the T-and the O-sites can be given by [44]

$$\Delta\overline{H} = \frac{\sum_{\text{site i}} P_i \Delta H_i \exp(-\Delta H_i / RT)}{\sum_{\text{site i}} P_i \exp(-\Delta H_i / RT)} . \qquad (5.21)$$

The activation energy E_a is given by the energy difference between the mean site energy and the saddle-point energy Q to which we allocated a constant value of -25.7 kJmol^{-1} for the Ti-V alloy (see Section 2.3) [35]. For $P_{\text{T-site}}$ and $P_{\text{O-site}}$ we assume to be proportional to the composition y. In this case, the population $P_{\text{T-site}}$ is given by 1-y and the $P_{\text{O-site}}$ is given by y. The composition dependence of E_a is calculated using Eq. (5.21) with the parameters $\Delta H_{\text{T-site}}$ = -50 kJ/mol and $\Delta H_{\text{O-site}}$ = -32 kJ/mol and the results are shown in Fig. 5.6(a) by broken line. In this case, the calculated E_a is approximately independent of the composition at 300 K and reaches the experimental data at the higher temperature such as 1000 K which is much higher temperature than that for the present work. Thus this situation is not reasonable to interpret the composition dependence of E_a.

Next, the composition dependence of E_a will be interpreted by means of the cluster model which take account of the short-range ordering of metals. Such an analysis brings about informations on the metal-hydrogen interaction and can derive the short-range order parameter which is one of the very important parameters characterizing the physical properties of disordered alloys. The cluster model assumes that the local framework structure of metal lattice around a hydrogen atom consists of octahedral $Ti_{6-i}V_i$ unit ; thus octahedron can assume seven different configurations depending on i. The bulk quantities are described by the statistical average of the various structure of the clusters. The activation energy $E_a(y, \sigma)$ for the hydrogen diffusion in the Ti-V alloys is represented by Eq. (2.17) ;

$$E_a(y, \sigma) = Q - \Delta\overline{H}(y, \sigma) ,$$

where y is the metal composition and σ the short-range order parameter as we explained in section 2.3. $\Delta\overline{H}(y, \sigma)$ is the enthalpy of solution of hydrogen in the metal, and given by Eq. (2.16) as a function of the alloy composition and the short-range order parameter. If the site

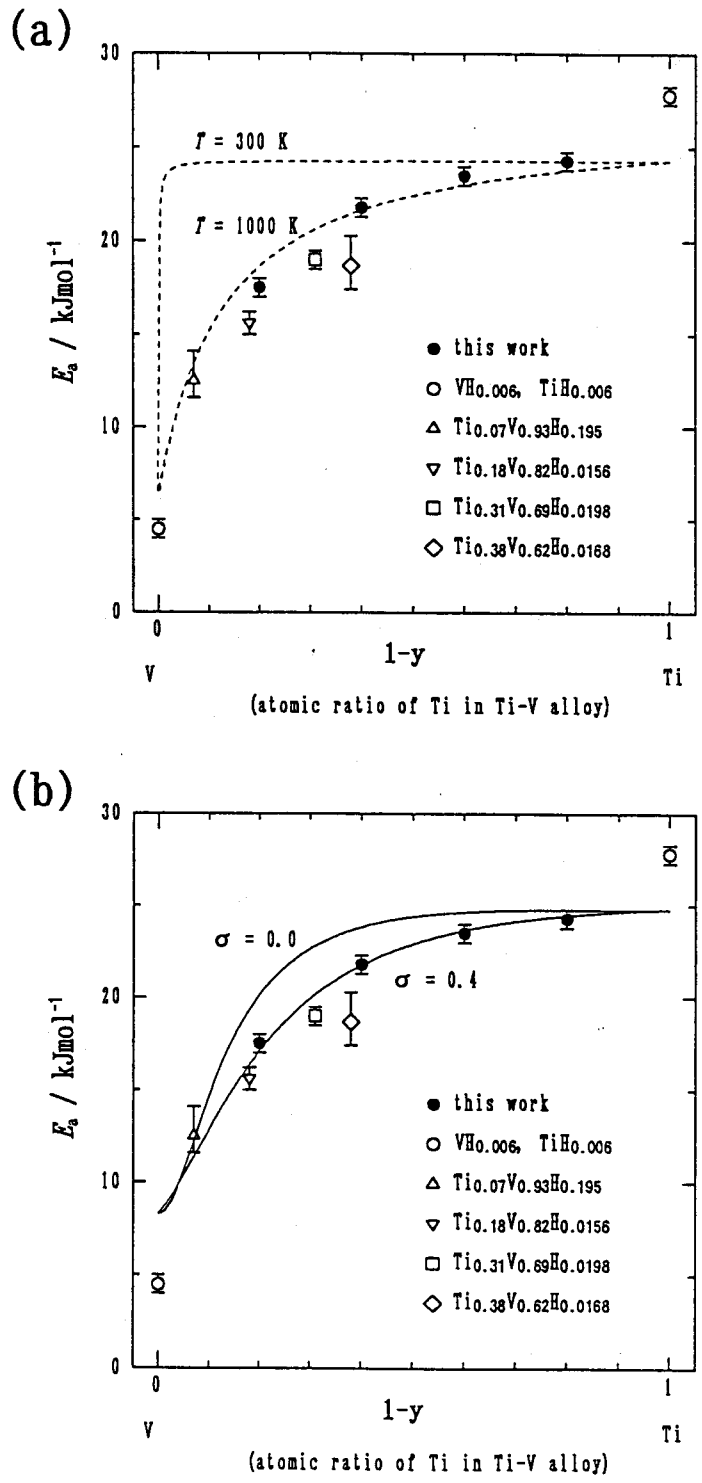

Figure 5.6 Alloy composition dependence of apparent activation energy E_a for proton diffusion in $Ti_{1-y}V_yH_x$. The calculated curves using the simple model (a) given by Eq.(5.21) on the different temperature 300 K and 1000 K, and the cluster model (b) given by Eqs. (2.15) - (2.17) on the different short-range order parameter $\sigma = 0$ and 0.4.

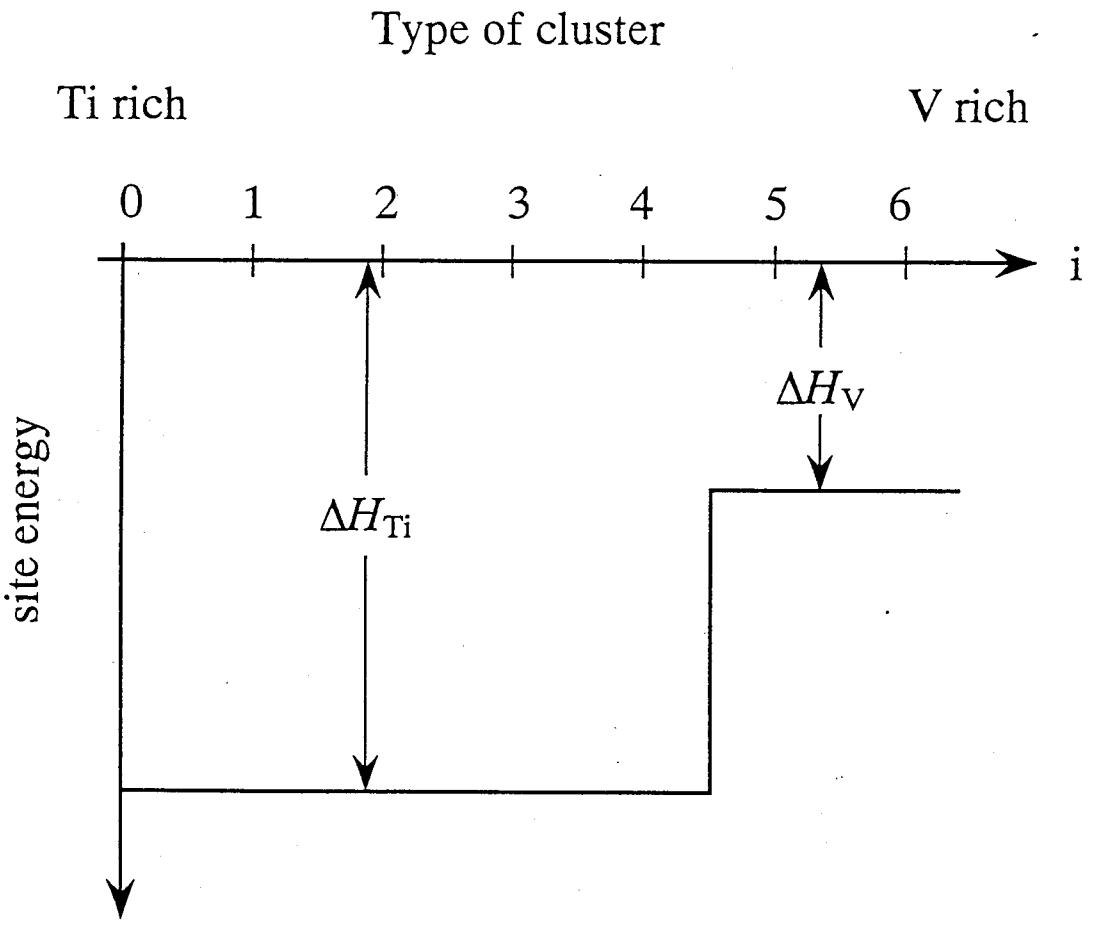

Figure 5.7 Schematic representation of the site energy, which depends on the type of clusters $Ti_{6-i}V_i$. The clusters with i values from 0 to 4 have a site energy ΔH_{Ti} which is the same as that in pure TiH_x, whereas the clusters with i = 5 and 6 have a site energy ΔH_V which is the same as that in pure VH_x. The site energy is assumed to vary discontinuously between i = 4 and 5 from ΔH_{Ti} to ΔH_V.

Table 5.3 Site energy, the chemical potential μ, and the short-range order parameter σ by the embeded cluster model.

System	ΔH_V (kJ/mol)	ΔH_{Ti} (kJ/mol)	μ (kJ/mol)	σ
Ti-V-H	-34	-50.5	-48.8	0.4
Ti-V-D	-40	-52	-52.8	0.4
V-H	-31.98(573K)[a)]	-------		
Ti-H	-------	-52.98(573K)[b)]		

a) Reference 37.

b) Reference 36.

energy $\Delta\overline{H}_i(y)$ in Eq. (2.16) is assumed to depend on the types of the clusters, the composition dependence of the activation energy can be evaluated theoretically according to the procedure described in section 2.3. The the energy scheme describing the relation between the site energy is assumed as shown in Fig. 5.7: In the Ti-rich regions the site energy is large and equal to the site energy of TiH_x, while in the V-rich regions the site energy is relatively small and equal to that of VH_x. The site energy in the border region was derived from the results of the neutron inelastic scattering. The clusters from i = 0 to 4 have the same site energy as TiH_x, meaning that the Ti-H interaction is dominat, whereas the clusters with i = 5 and 6 have the same site energy as VH_x, implying the V-H interaction is dominant. The composition dependence of E_a are calculated using Eq. (2.16) for $\sigma = 0$ and 0.4 at 298 K with ΔH_{Ti} = -50.5 kJ/mol and ΔH_V = -34 kJ/mol. The calculated curves are shown in Fig. 5.6(b) by the solid line. The calculated curves using this model are in agreement with the experimental data very well, comparing with the above simple model. Furthermore, the introduction of the short-range order parameter improve the agreement between the calculated and the experimental values. Using this model, the obtained metal-hydrogen interaction energies are ΔH_{Ti} = -50.5 kJ/mol and ΔH_V = -34 kJ/mol at 298 K and short-range order parameter is σ = 0.4 as listed in Table 5.3 with the results for the deuterides. The obtained metal-hydrogen interaction energies are in good agreement with -53 kJ/mol at 573 K for Ti-H [36] and -32 kJ/mol for V-H [37] in the pure metal hydrides. The difference in magnitudes between the Ti-H and V-H interaction energies affects obviously the configuration of cluster. For example, although Ti_2V_4 cluster contains more V atoms than Ti atoms its site energy is ΔH_{Ti}. This is caused by the larger affinity of the Ti atom to the hydrogen atom than the V atom. The short-range order parameter σ = 0.4 is also in good agreement with the previous value $\sigma = 0.43 \pm 0.05$ determined from the neutron inelastic scattering as well as other literature values $0.36 \le \sigma \le 0.51$ [35].

The dipolar strength of the ^1H-^{51}V dipolar interaction calculated by Eq. (5.16) and (5.20) are too large and so we introduced the reduction factor f. The reduction factor determined from data fitting and the calculated values of the dipolar strength are listed in Table 5.2. The f assumes the same value for $Ti_{0.6}V_{0.4}H_{0.91}$, $Ti_{0.4}V_{0.6}H_{0.91}$ and $Ti_{0.2}V_{0.8}H_{0.83}$, but much smaller for $Ti_{0.8}V_{0.2}H_{0.89}$. In the latter hydride the contribution of ^1H-^{51}V dipolar

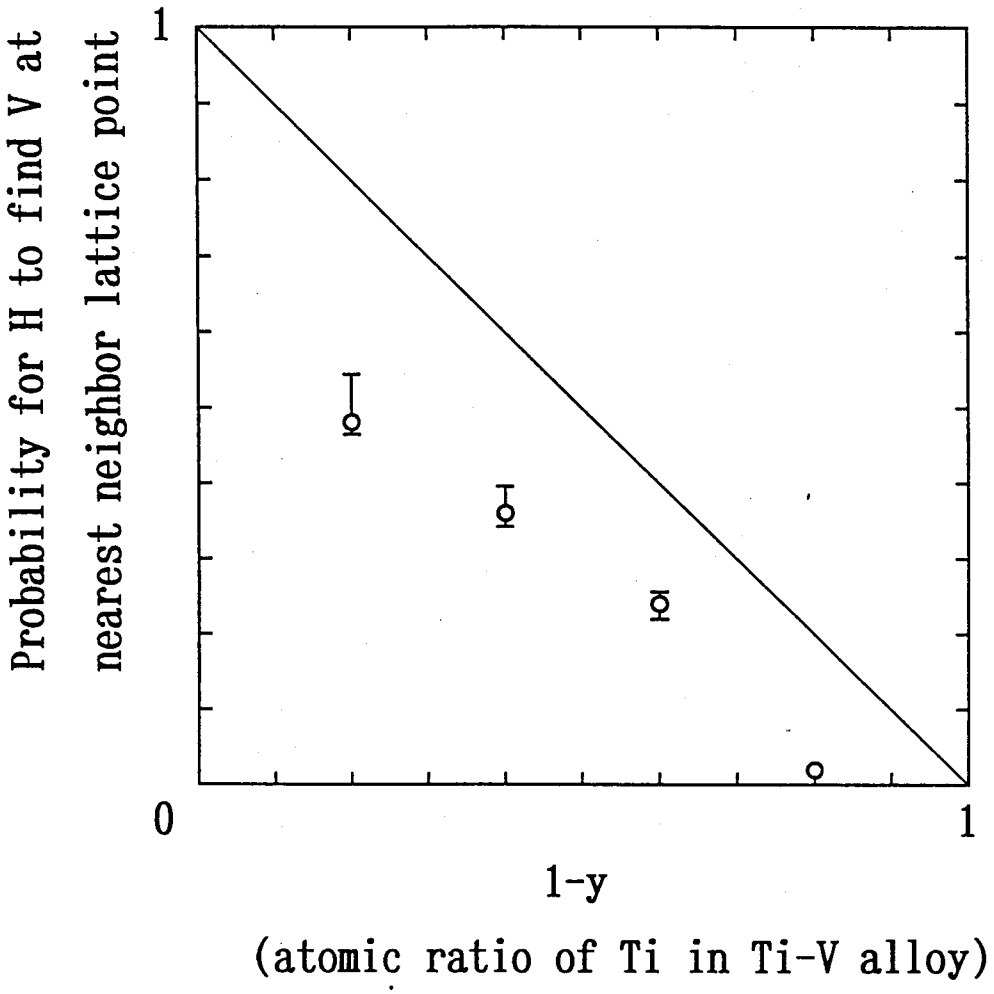

Figure 5.8 Effective concentration of V atom around a hydrogen atom in β-$Ti_{1-y}V_yH_x$, which is a product of the reduction factor *f* and the atomic ratio y of V to Ti+V. The solid line is an ideal concentration of V for the homogeneous distribution, which is equal to the alloy composition. The error bar indicates the range estimated under the assumptions that all the hydrogen atoms occupy the T- or O-site.

1. homogeneous distribution of hydrogen atoms

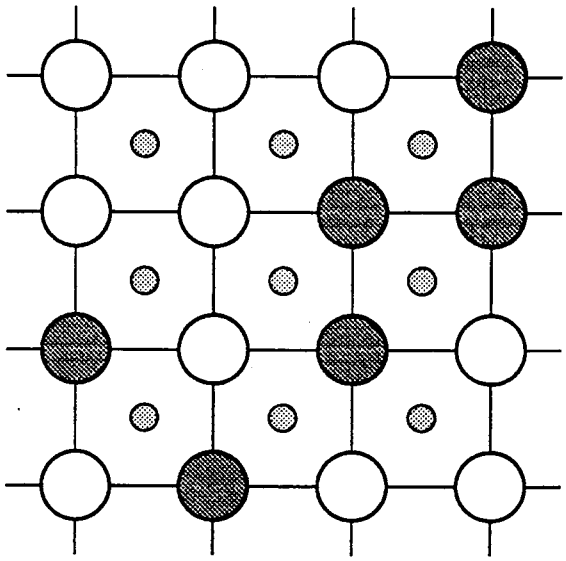

ex)

Metal : 9 atoms

Hydrogen : 4.5 atoms

V

Ti

1/2 H

2. inhomogeneous distribution of hydrogen atoms

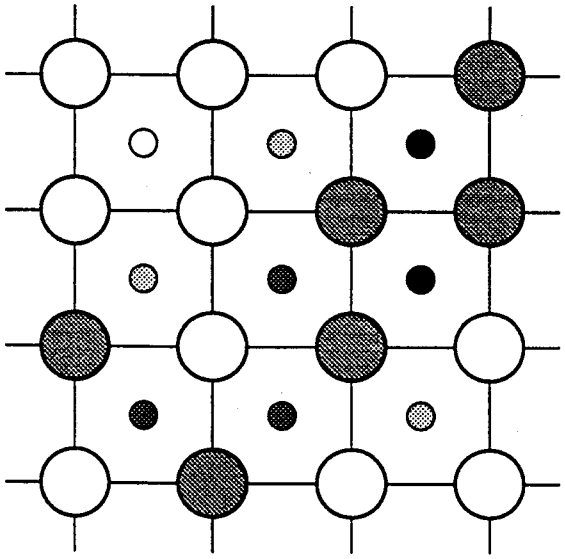

1 H

2/3 H

1/6 H

~ 0 H

Figure 5.9 Schematic representation of homogeneous and inhomogeneous distribution of hydrogen atoms in the Ti-V alloy. In this scheme, 9 metal atoms (Ti and V) form a two-dimensional square lattice, and 4.5 hydorgen atoms are able to enter its interstices. The large circles denote the metal atoms. The probability to find the hydrogen atom at an interstice depends on the framework arrangements of metals around the interstice. It is distinguished by the depth of the shade.

interaction is negligibly small, and the ^{1}H-^{1}H dipolar interaction governs the relaxation. The fact that the reduction factor for the ^{1}H-^{51}V dipolar interaction depends strongly on the alloy composition implies that there is a clustering or a short-range ordering with respect to the arrangements of the metals around a hydrogen atom and therefore a biased distribution of hydrogen atoms over the interstices is generated. Inhomogeneous distribution of hydrogen atoms in the Ti-V alloys can cause the composition dependence of the reduction factor in the ^{1}H-^{51}V dipolar interaction. If the hydrogen atoms are homogeneously distributed over all the interstices, the probability for a proton to find a V atom at the nearest neighbor lattice point is a function of only the alloy compositions y. The inhomogeneous distribution of hydrogen atoms changes the probability for a proton to find a V atom at the nearest neighbor. Using the reduction factor f, the probability is described by the effective concentration of V atoms, $f \cdot y$. Figure 5.8 shows the variation of this probability of V atoms as a function of the alloy composition. The reduction factor f for the dipolar strength with V content corresponds to selective clustering of metal atoms: That is, it implies that the hydrogen atoms tend to gather around Ti atoms. Such a situation is schematically shown in Fig. 5.9. The upper scheme represents the homogeneous distribution of the hydrogen atoms in the Ti-V alloy, in which all of interstices have the same probability for hydrogen occupation. For example, in the case of the scheme consisting of 9 metals and 9/2 hydrogen atoms, the 9 interstices are occupied by the hydrogen atom with the probability 1/2, irrespective of the kinds of metals around the interstices. The lower scheme represents the inhomogeneous distribution of the hydrogen atoms in the Ti-V alloy. In this case, the probability to find the hydrogen atoms at the interstices depends on the kind of the metal around the interstices. The interstice surrounded by three Ti and one V atoms is occupied by a hydrogen atom with a probability 1, whereas the interstice surrounded by four V atoms is hardly occupied. The probability to find a hydrogen atom at the interstices increases with increasing in the number of the Ti atoms. The inhomogeneous distribution of hydrogen atoms is caused by the difference in the interactions between Ti-H and V-H. As the affinity of a hydrogen atom to a Ti atom is higher than that to a V atom, the hydrogen atoms have a tendency to gather around Ti rich regions. This picture is consistent with the site energy scheme described above.

5.3 ^{2}H NMR

5.3.1 Experimental

^{2}H NMR measurements were carried out with a Bruker Model MSL-400 pulsed spectrometer with a superconducting magnet and the Larmor frequency for ^{2}H was 61.4 MHz. The rf irradiation coil in the probe-head for ^{2}H signal detection was changed to 5 mmϕ coil (0.8 mmϕ Cu wire with 28 turn ca. 30 mm long) from 10 mmϕ in order to improve the efficiency of the rf irradiation. For D_2O the length of 90° pulse was improved to 2.95 μs from 7 μs by this alternation. The deuteron spin-lattice relaxation times (T_1) were measured in the temperature range between 125 and 400 K using the 90° - τ - 90° and/or saturation recovery methods. The experimental uncertainty was less than ± 5 %. The temperature was controlled with the accuracy of ± 1 K by Bruker variable temperature unit VT-1000 by the flow of cooled or heated nitrogen gas. The deuterides used in ^{2}H NMR experiments had the following compositions ; $Ti_{0.8}V_{0.2}D_{0.79}$, $Ti_{0.6}V_{0.4}D_{0.86}$, $Ti_{0.4}V_{0.6}D_{0.80}$ and $Ti_{0.2}V_{0.8}D_{0.79}$. Each sample was sealed into a glass ampoule (5 mmϕ and ca. 30 mm long) with He heat exchange gas (~150 mmHg).

5.3.2 Results and analysis

The magnetization recovery curves for $Ti_{0.8}V_{0.2}D_{0.79}$, $Ti_{0.6}V_{0.4}D_{0.86}$, $Ti_{0.4}V_{0.6}D_{0.80}$ and $Ti_{0.2}V_{0.8}D_{0.79}$ show non-exponential behavior and the typical data are plotted in Fig. 5.10 and 5.11. The degree of non-exponential decay was relatively small and depended on the temperature and the alloy composition. For example, the recovery curves of $Ti_{0.4}V_{0.6}D_{0.80}$ could be approximated by a single exponential decay, except the data at 164 K, whereas the recovery curves of $Ti_{0.6}V_{0.4}D_{0.86}$ show non-exponential behavior over all temperature range. The non-exponential behavior may be caused by existence of multi-phases in deuterides, the cross-relaxation of ^{2}H through ^{51}V spin system, and different relaxation process between quadrupolar multi-levels. First of all, we tried to fit the recovery curves assuming the superimpose of two single exponential decays. The two components of T_1 were distinguished below the temperature of the T_1 minimum and had similar slope of T_1 vs. $1/T$ curve to each other as shown in Fig. 5.12 (a) - (d). These results suggest that the dynamical behavior of deuterons can be deduced from either of those two components, if it is reasonable to have

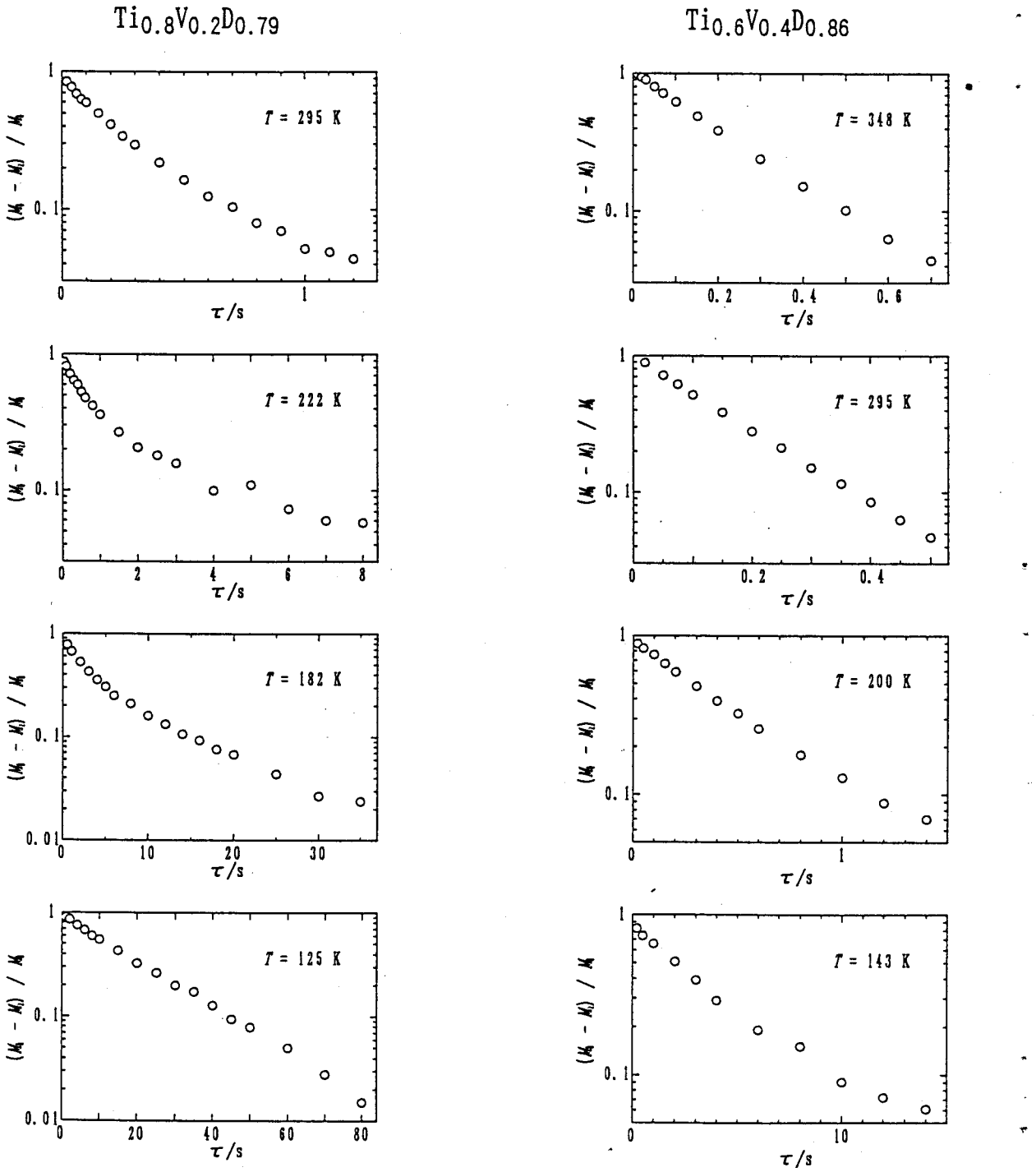

Figure 5.10 Recovery curves of ^2H magnetization of β-$Ti_{0.8}V_{0.2}D_{0.79}$ (left hand column) and β-$Ti_{0.6}V_{0.4}D_{0.86}$ (right hand column).

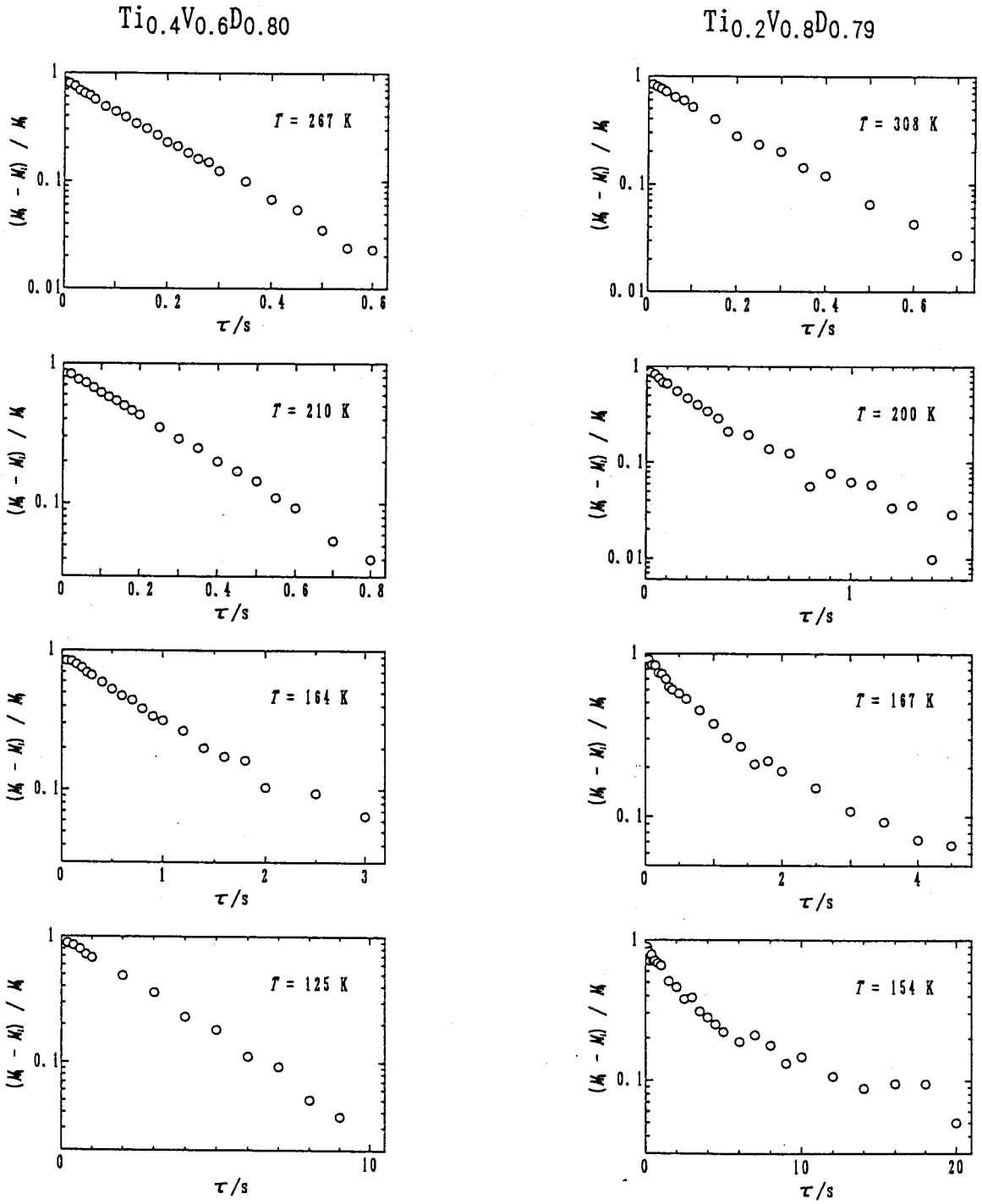

Figure 5.11 Recovery curves of ^2H magnetization of β-$Ti_{0.4}V_{0.6}D_{0.80}$ (left hand column) and β-$Ti_{0.2}V_{0.8}D_{0.79}$ (right hand column).

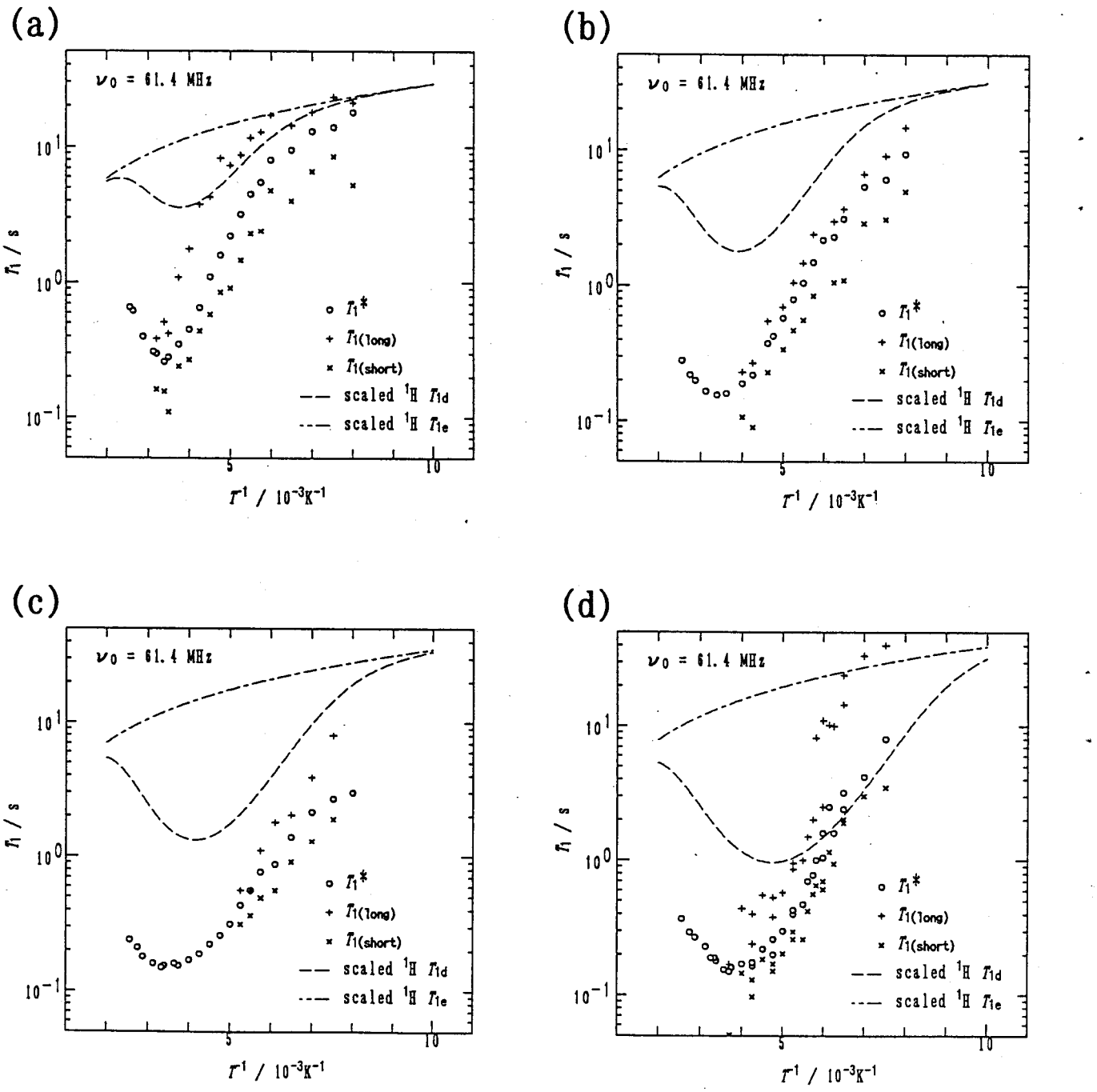

Figure 5.12 Temperature dependence of ^2H spin-lattice relaxation times for $Ti_{0.8}V_{0.2}D_{0.79}$ (a), $Ti_{0.6}V_{0.4}D_{0.86}$ (b), $Ti_{0.4}V_{0.6}D_{0.80}$ (c) and $Ti_{0.2}V_{0.8}D_{0.79}$ (d). The T_1^* (O), $T_{1(long)}$ (+) and $T_{1(short)}$ (X) are plotted as afunction of the reciprocal temperature. The resonance frequency is 61.4 MHz. The broken and dashed lines show the contribution of ^2H-^{51}V dipole interaction and of the conduction electrons, respectively, which are given by scaling of the ^1H spin-lattice relaxation times by multiplying the factor, 42.44 (= γ_H^2/γ_D^2).

assumed the two component relaxation mechanism for these deuterides. However, the validity of such analysis cannot be ascertained because of the complexities of the systems. Anyway, as it was difficult to determine the unique ^2H T_1 values, the apparent relaxation time T_1^* was defined as the time at which the longitudinal magnetization reduces to 1/e of the initial value and it will be used in the following discussion. The obtained T_1^* values are plotted as a function of inverse temperature in Fig. 5.12 (a) - (d). The T_1^* vs. $1/T$ curves show a minimum for all samples. The values and temperatures at T_1^* minimum depend on the composition of the Ti-V alloys in the similar way as the hydrides. The temperatures at which the T_1^* minimum was observed were 274, 275, 287 and 292 K for $Ti_{0.2}V_{0.8}D_{0.86}$, $Ti_{0.4}V_{0.6}D_{0.80}$, $Ti_{0.6}V_{0.4}D_{0.86}$ and $Ti_{0.8}V_{0.2}D_{0.79}$, respectively. On the other hand, the T_1^* minimum values for $Ti_{0.2}V_{0.8}D_{0.86}$, $Ti_{0.4}V_{0.6}D_{0.80}$, $Ti_{0.6}V_{0.4}D_{0.86}$ coincided with each other to be 150 ms within the experimental error. For $Ti_{0.8}V_{0.2}D_{0.79}$ the minimum value of T_1^* was 260 ms. On the basis of these results of the ^2H T_1 measurements for the β-$Ti_{1-y}V_yD_x$ the relaxation data are analyzed to obtain the activation parameters for deuteron dynamics in these deuterides, which are used to specify the favorable deuteron sites and to examine the isotope effect on the restricted potential wells at the interstices.

For β-$Ti_{1-y}V_yD_x$ the total spin-lattice relaxation rate (T_1^{-1}) are mainly described by three components as follows [38]:

$$T_1^{-1} = T_{1Q}^{-1} + T_{1(DV)}^{-1} + T_{1e}^{-1}, \qquad (5.22)$$

where T_{1Q}^{-1} is a contribution of the quadrupole interaction of deuteron, $T_{1(DV)}^{-1}$ of the ^2H-^{51}V dipolar interaction and T_{1e}^{-1} of the interaction with conduction electrons. T_{1e}^{-1} is assumed to satisfy the Korringa relation, $T_{1e} \cdot T = K_D$. Contributions of the ^{47}Ti-^2H and ^{49}Ti-^2H and ^2H-^2H dipolar interactions to the total T_1 are negligible because of the small gyromagnetic ratios of ^{47}Ti, ^{49}Ti and ^2H. It is difficult to estimate three contributions in Eq. (5.22) independently from the experimental data. Assuming that the $T_{1(DV)}^{-1}$ and T_{1e}^{-1} are dominated by the similar fluctuation to dipolar interactions in the hydrides, the $T_{1(DV)}^{-1}$ and T_{1e}^{-1} for deuterides can be represented by the scaling the total spin-lattice relaxation rates of proton in the hydrides with the

square of the nuclear gyromagnetic ratios (γ_H^2/γ_D^2). We used the ^{1}H spin-lattice relaxation times to estimate the contribution of ^{2}H-^{51}V dipolar interaction and the interaction with conduction electrons of deuterons. The $T_{1(DV)}^{-1}$ and T_{1e}^{-1} estimated from ^{1}H data are shown in Fig. 5.12 (a) - (d) with dotted and broken lines, respectively. The estimated total T_1 values were too long to interpret the experimental data by an order of magnitude. Hence it was revealed that the quadrupolar relaxation process of ^{2}H nuclei is the dominant relaxation mechanism in the deuterides. The quadrupolar relaxation time, T_{1Q}^{-1} for ^{2}H nuclei is represented by BPP equation with a gaussian or lognormal distribution $F(S)$ of the correlation times (see in Eq.(5.17)) and the distribution parameter β which depends on temperature as described in Eq. (5.18), as follow :

$$T_{1Q}^{-1} = \frac{3}{40}(1+\frac{\eta^2}{3})(\frac{e^2Qq}{\hbar})^2 \int_{-\infty}^{+\infty} F(S)[\frac{\tau_c}{1+\omega_L^2\tau_c^2} + \frac{4\tau_c}{1+4\omega_L^2\tau_c^2}]dS, \quad (5.23)$$

where $e\,^2Qq$ /h is the quadrupole coupling constant (QCC) representing the strength of quadrupole interaction. The η is the asymmetry parameter of the electric field gradient at the deuteron site, and ω_L is the Larmor frequency of ^{2}H nucleus. In Eq. (5.23) τ_c is the correlation time describing the time fluctuation of the electric field gradient and τ_{cm} the mean correlation time. The temperature dependence of the correlation time is represented by the Arrhenius' activation law in Eq. (5.14). Equation (5.23) is used to analyze the experimental data of the ^{2}H T_1 in our disordered systems.

For the data analysisby the case of the above equation the fitting parameters (adjustable parameters) are QCC, η, β_0, β_Q, τ_{0m} and E_a. We put two assumptions on η and τ_{0m} to reduce the number of the fitting parameters. The first assumption is on the asymmetry parameter of the electric field gradient, η. This parameter reflects generally the site symmetry of the ^{2}H nuclei. In the alloys the ^{2}H nuclei is assumed to exist in the ionic form, $^2H^+$ (deutron). Since the symmetry of the T- and O-sites for deuteron is not considered to be low to produce large asymmetry in the electric field gradient, we assume that the η is zero. Next the same

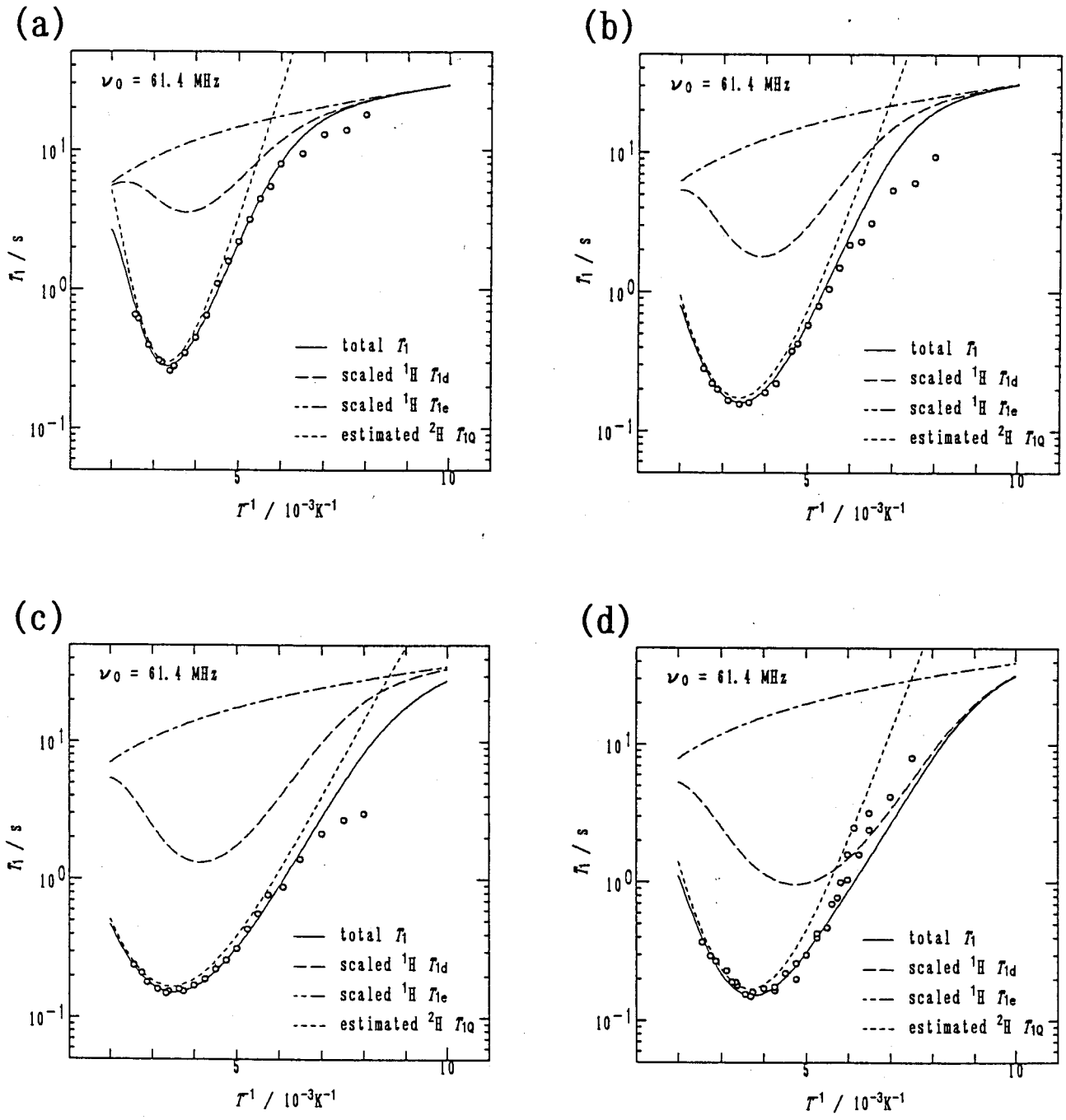

Figure 5.13 Temperature dependence of apparent ^2H spin-lattice relaxation times (T_1^*) for $Ti_{0.8}V_{0.2}D_{0.79}$ (a), $Ti_{0.6}V_{0.4}D_{0.86}$ (b), $Ti_{0.4}V_{0.6}D_{0.80}$ (c) and $Ti_{0.2}V_{0.8}D_{0.79}$ (d). The resonance frequency is 61.4 MHz. Solid lines are the results of data fitting with Eq. (5.23), and dotted line represents contribution of quadrupole relaxation time of deuteron. The broken and dashed lines show the contribution of ^2H-^{51}V dipole interaction and the conduction electrons, respectively, which are given by scaling the ^1H spin-lattice relaxation times with a factor of the square of the nuclear gyromagnetic ratios, 42.44 ($= \gamma_H^2/\gamma_D^2$).

Table 5.4 Quadrupole relaxation parameters deduced from the T_1^* data.

Substance	QCC (kHz)	E_a (kJmol^{-1})	τ_{0m} (10^{-14} s)	β_0	β_Q (kJmol^{-1})
$Ti_{0.2}V_{0.8}D_{0.79}$	30	20.7	13.0	1.8	3.3
$Ti_{0.4}V_{0.6}D_{0.80}$	36	24.0	4.2	3.2	5.2
$Ti_{0.6}V_{0.4}D_{0.86}$	32	25.5	4.2	2.3	4.5
$Ti_{0.8}V_{0.2}D_{0.79}$	21	26.0	4.2	0.0	4.5

assumption as in the case of the analysis of ^1H T_1 is imposed upon the pre-exponential factor, τ_{0m}. The correlation time for the fluctuation of the EFG tensor in the deuterides is twice as large as that for the fluctuation of the H-H vector in the hydrides. Thus, the correlation time is the deuterides is given by $\tau_{0m} = \nu_0^{-1}$. In this case, the ν_0 is the local vibrational frequency of deuterium atoms in Ti-V alloy. Its value for each deuteride was evaluated from the ν_0 deduced by INIS for hydride using the relation [39]

$$\nu_0^{D} \sim \nu_0^{H} \cdot \sqrt{\frac{m_H}{m_D}}. \qquad (5.24)$$

The values of ν_0^D are listed in Table 5.4 with the ν_0 of the hydrogen for Ti-V-D systems.

The results of the analysis of T_1 of ^2H using Eq. (5.23) are shown in Fig. 5.13 (a) - (d). The broken and solid lines correspond to the contribution of the quadrupole relaxation and the total one, respectively. The activation parameters determined from the data fitting are listed in Table 5.5.

5.3.3 Discussion

The activation parameters detremined from the data fitting give us the useful informations on the nature of the deuterium sites and the isotope effect on the metal-H(D) interaction. The quadrupole coupling constant (QCC) is an excellent clue to the deuteron site symmetry and the strength of the metal-deuterium interaction. Comparsion of the QCC with those in other deuterides reveals the deuteron site symmetery in β-$Ti_{1-y}V_yD_x$. The alloy composition dependence of the activation energy, E_a, is an excellent clue to the local framework structure around a deuterium and the comparsion of the E_a between hydrides and deuterids brings about the detailed information on the potential wells at interstices for the H and/or D.

At first, we evaluate the feature of the deuteron sites in the Ti-V alloys on the basis of the QCC values determined. The QCC values in some deuterides at the specified sites are listed in Table 5.5 together with the present results. The deuteron occupies the T-site in α'-TaD_x, β-NbD_x and δ-VD_x [40]. These deuterides give small QCC values ranging in 37 ~ 55 kHz regardless of the difference in the way of the deuterium distribution (ramdom or ordered) [38].

Table 5.5 Quadrupole coupling constant for metal deuterides.

Substance	QCC / kHz	Site for D	reference
$Ti_{0.2}V_{0.8}D_{0.79}$	30	T-site	this work
$Ti_{0.4}V_{0.6}D_{0.80}$	36	T-site	this work
$Ti_{0.6}V_{0.4}D_{0.86}$	32	T-site	this work
$Ti_{0.8}V_{0.2}D_{0.79}$	21	T-site	this work
α'-TaD_x ($0.43<x<0.60$)	40	T-site (random)	38
α'-$TaD_{0.76}$	37	T-site (random)	38
α-TaD_x	40	T-site (random)	38
β-$TaD_{0.60}$	43 (at 313 K)	T-site (ordered)	38
β-$NbD_{0.55}$	45 (at 217 K)	T-site (random)	38
β-VD_x ($0.5<x<0.6$)	105 (< 210 K)	O-site (ordered)	41
δ-VD_x ($0.5<x<0.6$)	55 (< 210 K)	T-site (ordered)	38

In β-VD_x, in which the deuterons are occupying the O-site and forming bcc sub-lattice, the QCC value has been known to be 105 kHz below 210 K [41]. In the present work the QCC in $Ti_{1-y}V_yD_x$ have the values of 21 ~ 36 kHz. These QCC values implies that the deuterons are dominantly occupying the T-site in $Ti_{1-y}V_yD_x$. In Chapter 2 we found by INIS that in the case of the hydrides the hydrogens are distributed over two kinds of tetrahedral sites (T_1- and T_2-site) and the octahedral site. The fraction in the T_1-site increases with increase in Ti content, whereas that is the O-site increases with increase in V content. The T_2-site fraction is approximately independent of the composition. It is remarkable that the manner of the distribution of hydrogen is different between the hydride and the deuteride in the case of Ti-V alloy. Such remarkable difference in the atomic distributions is also found between the pure metal hydride VH_x and deuteride VD_x. These results suggest that the V-H and/or V-D interactions in the pure metals are still existing in the alloys. The QCC values of $Ti_{1-y}V_yD_x$ are relatively small by comparison with those of deuterons occupying the T-site in other hydrides. The magnitude of the QCC is considered to reflect the degree of disorder of the host alloys. The disorder work to average the electric-field-gradent (EFG) partially and as a result the QCC value decreases.

Next we examine the alloy composition dependence of the activation energy E_a for the diffusion of deuterons. The alloy composition dependence of activation energy is shown in Fig.5.14 together with that in the hydrides. The E_a for the deuteron diffusion decreases gradually from 26 $kJmol^{-1}$ for y = 0.2 to 24 $kJmol^{-1}$ for 0.6, and decreases drastically to 20.7 $kJmol^{-1}$ for y = 0.8. This composition dependence of the E_a is analyzed by the same procedure as that applied to the hydrides, details of which were already described in Section 5.2.3. The similar composition dependence of E_a in the hydride and the deuteride implies that the degree of disroder and the framework arrangements of metal atoms are similar in the hydride and the deuteride of Ti-V alloys. Thus we analyzed the deuterium T_1 data by adopting the same value of short-range order parameter, σ = 0.4 to that in the hydride. The calculated E_a as a function of the alloy composition is shown in Fig. 5.14 with solid line, and the parameters obtained were listed in Table 5.4.

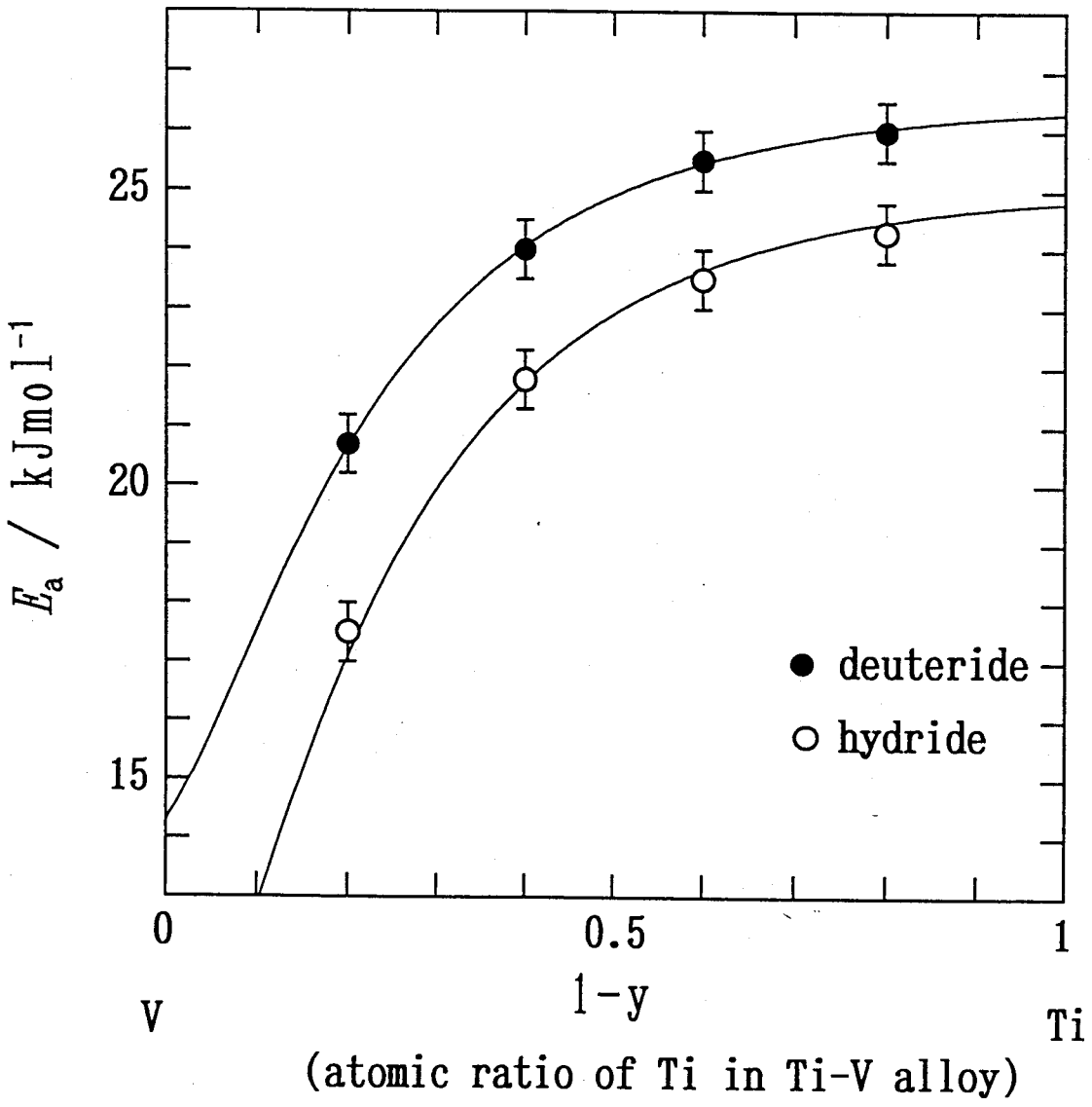

Figure 5.14 Alloy composition dependnce of apparent activation energy E_a for diffusion of interstitial atoms in Ti-V alloys ; $Ti_{1-y}V_yD_x$ (●) and $Ti_{1-y}V_yH_x$ (○). The solid lines are the theoretical curves calculated using Eqs. (2.15) - (2.17).

The isotope effect on the E_a is an important measure of the M-H(D) interactions which determine the potential wells restricting the H or D motion in the interstices in Ti-V alloys. For the M-H(D) interaction discussed above, the absolute values of the ΔH_V and the ΔH_{Ti} in the deuterides are larger than those in the hydrides. These differences brings about the difference of activation energy between H and D. The difference between the activation energy for diffusion in the hydride and the deuteride are shown in Fig. 5.15. The relation $|\Delta H_{Ti}^D| > |\Delta H_{Ti}^H|$, $|\Delta H_V^D| > |\Delta H_V^H|$ and $|E_a{}^D| > |E_a{}^H|$ holds (see in Table 5.3) and it can probably interpreted by the difference in the zero point energies between the hydride and the deuteride caused by the atomic mass effect. Suppose that the hydrogen and/or deuterium local vibrational motion is approximated by a harmonic ocillator. Then the magnitude of the difference in the E_a is given by

$$\Delta E_a = E_a^D - E_a^H = \frac{1}{2}h(\nu_0^D - \nu_0^H) = \frac{1}{2}h\nu_0^H(1 - \frac{1}{\sqrt{2}}), \qquad (5.25)$$

where $\nu_0{}^H$ is the frequency of the local vibrational mode for the hydride [42] and Eq. (5.24) was applied. Using Eq. (5.25) with the values of $\nu_0{}^H$ in Table 5.1 the differences in the activation energy between the hydrides and the deuterides are estimated to be ~20 mev (~2 kJ/mol) for $h\nu_0{}^H$ = 140 meV and ~6 meV (~0.6 kJ/mol) for $h\nu_0{}^H$ = 44 meV. For $Ti_{0.8}V_{0.2}H_{0.89}$, $Ti_{0.6}V_{0.4}H_{0.91}$ and $Ti_{0.4}V_{0.6}H_{0.91}$, in each of which the hydrogen atom occupies the T-site, the predicted energy differences are in good agreement with the experimental ones. The energy difference of ~22 meV (~2.2 kJ/mol) is predicted for the Ti-H interaction if we use the local vibrational mode $h\nu_0{}^H$ = 147.6 meV observed in TiH_2 at 300 K [43]. This estimated energy difference is also in good agreement with the experimental value $|\Delta H_{Ti}^D| - |\Delta H_{Ti}^H|$ = 2.5 kJ/mol. However, for $Ti_{0.2}V_{0.8}H_{0.83}$, in which the hydrogen atom occupies the O-site, the predicted energy difference is about 5 times greater than the experimental value. The predicted energy difference for the V-H interaction is ~8 meV (~0.8 kJ/mol) for the mean value $h\nu_0{}^H$ = 53.5 meV of two local vibrational modes (100) and (010), $h\nu_0{}^H$ = 50 meV and 57 meV, respectively, in $VH_{0.33}$ at 30 K [43]. The theoretical value is much smaller than the experimental value, $|\Delta H_V^D| - |\Delta H_V^H|$ = 6 kJ/mol, suggesting that there may

be some other origin bringing about the energy shift in addition to the zero point energy difference in the $Ti_{0.2}V_{0.8}D_{0.79}$ and the $VH_{0.33}$. This big difference may be originated from the difference in the site occupation between hydrogen and deuterium in the compounds. The isotope effect on the zero point energy levels is schematically shown in Fig. 5.16. In the region of the Ti rich compositions (y = 0.2, 0.4, 0.6) the restricted potential well can be approximatly regarded to be the same because the hydrogen and deuterium sites have the tetrahedral symmetry. Thus the isotope shift of the site energy is brought about by only the atomic mass effect. On the other hand, in the region of the V rich compositions (y = 0.8, 1), hydrogen populates at the O-site but deuterium at the T-site only. If we assume that the potential energy function is not given by the simple harmonic potential either in the T-site or the O-site the difference is the zero-point energy between hydrogen in the O-site and deuterium in the T-site may be much larger than predicted by the simple harmonic vibrators. Provided that such mechanism works we estimate the zero-point energy difference due to the potential deformation to be about 2.6 and 5.2 kJ/mol for the $Ti_{0.2}V_{0.8}D_{0.79}$ and the $VH_{0.33}$ (by the subtraction of the mass effect (0.6 and 0.8 kJ/mol) from the total energy shift (3.2 and 6.0 kJ/mol), respectively). The schematic model suggests that the isotope effect of the pure metal hydride and deuteride are remained in the Ti-V alloys and the effect can be qualitaitively described by the M-H(D) interactions in the pure metal hydride and deuteride.

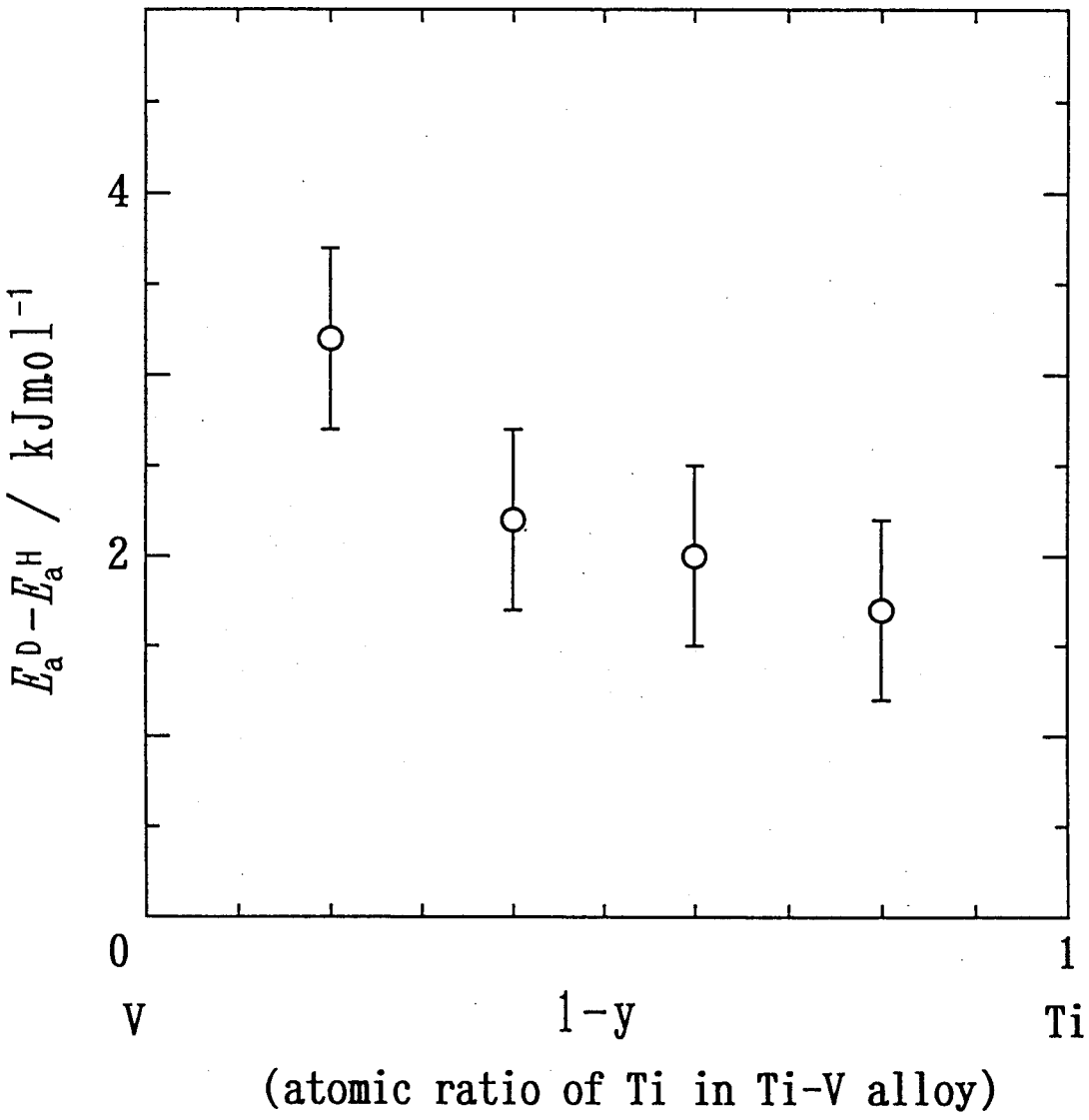

Figure 5.15 Alloy composition dependence of energy difference between deuterides and hydride, $E_a^D - E_a^H$.

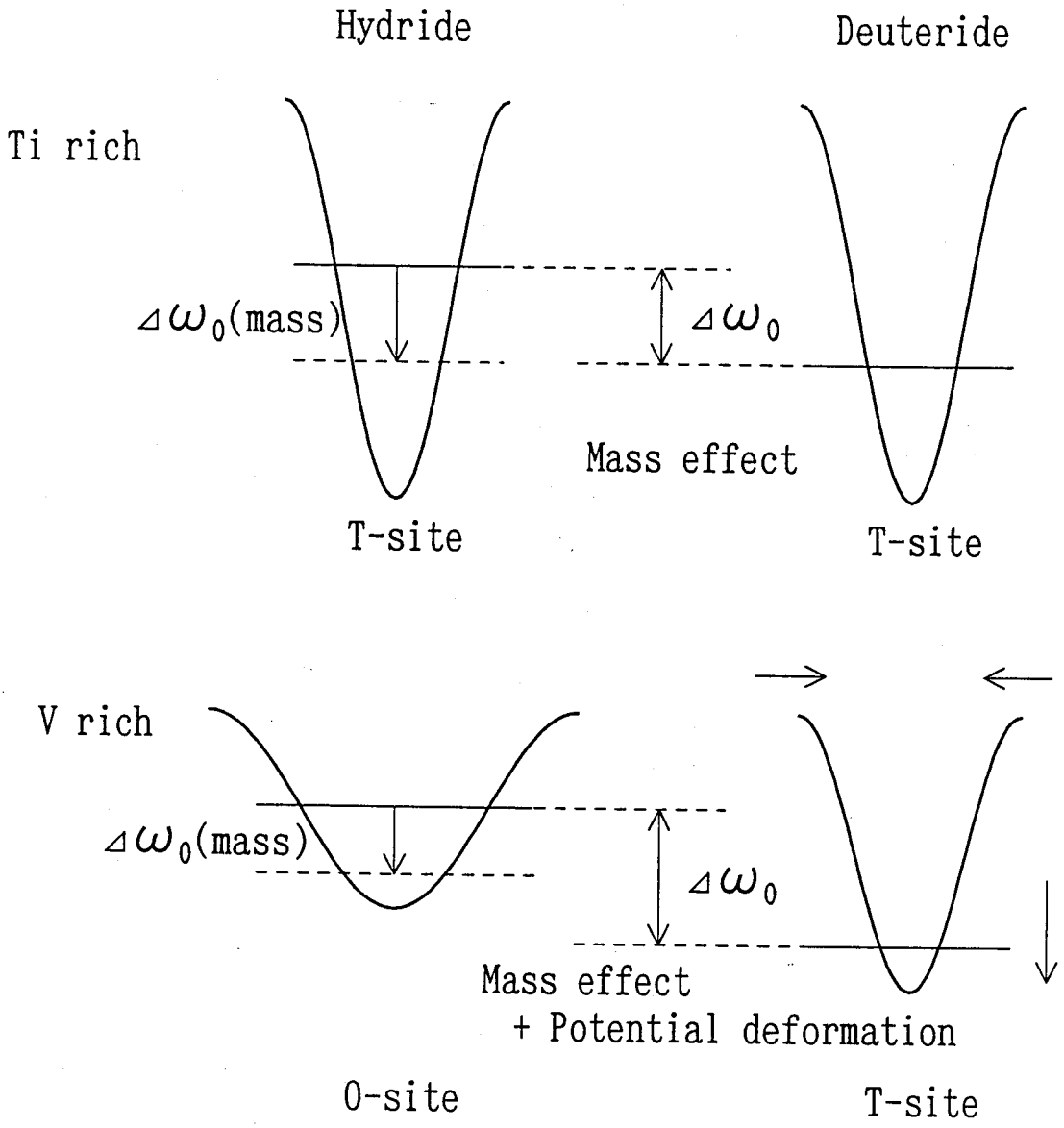

Figure 5.16 Schematic representation of isotope effect on the potential walls at interstices. At Ti-rich conpositions in Ti-V alloy, the isotope effect on the activation energy is caused by only the zero-point energy shift due to the mass effect (upper scheme). Then, both of hydrogen and deutrium atoms enter the tetrahedral site and the shape of potential walls are same as both compounds approximately. At V-rich compositions in Ti-V alloy, the isotope effect is caused by both of the zero-point energy shift due to the mass effect and the potential deformation. Then, the hydrogen atoms enter the octahedral site, but the deuterium atoms enter the tetrahedral site. The potential deformation will be brought by the change in the symmetry of interstices.

References

[1] N. Bloembergen, E. M. Purcell and R. V. Pound, *Phys. Rev.*, **73**, 679(1948).

[2] A. Abragam, *The principles of Nuclear Magnetism*, Oxford University Press, 1961, Chapter VIII.

[3] F. Borsa, D. R. Torgeson, S. W. Martin and H. K. Patel, *Phys. Rev.* **B46**, 795(1992).

[4] C. A. Sholl, *J. Phys. C: Solid State Phys.*, **7**, 3378(1974).

[5] C. A. Sholl, *J. Phys. C: Solid State Phys.*, **8**, 1737(1975).

[6] W. A. Barton and C. A. Sholl, *J. Phys. C: Solid State Phys.*, **9**, 3378(1976).

[7] W. A. Barton, *J. Phys. C: Solid State Phys.*, **15**, 5123(1982).

[8] T. K. Halstead, K. Metcalfe and T. C. Jones, *J. Magn. Reson.*, **47**, 292(1982).

[9] J. -M. Chezau, J. H. Strange and C. Brot, *J. Chem. Phys.*, **56**, 1380(1972).

[10] E. R. Andrew, D. J. Bryant and E. M. Cashell, *Chem. Phys. Lett.*, **69**, 551(1980).

[11] E. R. Andrew, D. J. Bryant, E. M. Cashell and Q. A. Meng, *Phys. Lett.*, **88A**, 487(1982).

[12] J. Schaeher, *Macromolecules*, **6**, 882(1973).

[13] F. A. Bovey and L. W. Jelinski, *J. Phys. Chem.*, **89**, 571(1985).

[14] J. Shinar, *J. Less-Common Met.*, **104**, 87(1984).

[15] K. Morimoto, M. Saga, H. Fujii, T. Okamoto and T. Hihara, *J. Phys. Soc. Jpn.*, **57**, 647(1988).

[16] A. V. Skripov, S. V. Rychkova, M. Yu Belyaev and A. P. Stepanov, *J. Phys.: Condens. Matter*, **2**, 7195(1990).

[17] A. V. Skripov, S. V. Rychkova, M. Yu Belyaev and A. P. Stepanov, *J. Phys.: Condens. Matter*, **3**, 6277(1991).

[18] L. D. Bustard, *Phys. Rev.* **B22**, 1(1980).

[19] P. A. Fedders, *Phys. Rev.* **B25**, 78(1982).

[20] E. Rössler, H. Sillescu, *Chem. Phys. Lett.*, **112**, 94(1984).

[21] P. A. Beckmann, *Phys. Rep.*, **171**, 85(1988).

[22] S. Hayashi and K. Hayamizu, *J. Less-Common Met.*, **161**, 61(1990).

[23] T. Ueda, S. Hayashi and K. Hayamizu, *Phys. Rev.* **B48**, 5837(1993).

[24] A. S. Nowick and B. S. Berry, *IBM J.*, 297(1961).

[25] R. E. Walstedt, R. Dupree, J. P. Remeika and A. Rodriguer, *Phys. Rev.* **B15**, 3442(1977).

[26] C. Wert and C. Zener, *Phys. Rev.*, **76**, 1169(1949).

[27] J. C. Wang, M. Gaffari and Sang-il Choi, *J. Chem. Phys.*, **63**, 772(1975).

[28] S. J. Allen, Jr. and J. P. Remeika, *Phys. Rev. Lett.*, **33**, 1478(1974).

[29] A. C. Switendick, *Z. Phys. Chem. Neue Folge*, **117**, 89(1979).

[30] B. K. Rao and P. Jena, *Phys. Rev.* **B31**, 6726(1985).

[31] S. Hayashi, K. Hayamizu and O. Yamamoto, *J. Chem. Phys.*, **78**, 5096(1983).

[32] E. F. Khodosov and N. A. Shepilov, *Phys. Stat. Sol.*, **(b)47**, 693(1971).

[33] E. H. Sevilla and R. M. Cotts, *Phys. Rev.* **B37**, 6813(1988).

[34] Y. Fukai and S. Kazama, *Acta Metall.*, **25**, 59(1977).

[35] R.C. Brouwer, J. Rector, N. Koeman and R. Griessen, *Phys. Rev.* **B40**, 3546(1989).

[36] P. Dantzer, O. J. Kleppa and M. E. Melnichak, *J. Chem. Phys.*, **64**, 139(1976).

[37] O. J. Kleppa, P. Dantzer and M. E. Melnichak, *J. Chem. Phys.*, **61**, 4048(1974).

[38] N. Salibi, B. Ting, D. Cornell and R. E. Norberg, *Phys. Rev.* **B38**, 4416(1988).

[39] N. L. Peterson, in *Diffusion in Solids. Isotope effects in Diffusion*, edited by A. S. Nowick and J. J. Burton, Academic Press, New York, 1975, pp. 120.

[40] T. Schober and H. Wenzl, *Hydrogen in Metals II. The Systems NBH(D), TaH(D), VH(D): Structures, Phase Diagrams, Morphologies, Methods of Preparation*, edited by G. Alfled and J. Völkl, Springer-Verlag, Berlin, 1978, pp. 11.

[41] R. R. Arons, H. G. Bohn and H. Lütgemeier, *J. Phys. Chem. Solids*, **35**, 207(1974).

[42] K. W. Kehr, *Hydrogen in Metals I. Theory of the Diffusion of Hydrogen in Metals*, edited by G. Alfled and J. Völkl, Springer-Verlag, Berlin, 1978, pp. 222.

[43] S. Ikeda and N. Watanabe, *J. Phys. Soc. Jpn.*, **56**, 565(1987).

[44] R. B. Mclellan and M. Yoshihara, *J. Phys. Chem. Solids*, **48**, 661(1987).

[45] L. R. Lichty, J-W. Han, R. Ibanez-Meier, D. R. Torgeson, R. G. Barnes, E. F. W. Seymour, C.A. Sholl, *Phys. Rev.* **B39**, 2012(1989).

6. ^{2}H NMR spectra

6.1 Introduction

A ^{2}H nucleus with spin quantum number I =1 has a finite electric quadrupole moment (eQ). The electric quadrupole moment interacts with the electric field gradient (EFG) tensor which is defined by the second derivative $V_{pq} = \partial^2 V/\partial p \partial q$ of the electrostatic potential V produced at the deuteron position by its surrounding charges. The line shape in the ^{2}H NMR spectrum is mainly determined by the nuclear quadrupole interaction. The magnitude of the quadrupole splitting is theoretically derived by the first order perturbation treatment of the nuclear quadrupole interaction to the Zeeman interaction, and is given by [1]

$$\Delta\nu = \frac{3}{4}\frac{e^2Qq}{h}(3\cos^2\beta - 1 - \eta\sin^2\beta\cos\alpha), \qquad (6.1)$$

where e^2Qq/h is the quadrupole coupling constant (QCC) and α and β the Eulerian angles to transform the coordinate system from the laboratory fixed frame to the principal axis system of the EFG tensor. η is the asymmetry parameter for the EFG defined by

$$\eta = \frac{(V_{xx} - V_{yy})}{V_{zz}}, \qquad (6.2)$$

using the principal values of the EFG tensor which satisfy the relation, $|eq| = |V_{zz}| \geq |V_{yy}| \geq |V_{xx}|$. η takes the value in the range of $0 \leq \eta \leq 1$. Thus, the EFG tensor reflects the charge distribution around the nucleus. The QCC and η are very useful parameters to discuss the microscopic environments of an atom such as the site symmetry, the directionality of the chemical bond and the valences of the atom in the solid state.

For a powdered or polycrystalline material, ^{2}H NMR line shape is given by the spacial average of Eq. (6.1) with respect to the Eulerian angles α and β. The line shape for the powdered specimen consists of the famous Pake doublet when η = 0, and varies with increase in η, as shown in Fig. 6.1. The fluctuation of the EFG tensor due to the deuterium motion causes the averaging of the nuclear quadrupole interaction. As the results, the line shape varies depending on both the frequency and the mode of the fluctuation of the EFG tensor. Thus, the

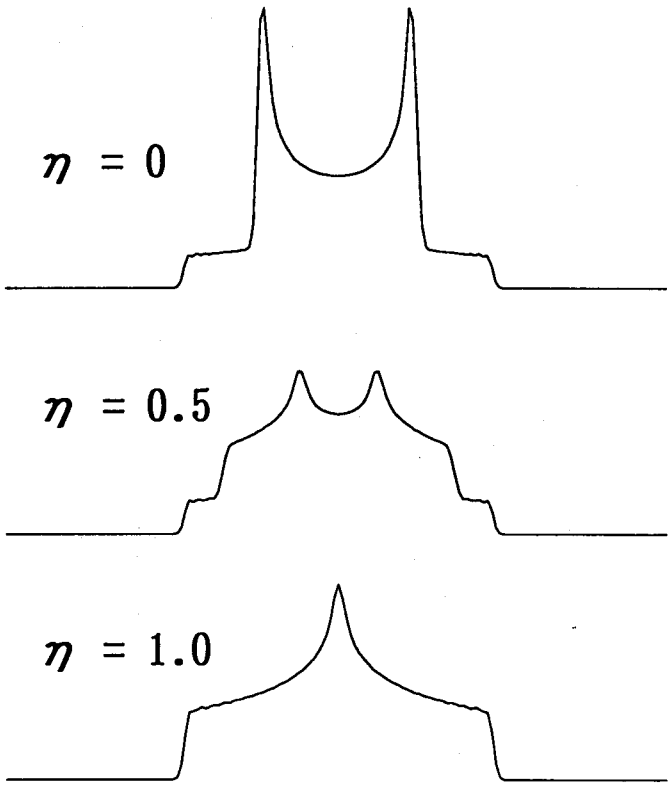

Figure 6.1 Typical ^2H NMR line shapes for the powdered material with the asymmetry parameter of the EFG tensor, $\eta = 0$, 0.5 and 1.

^{2}H NMR spectrum for the powdered specimen is also used to investigate the dynamical behavior of the molecules containing ^{2}H nucleus.

The measurements of ^{2}H NMR line shape for the metal deuterides have been performed to study the type of ^{2}H interstitial site, the valence and the dynamics of the deuterium in the host metal framework by a number of researchers. The deuterides of Ta, Nb and V were studied using the powdered samples by Salibi *et al.* by measuring the spectra and the magnetic relaxation times [2]. For $VD_{0.59}$, in which the deuterium occupy both the octahedral (O-) and the tetrahedral (T-) sites, they demonstrated that the magnitude of the nuclear quadrupole interaction is closely related to the deuterium site symmetry. The QCC for ^{2}H occupying the O- and the T-sites are 106 kHz at 244 K and 54 kHz at 194 K, respectively. The asymmetry parameter of the EFG tensor η was about 0.1 in both the O- and the T-sites. Thus, the type of the interstitial sites occupied by the deuterium can be investigated by measuring the QCC in the ^{2}H NMR. In the present work the measurements of ^{2}H NMR spectra are performed to investigate the nature of the ^{2}H site in the Ti-V alloy. The temperature depndence of the line shape is also observed to study the dynamical behavior of the deuterons in the deuterides.

6.2 Experimental

^{2}H NMR measurements were carried out with a Bruker Model MSL-400 pulsed spectrometer with a superconducting magnet at the Larmor frequency for ^{2}H of 61.4 MHz. The modification of the instrument was described in Section 5.2. The length of 90° pulse for liquid D_2O was improved to 2.95 μs from 7 μs. ^{2}H NMR spectra were measured using solid echo method over the temperature range 125 ~ 298 K. The delay time between the first and the second pulses in the solid echo pulse sequence was 15 μs. The 90° pulse length for the Ti-V-D system were 8 ~ 11 μs depending on the volume susceptibility of the sample, which varied with the size and the shape of the particles and the metallic character of sample. The temperature control was achieved by Bruker variable temperature unit VT-1000, which was controlled to ± 1 K by the flowing cooled or heated nitrogen gas. The samples for the experiments were the same as those used in the ^{2}H T_1 measurements.

6.3 Results and Discussion

The temperature dependence of the ^2H NMR spectra for $Ti_{1-y}V_yD_x$ is shown in Fig. 6.2 ~ 6.5. The full line width at the half maximum (FWHM) and the shift ($\Delta\nu$) in the peak frequency to the Larmor frequency 61.4 MHz are plotted against temperature in Fig. 6.6 ~ 6.9. There are no significant dependence of the spectral patterns on the alloy composition of the deuteride and the spectra of all the deuterides give similar temperature dependence. For example, at 125 K, the ^2H NMR spectrum of $Ti_{0.6}V_{0.4}D_{0.86}$ has the broad line width with that FWHM of larger than 20 kHz, and as its $\Delta\nu$ value is -7.8 kHz. The line shape is asymmetric and there is a shoulder at the higher frequency side of the peak. The intensity of the shoulder decreases with increase in temperature, and it disappears above 200 K. The line width narrows rapidly from 21 kHz to 5 kHz on heating from 125 K to 225 K, and remains almost constant above 225 K as shown in Fig. 6.7. The $\Delta\nu$ value shifts from -7.8 kHz to -5.3 kHz on heating from 125 K to 200 K, and is constant above 200 K. The spectra of other metal deuterides have similar temperature dependence. The $\Delta\nu$ value in each deuteride shift from about -8 kHz to about -5 kHz with increasing on heating from 125 K to 200 K as shown in Figs. 6.6-6.9. The line widths at 125 K was 10 kHz for $Ti_{0.8}V_{0.2}D_{0.79}$ and 30 kHz for $Ti_{0.2}V_{0.8}D_{0.79}$, and narrow to about 5 kHz on heating from 125 K to 225 K.

When the powder line shape in the ^2H NMR spectrum is governed by the nuclear quadrupole interaction it should have an ideally symmetric shape as shown in Fig. 6.1. The experimental line shapes in the Ti-V-D systems are largely different from the theoretical powder patterns of the ^2H NMR spectrum, especially with respect to the symmetry of the patterns. These results suggest that some other interaction contributes to the broadening and the asymmetrization of the line shape in addition to the weak nuclear quadrupole interactionin the $Ti_{1-y}V_yD_x$. In the case of metal deuterides there have been known two kinds of interactions which cause the line broadening and the aymmetrization; one is the anisotropy in the Knight shift tensor [3], and the other the magnetic susceptibility broadening [4, 5]. In the present alloy-deuterium system the co-existence of the multi-phases caused as described in Chapter 3 may bring about an apparent broadening of the ^2H spectral line. The Knight shift is caused by the interaction between the nuclear spins and the hyperfine field produced at the site of the

nucleus by the conduction electrons. The hyperfine field has a tensor properties, and gives a similar effect to that by the chemical shift anisotropy on the powder NMR pattern. However, the magnitude of the hyperfine field for the deuteron is comparable to that of the normal demagnetization field originated from the bulk susceptibility of the sample. Hence the Knight shift anisotropy can cause the line broadening of at most 10 kHz. On the other hand, the magnetic susceptibility broadening is caused by the inhomogeneous field produced by the scattering of the uniform external field by an ellipsoidal or, more generally, non-spherical particles with non-zero magnetic susceptibility. Therefore, the degree of the broadening depends strongly on the shape of the particles, on the bulk magnetic susceptibility (χ) of each particle, and on the magnitude of the external static field. The line broadening of the ^2H NMR spectra in the $Ti_{1-y}V_yD_x$ is therefore considered to be caused by both the nuclear quadrupole interaction and the magnetic susceptibility effect. However, these effects do not cause the asymmetry of the spectra. Furthermore, the QCC values, which were determined from the minimum values of the T_1 for $Ti_{1-y}V_yD_x$, lie in the frequency range 21 ~ 36 kHz. If the deuteron diffusion is completely frozen, the splitting of the Pake doublet in the case of $\eta = 0$ amount to 40 ~ 70 kHz. Acutaully, in the temperature range between 125 K and 200 K the deuteron diffusional motion is rapid and isotropic enough to cause the complete motional narrowing of the nuclear quadrupole interaction in the $Ti_{1-y}V_yD_x$ because the line width in this temperature region is much smaller than the rigid lattice value. Therefore the inhomogeneous and asymmetric line shape of ^2H in Ti-V-D system is considered to be originated from the co-existence of the multi-phases (two or three phases) and its partial variations with temperature. The shoulder observed below 200 K is regarded as a peak with a significantly broad line width originated from some co-existing phase with the β-phase. The decrease in the intensity of this peak on heating may correspond to some change in the additional phase such as phase transition (see in Chapter 3).

The α-phase of the $Ti_{1-y}V_yD_x$ is the most possible condidate for the co-existing phase with the β-phase. It is known that when the metallic character of the metal deuteride is high, the magnetic susceptibility and the hyperfine field become larger [6], causing the larger line broadening and the higher frequency shift of the ^2H NMR sepctrum in the deuterides. On the

other hand, the metallic character of the metal deuterides becomes large with decrease in the concentration of the deuterium in the metal deuterides [7]. Comparing the degree of the metallic character between the α- and β-phases, which have the same crystal lattice formed by the metals, the metallic character in the β-phase is lower than that in the α-phase. On the basis of the consideration, the high frequency shoulder can be assigned to the deuterons in the α-phase.

These results suggest that the apparent spin-lattice relaxation time T_1^* for ^2H below 200 K corresponds to an average value among the T_1 values is individual multi-phases. This is one of the origins of the discrepancy between the calculated and the experimental values for the ^2H T_1^* in Ti-V-D system below 200 K.

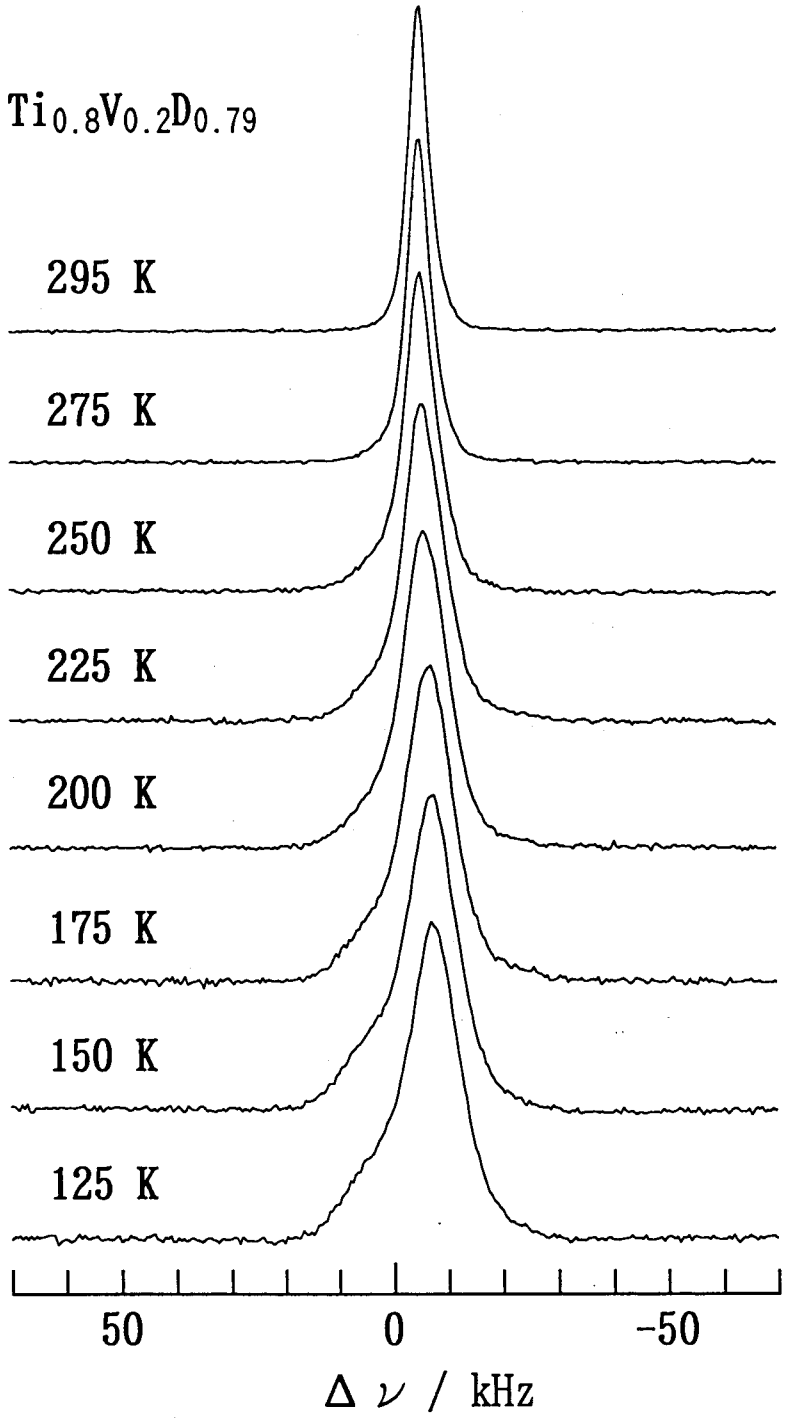

Figure 6.2 Temperature dependence of the ^2H NMR line shape in β-$Ti_{0.8}V_{0.2}D_{0.79}$ powdered sample.

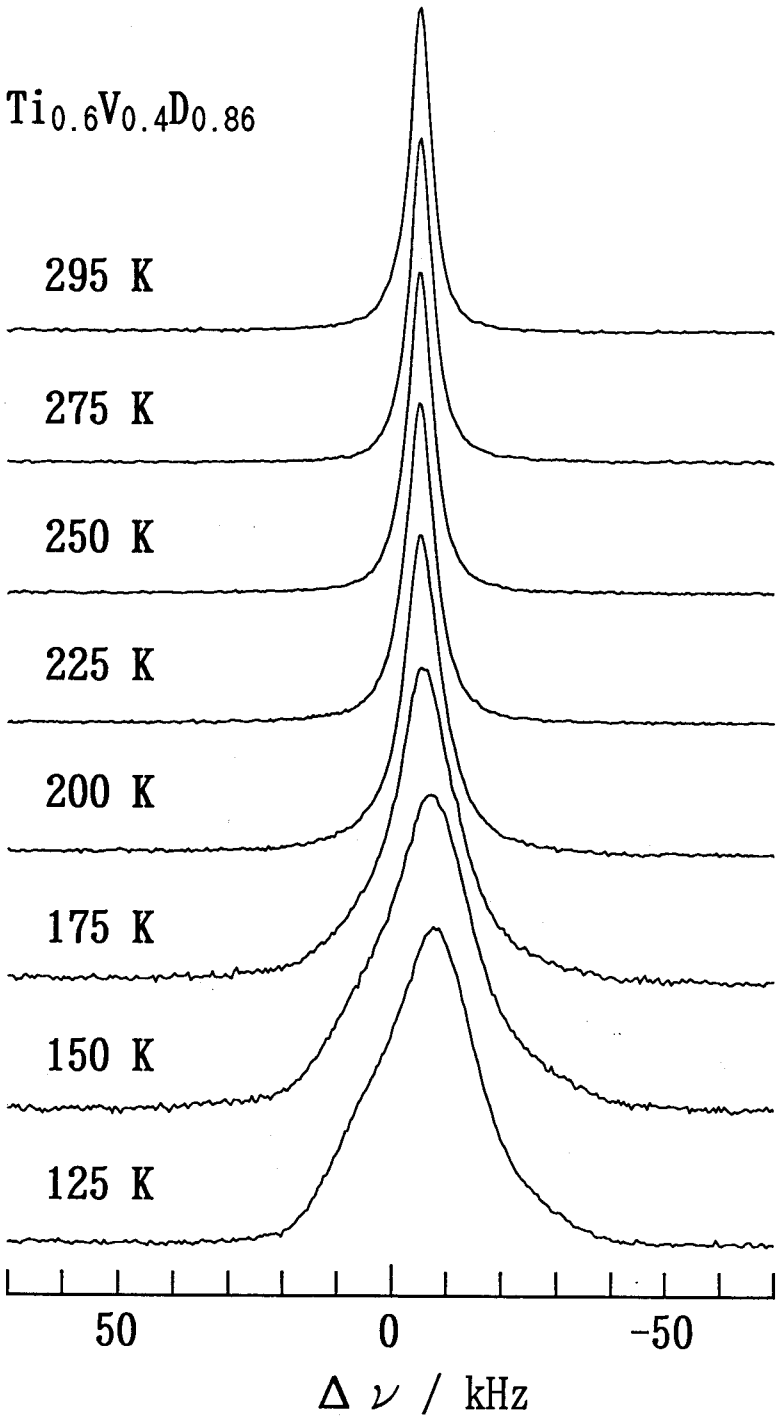

Figure 6.3 Temperature dependence of the ^2H NMR line shape in β-$Ti_{0.6}V_{0.4}D_{0.86}$ powdered sample.

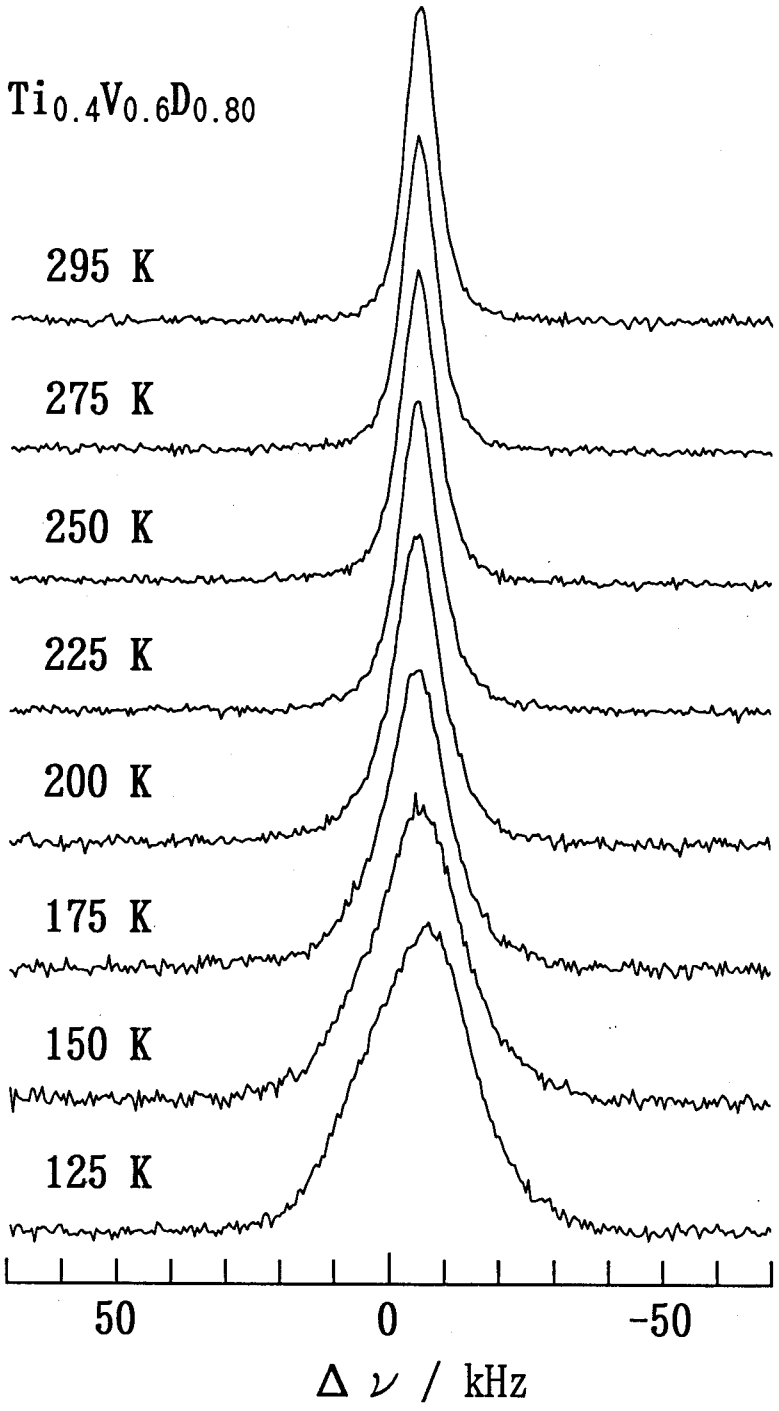

Figure 6.4 Temperature dependence of the ^2H NMR line shape in β-$Ti_{0.4}V_{0.6}D_{0.80}$ powdered sample.

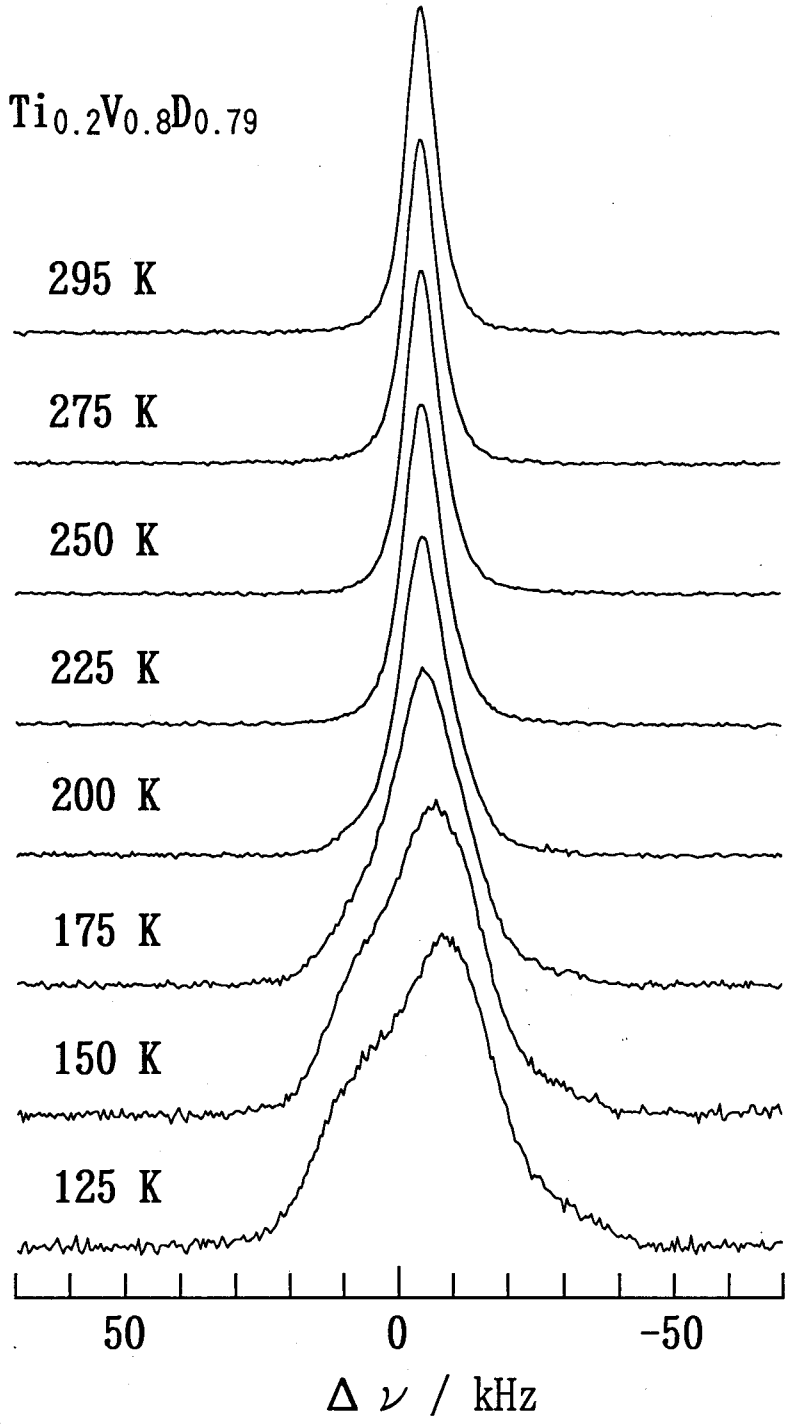

Figure 6.5 Temperature dependence of the ^2H NMR line shape in β-$Ti_{0.2}V_{0.8}D_{0.79}$ powdered sample.

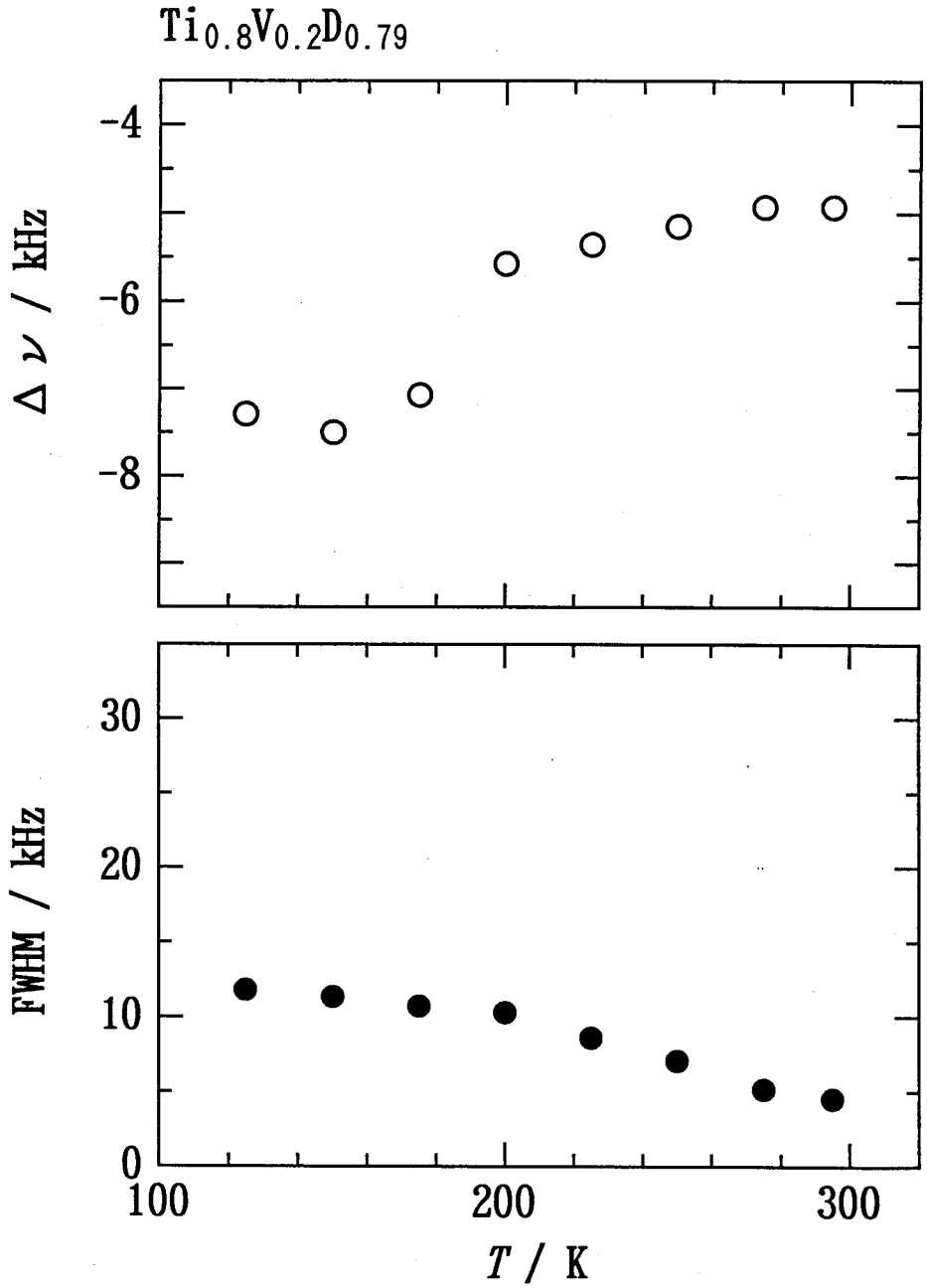

Figure 6.6 Temperature dependence of the frequency shift ($\Delta\nu$) and the full line width at the half maximum (FWHM) of ^{2}H NMR spectrum in β-$Ti_{0.8}V_{0.2}D_{0.79}$.

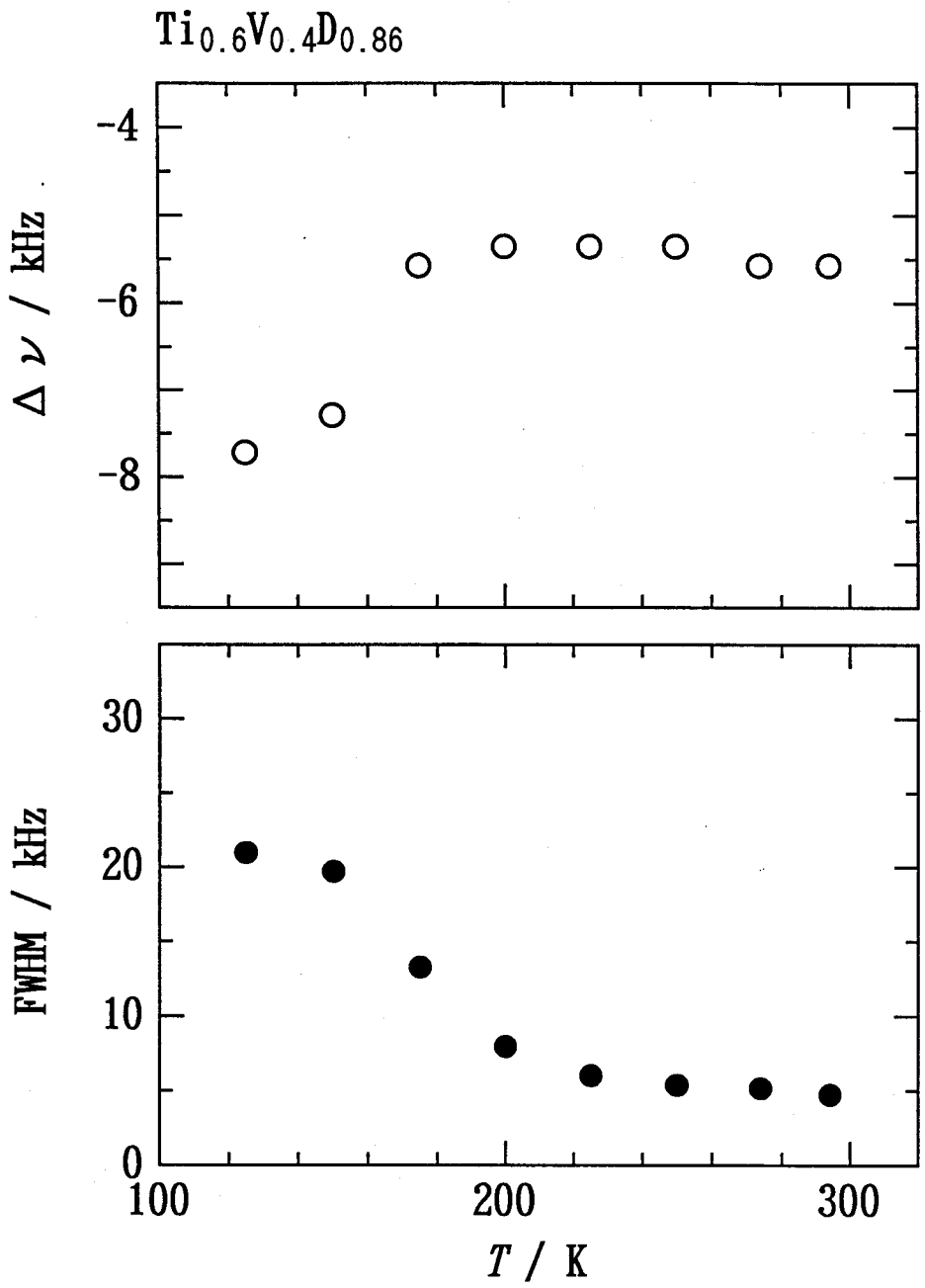

Figure 6.7 Temperature dependence of the frequency shift ($\Delta\nu$) and the full line width at the half maximum (FWHM) of ^{2}H NMR spectrum in β-$Ti_{0.6}V_{0.4}D_{0.86}$.

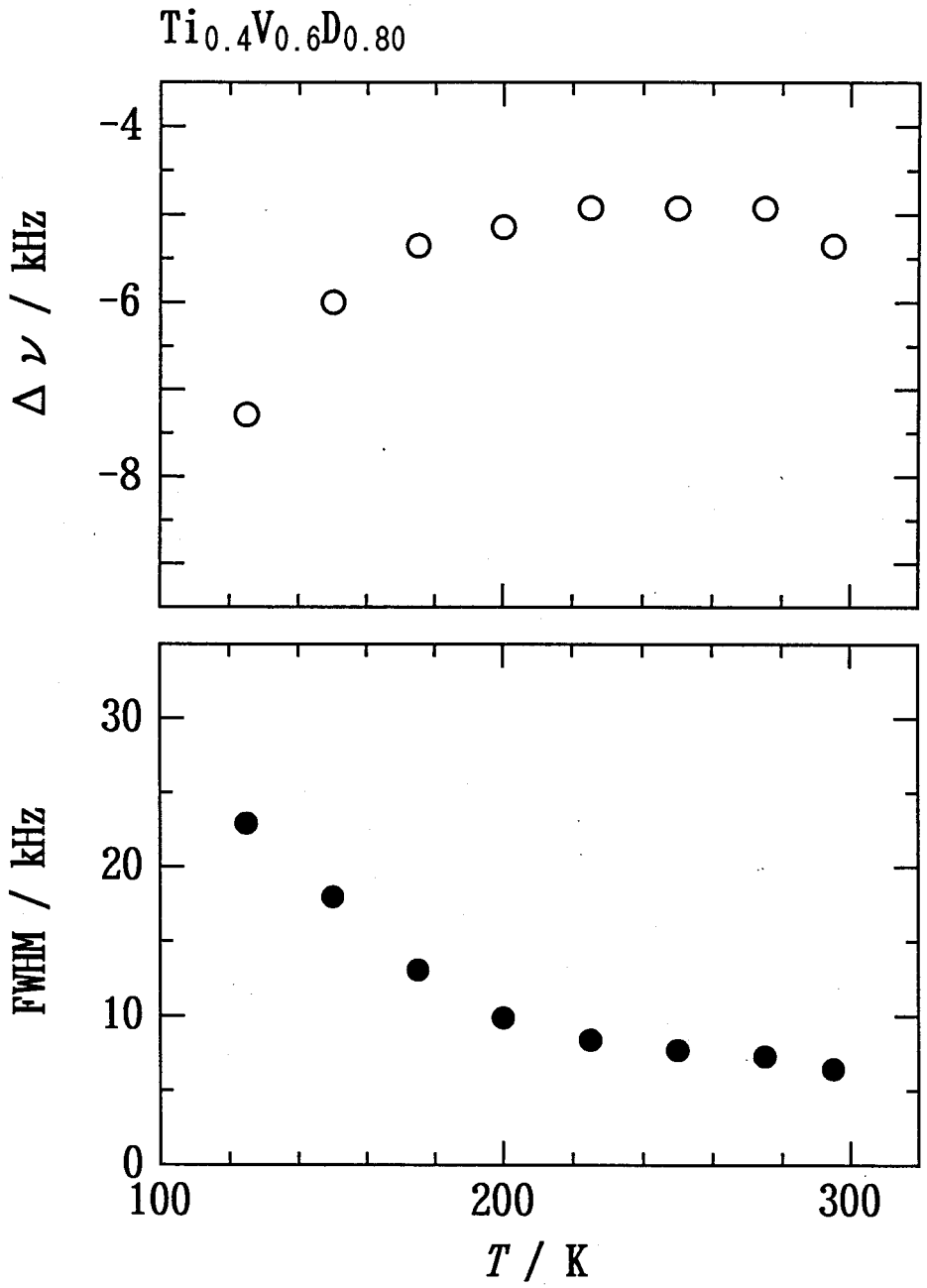

Figure 6.8 Temperature dependence of the frequency shift ($\Delta\nu$) and the full line width at the half maximum (FWHM) of ^{2}H NMR spectrum in β-$Ti_{0.4}V_{0.6}D_{0.80}$.

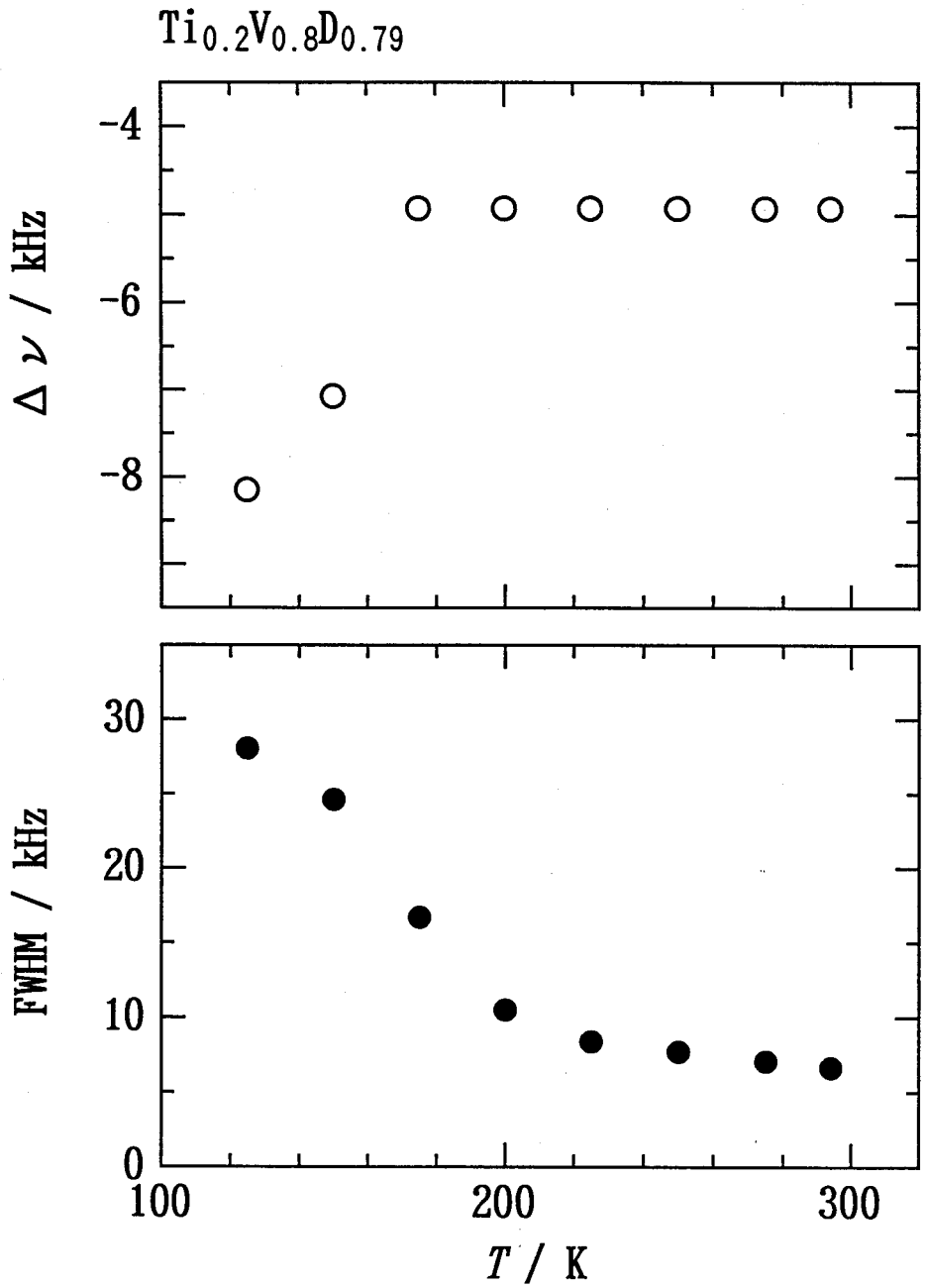

Figure 6.9 Temperature dependence of the frequency shift ($\Delta\nu$) and the full line width at the half maximum (FWHM) of ^{2}H NMR spectrum in β-$Ti_{0.2}V_{0.8}D_{0.79}$.

References

[1] A. Abragam, *The principles of Nuclear Magnetism*, Oxford University Press, 1961, Chapter VII.

[2] N. Salibi, B. Ting, D. Cornell and R. E. Norberg, *Phys. Rev.* **B38**, 4416(1988).

[3] D. R. Torgeson, R. J. Schoenberger and R. G. Barnes, *Bull. Am. Phys. Soc.*, **31**, 270(1986).

[4] L. E. Drain, *Proc. Phys. Soc.*, **80**, 1380(1962).

[5] M. E. Stoll and T. J. Majors, *J. Magn. Reson.*, **46**, 283(1982).

[6] W. Baden, P. C. Schmidt, A. Weiss, *J. Less-Common Met.*, **88**, 171(1982).

[7] T. Ueda, S. Hayashi and K. Hayamizu, *Solid State Commun.*, **87**, 429(1993).

7. Summary

Nuclear magnetic resonance and neutron inelastic scattering methods are useful tools in the study of the structure and dynamics of hydrogen atom in the metal-hydrogen system from the microscopic point of view and can give the information on the local environment around the interstitial hydrogen atom. This work has been planed to apply ^1H and ^2H NMR and neutron inelastic scattering methods to the study of the dynamics of hydrogen atom and the local framework structure of the host metal lattice around the hydrogen atom in disordered Ti-V-H(D) system with the β-form. These experiments were done on the disordered metal hydrides, β-$Ti_{1-y}V_yH_x$ ($x \sim 1$ and $0.2 < y < 0.9$) and the deuterides, β-$Ti_{1-y}V_yD_x$ ($x \sim 1$ and $0.2 \leq y \leq 0.8$). The neutron inelastic scattering of β-$Ti_{1-y}V_yH_x$ and the ^2H NMR measurements of the deuterides provide the first research data for the microscopic properties of those materials.

The neutron inelastic scattering measurements elucidated the type of the interstitial sites occupied by the hydrogen atom in the β-phase of Ti-V-H system. It distingushed the two kinds of the tetragonal sites and the octahedral site for hydrogen accommodation in the metal framework and succeeded to estimate the population in between these sites. The dynamics of interstitial atoms in disordered metal hydrides and deuterides were studied by the spin-lattice relaxation times (T_1) measurements on ^1H and ^2H. The remarkable isotope effect on the activation energy for the hydrogen diffusion was found between hydride and deuteride. Broadline ^2H NMR spectra were also measured to investigate the deuteron diffusive motion. The obtained spectra showed no remarkable quadrupole broadening even at 125 K, implying that the deuteron diffusive motion is rapid enough to average out the quadrupole interaction. A shoulder detected near the main ^2H signal in each β-Ti-V-D was attributed to phase transition which was observed by DSC measurments. In order to describe the local structure of the disordered host alloy framework a cluster model adopting the short-range ordering of metal atoms was applied. The original cluster model is developed to examine the distribution of hydrogen over only the $Ti_{4-i}V_i$-type tetragonal interstitial sites; In this work this model was improved to a general theory which deals with the simultaneous hydrogen distribution over the $Ti_{6-i}V_i$-type octahedral interstitial sites and the tetragonal sites. Application of the newly developed cluster model to Ti-V-H(D) system made it possible to analyze the composition

dependence of the activation energy and of the population of the hydrogen sites in this system. The analyses revealed that the alloy system of disordered state is not homogeneous in the microscopic point of view and the hydrogen is apt to enter interstitial site rich in Titanium. The short-range order parameter, which is a measure of microscopic inhonogeneity, was evaluated to be 0.4.

In this work, two remarkable characteristices of the framework structure and the hydrogen dynamics in the β-phase for the Ti-V-H(D) system were revealed as follows; One is that the hydrogen atoms occupy both the tetrahedral and the octahedral sites and the occupancy of each site varies with the alloy composition. Other is that the hydrogen atoms diffuse rapidly even at 125 K and the activation energy increases with increase in Ti content. Assuming the equation $D = <s^2>/6\tau_c$ between the correlation time τ_c and the diffusion constant D and the mean jump distance $<s^2> \sim 2 \times 10^{-16}$ cm^2 which corresponds to the mean distance among the nearest neighbor T- and the O-sites, the order of the diffusion constant in the β-phase was estimated to be 10^{-7} cm^2/s at 40 °C using the activation parameters in Table 5.2. In contrast to the β-phase examined in this study, in the case of the γ-phase the hydrogen atoms occupy only the T-sites in the fcc metal lattice and form the simple cubic sub-lattice. The hydrogen atoms in the γ-phase cannot diffuse in the same temperature range as this work. On the other hand, in the α-phase the hydrogen atoms are diffusing between the T-sites in the bcc metal lattice with the order of the diffusion constant $10^{-5} \sim 10^{-4}$ cm^2/s at 40 °C. The difference in the diffusion rate between the α- and the β-phase will reflect the H-H interaction depending on the hydrogen concentration. This work revealed that the tetrahedral-tetrahedral (T-T), tetrahedral-octahedral (T-O) and octahedral-octahedral (O-O) diffusion processes take place in the β-phase.

The short-range order of the metallic atoms is the most important characteristic of the Ti-V alloy system. The value of the short-range order parameter was determined in the β-phase for the first time in this work. The value obtained in this work was in good agreement with the literature values which were determined for the α-phase. This work thus clarified the local metallic framework structure and the dynamics of hydrogen atoms in the β-phase for the disordered Ti-V-H(D) system, and indicated that very important parameters which describe the

microscopic structure and properties of the disordered Ti-V alloy system can be derived by the use of an extended cluster model.